5-2020

Numerical Simulations of Spread Foundations Supported on Stone Columns Using the Discrete Element Method

Anibal Enrique Santos Marin
University of Arkansas, Fayetteville

Numerical Simulations of Spread Foundations Supported on Stone Columns Using the Discrete Element Method

A dissertation submitted in partial fulfillment
of the requirements for the degree of
Doctor of Philosophy in Engineering

by

Aníbal Enrique Santos Marín
Technological University of Panama
Bachelor of Science in Civil Engineering, 2010
University of Arkansas
Master of Science in Civil Engineering, 2017

May 2020
University of Arkansas

This dissertation is approved for recommendation to the Graduate Council.

_____
Michelle L. Barry, Ph.D.
Committee Chair

_____
Richard A. Coffman, Ph.D.
Committee Member

_____
Paul C. Millett, Ph.D.
Committee Member

_____
Clinton M. Wood, Ph.D.
Committee Member

ABSTRACT

The implementation of stone columns as a ground improvement technique has become more popular in geotechnical construction practice as a result of their ability to improve strength, stiffness and permeability characteristics of weak clayey soil deposits. There are several analytical and empirical approaches to estimate the bearing capacity of stone column foundation systems; however, there is notable variation in the performance of these existing methods when compared with full-scale experimental results. For very weak cohesive soils (i.e., undrained shear strength less than 15 kPa), the use of conventional stone columns becomes restricted because of the insufficient confinement that these types of soils can provide to the columns. Hence, the inclusion of cement-coated aggregate has been developed as an alternative method to improve the efficacy of stone columns in soft soils. Limited information is available regarding the global performance, load-transfer mechanism, and design of these types of cemented stone columns under various field conditions. Efforts to refine the accuracy of current design methods and reinforcement techniques for conventional stone columns naturally point to the need for improving the understanding of the fundamental load-transfer mechanisms of stone columns.

Three-dimensional discrete element method (DEM) simulations of small- and full-scale footing loading tests were developed to investigate the effects of aggregate strength, pier length, aggregate Young's modulus, area replacement ratio, cement content, and undrained shear strength of the matrix soil on the bearing pressure-displacement responses of isolated foundations supported on stone columns. The elemental responses of the aggregate and plastic matrix soil were calibrated against laboratory and in-situ test data from a well-characterized site and compared against the results of small- and full-scale footing loading tests. The column aggregate material was represented by discrete-deformable tetrahedrons in conjunction with

strain-softening and strain-hardening models in order to improve the simulation of the nonlinear response of the cemented aggregate. Joined deformable blocks were employed to represent the continuous mechanical behavior of the surrounding clayey soil. The numerical results are in excellent agreement with the experimental laboratory and field data and provide improved estimates of the bearing pressure-displacement curves of the column-foundation systems investigated in this study. The Young's modulus of the aggregate column and the area replacement ratio were found to have the greatest influence on the bearing pressure-displacement response. The DEM results also improve the understanding of the effects of granular material-cementation on the performance of stone columns. At low cement contents the stone column exhibits a type of bulging failure mechanism similar to uncemented stone columns, but at higher cement contents (10 % in this study), bulging is not observed, and the behavior resembles more like that of a concrete pile. These types of behavioral differences also have different implications for single isolated stone columns and group column behavior.

ACKNOWLEDGMENTS

I want to thank my wife, Carolina, family and friends who have supported me during all this academic journey. Also, I would like to thank my advisor, Dr. Michelle Bernhardt-Barry, for the opportunity to work in her research group, her encouragement in developing this dissertation, and her academic and personal support not only as my advisor, but as a friend over these five years at the University of Arkansas. I am thankful to Dr. Armin Stuedlein for providing the field experimental data used in this research and reviewing some of the results obtained from this numerical investigation. Additionally, I would like to thank Dr. Richard Coffman, Dr. Paul Millett, and Dr. Clinton Wood for accepting to be members of my committee, sharing knowledge in classes, and reviewing this research. I also want to thank to my dear friend Victorino Rodriguez and Professor Tomas Guevara for agreeing to co-sign and be my guarantors of my scholarship. Finally, I would like to thank the Panamanian Institute for the Formation and Use of Human Resources (IFARHU) for providing student support for this research.

DEDICATION

I would like to dedicate this work to my Lord, Jesus Christ, my wonderful and beautiful wife, Carolina, my mother, Enriqueta, and all my family in Panama (Daisy, Yessica, Aida, Jormel, Reid, Ashly, Héctor, Lía, Aníbal, Roberto).

TABLE OF CONTENTS

LIST OF FIGURES

LIST OF TABLES

CHAPTER 1. INTRODUCTION

1.1 Research motivation

Ground improvement and reinforcement techniques developed by specialty contractors have proven effective for mitigating poor deformation performance in weak soil deposits (Schaefer et al. 1997). Aggregate piers are typically used to increase the bearing capacity and decrease total and differential settlement of foundations and embankments, and they have been shown to be a cost-effective ground improvement alternative (Van Impe and de Beer 1983; Vahedian et al. 2014; Stuedlein and Holtz 2013, 2014). Aggregate piers are particularly advantageous for layered soils of contrasting stiffnesses and hydraulic conductivities, as they can accelerate the rate of consolidation (Han and Ye, 2001; Castro and Sagaseta 2009), reduce liquefaction potential (Ashford et al. 2000; Adalier et al. 2003; Rayamajhi et al. 2014a, 2014b; Stuedlein et al. 2015), and improve the stability of slopes (Vautrain 1977; Barksdale and Bachus 1983).

Typically for aggregate pier projects, between 15 to 40% of the treated soil area is replaced with compacted granular material using different types of installation techniques such as vibro-displacement, vibro-replacement, or tamping (Nazari and Ghazavi 2014; and Stuedlein and Holtz 2012a). When the vibrational installation technique is used, aggregate piers are better known as stone columns. Provided that sufficient densification is achieved in the aggregate during construction, the performance of spread footings on stone column-reinforced clayey soils has been satisfactory for a variety of installation methods and aggregate gradations (Stuedlein and Holtz 2012a). However, despite their history of good performance, available methods for the static design of shallow foundations with regard to capacity (Greenwood 1970; Hughes and Withers 1974; Brauns 1978; Madhav and Vitkar 1978; Mitchell 1981) and displacement (Fox

and Cowell 1998; Wissmann et al. 2007; White et al. 2007) have been shown to exhibit poor accuracy (Stuedlein and Holtz 2013; 2014). This generates not only lack of confidence in these methods that could consequently lead to over-engineered designs, but also the need for verification of the column performance through expensive field testing (Stuedlein, 2008).

For very weak strata with high compressibility and low shear strength characteristics (e.g., peat, organic material), the implementation of conventional stone columns is questionable because of the lack of lateral support that these types of soft soils can provide (Barksdale and Bachus 1983). Approaches for improving the effectiveness of stone columns in low shear strength soils consists of increasing the column's stiffness (e.g., cemented aggregates, high compaction), restricting the column's lateral deformation (e.g., geosynthetic encasement), or some combination of the two. Recent experimental investigations have shown that the use of cemented aggregates produces substantial improvement in the performance of stone column-foundation systems, with no significant increase in the construction cost (Golait and Padade 2016). However, there is lack of information regarding design and modeling parameters and the global performance of these type of columns under different field conditions in comparison with conventional uncemented aggregate columns. Advancements in the performance of stone columns requires further refinement of the accuracy of the current design methods and improvement in the understating of the mechanical behavior of reinforcement techniques developed.

Because of the difficulties in measuring the load transfer and deformation occurring around a stone column in either small- or full-scale experiments, numerical analyses have been used to investigate the complex soil-column-foundation interaction. To date, continuous analytical and numerical approaches have primarily been used to simulate stone columns. One

issue with these methods is that they cannot properly capture the internal interaction occurring between the individual aggregate particles comprising a stone column (Ngo et al., 2016). An alternative solution is to use the discrete element method (DEM), which is a numerical approach used to calculate the mechanical behavior of a system consisting of a large number of distinct blocks or elements such as granular material (Cundall 1988; and Luding 2008). Experimental calibration or verification of these models is important in order to provide confidence in the numerical findings. The experimental data can be derived from either laboratory element or scaled tests, or full-scale field tests. Stuedlein and Holtz (2012a) described a comprehensive full-scale footing loading test program designed to investigate the effects of aggregate pier installation method, aggregate gradation, and column length on the bearing pressure-displacement performance. This experimental program was conducted on single, isolated cemented and uncemented stone columns, as well as small groups of stone columns. Newton (2014) further characterized the aggregates used in Stuedlein and Holtz (2012a) using triaxial consolidated drained tests to examine the stress-strain and volumetric response of the cemented and uncemented aggregates. Golait and Padade (2016) conducted a scaled-model laboratory experimental program to evaluate the effectiveness of cemented stone columns and developed a theoretical procedure to estimate the bearing capacity of weak clayey deposits reinforced with these types of columns. These experimental investigations provide excellent field and laboratory data for calibrating and validating the three-dimensional discrete element models (3D-DEM) conducted in this research.

1.2 Goal and objectives of this research

The overall goal of this research was to improve understanding of the complex, nonlinear, and progressive nature of load transfer in uncemented and cemented stone columns

using three-dimensional multiscale DEM simulations. The elemental responses of the aggregate and clayed soil were calibrated against laboratory and in-situ test data compared against the results of small-and full-scale footing loading tests. The main factors governing the global performance and load transfer mechanism of single and group aggregate columns (e.g., strength and stiffness of the surrounding soil, area replacement, pressure-dependence of the stiffness and strength of the aggregate, column geometry) were systematically varied and examined. The results obtained from this numerical investigation are used to advance the current design methods and reduce uncertainties in the prediction of the performance of spread foundations on aggregate columns reinforced clay in order to obtain more cost-effective designs.

The research objectives aimed at achieving this goal include:

1. Improve understanding of the behavior of isolated foundations supported on conventional stone columns through calibrated and validated DEM simulations. This objective includes the following research tasks:
    1.1 Conduct element test simulations to calibrate the responses of the uncemented aggregate reported in Duncan et al. (2007) and Newton (2014).
    1.2 Develop and calibrate full-scale 3D-DEM models to evaluate the bearing pressure-displacement responses of single uncemented stone columns investigated by Stuedlein et al. (2012a).
    1.3 Conduct a parametric study of single uncemented stone columns to investigate the effect of parameters (e.g., column length, aggregate gradation, area replacement ratio) on the bearing pressure-displacement response.

2. Evaluate the performance of isolated footings resting on cemented stone columns by conducting a DEM numerical investigation. This objective includes the following research tasks:
    2.1 Conduct calibrated and validated small- and full-scale 3D-DEM models to evaluate the effectiveness of cemented stone columns investigated by Stuedlein (2008) and Golait et al. (2016)
3. Reduce uncertainties in the prediction of the bearing capacity of spread foundations on stone column groups. This objective includes the following research tasks:
    3.1 Compare the differences in the bearing pressure-displacement responses of external and internal columns within a small stone column group with the results obtained from a unit-cell model.
    3.2 Compare estimations of the ultimate bearing pressure obtained using the calibrated 3D-DEM simulations with existing methods for footings on small stone column groups.

1.3 Dissertation overview

This dissertation contains a description of the numerical investigation conducted to increase the understanding of the global behavior and load transfer mechanisms of isolated foundations supported on aggregate column reinforced clay. This dissertation is organized into six chapters. Chapter 2 presents a summary of the relevant literature on aggregate columns including: general aspects of stone column installation, current methods for estimating the bearing capacity of single stone columns and small aggregate column groups, and an outline of previous DEM investigations conducted on stone columns. A description of the laboratory and

field experimental database used for calibration and validation of the 3D-DEM simulations is provided in Chapter 3. Details of the test site characterization and footing loading test program conducted by Stuedlein and Holtz (2012a), as well as information related to the laboratory experimental program developed by Golait and Padade (2016) are given. Chapter 4 provides detailed aspects of the development of the 3D-DEM simulations. Description of the numerical framework features, selection of model geometries and boundary conditions, as well as calibration of selected material properties and constitutive stress-strain relationships are presented. Chapter 4 also includes the validation of the small- and full-scale footing loading test simulations against experimental data. Chapter 5 presents the numerical results obtained from a parametric study conducted to investigate the effects aggregate strength and stiffness, column length, cement content, area replacement ratio, and undrained shear strength of the matrix soil have on the load transfer mechanisms of isolated spread foundations on aggregate columns. A summary of the numerical investigation is presented in Chapter 6 along with the significant findings of the research and suggestions for future work.

CHAPTER 2. LITERATURE REVIEW

2.1 Introduction

The need to construct civil engineering projects on weak soils has led geotechnical engineers and specialty contractors to develop cost-effective techniques for improving the strength, stiffness and permeability of compressible soils. Because they are economically viable and environmentally acceptable, vibrated stone columns are considered one of the best soil improvement alternatives (Vahedian et al. 2014). Typically, stone columns are used for increasing the bearing capacity and reducing the total and differential settlement of foundations supported on soft to medium stiff fine-grained soils. Other advantages of using stone columns include: acceleration of consolidation and permeability, reduction of liquefaction potential and stabilization of slopes (e.g., Vahedian et al. 2014; Zhang et al. 2013; Ambily et al. 2007; and Stuedlein and Holtz 2012).

This chapter contains general aspects of single and group of stone columns, followed by a summary of several methods that have been developed to estimate the bearing capacity of uncemented and cemented stone columns. A review of the numerical modeling conducted on stone columns using DEM is also presented in this section.

2.2 Stone column construction

Stone column-foundation systems are comprised either of a single column or a small group of columns. For a group of columns, the typical installation configurations are triangular, square or rectangular patterns, and the columns are distributed on the treated surface area using center-to-center column spacing ranging from 1.5 to 3 times the diameter of the column as illustrated in Fig. 2.1. Aggregate columns can be designed and installed to bear on a firm soil

layer (end-bearing columns), or as a floating system (frictional columns) where the load is transferred along the length of the column (Barksdale and Bachus 1983). The installation techniques used for placing, vibrating and compacting the granular material into the weak strata are widely known as wet-top feed method (vibro-replacement), and dry-bottom feed method (vibro-displacement). These stone column installation techniques are generally employed in soils with fines contents greater than 20% and undrained shear strengths typically greater than 15 kPa.

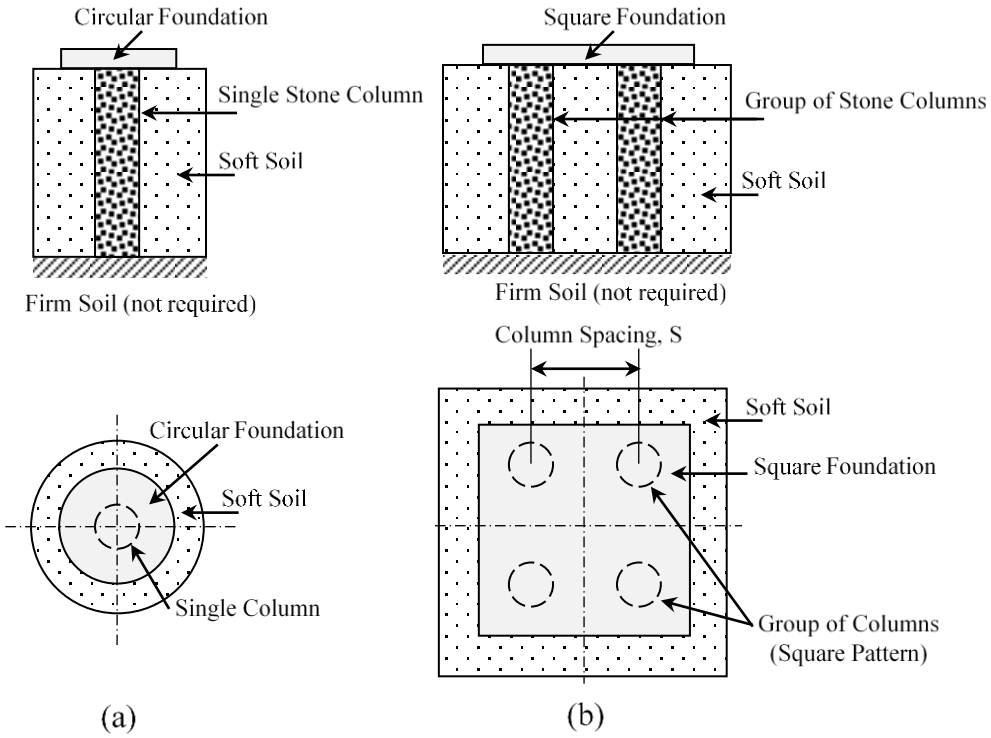

Fig. 2.1. Stone column-foundation systems. (a) single, isolated stone column and (b) small group of stone columns.

To begin the column installation process, the vibro-flot is positioned over the location where the aggregate column will be constructed, and it is lowered into the soil until the desired depth is reached. While the vibro-flot penetrates into the ground, its jets are opened expelling water or air to facilitate the drilling process. When water is used, the procedure is known as a wet

process. If air is employed, it is termed a dry process. Once the vibro-flot has reached the desired depth, the void created by displacing the in-situ soil is filled with granular material using either the top feed or bottom feed method. The wet-top feed method is typically used below the water table and has been effective in soft cohesive soil; however, its use has been significantly reduced because of the environmental regulations due to the water flush on the surface (Kelly 2014). In this system, the water circulating around the vibro-flot helps the borehole to remain open, while the aggregate is discharged from the top of the surface falling through the cylindrical space between the vibro-flot and the borehole wall. This method does not significantly disturb the native soil so that no marked change in the lateral effective stress occurs.

The dry-bottom feed method is the most predominantly used stone column installation technique today (McCabe et al. 2009). Advantages of the dry-bottom feed method include: more effective horizontal densification, no environmental issues related to water flush, no need for water supply, less aggregate waste, and better differential settlement performance. In addition, McCabe et al. (2009) reported that this method has been successfully used in very soft soil with undrained shear strength (s_u) as low as 5 kPa if the installation process is controlled and monitored automatically. Another advantage of the dry bottom feed method is that the vibro-flot does not have to be withdrawn during the installation procedure, which improves radial densification. In the dry-bottom feed procedure, the granular material is directly placed to the desired depth through a pipe that is attached to the vibro-flot edge and connected at its top to a hopper where the aggregate is initially deposited (Kelly 2014). Fig. 2.2 shows the procedures described for wet-top feed and dry-bottom feed methods. Regardless of the selected installation method, the aggregate is usually vibrated and compacted by the probe in lifts ranging from 1.0 ft to 4.0 ft depending on the slenderness ratios (column length over diameter, L_{sc}/D_{sc}). Common

values for the L_{sc}/D_{sc} ratio range from six to 10; however, values of up to 15 can be used depending on the thickness of the weak soil layer. It is important to highlight that the effects of the installation process on the performance of the stone columns analyzed in this study were not directly incorporated in the DEM simulations.

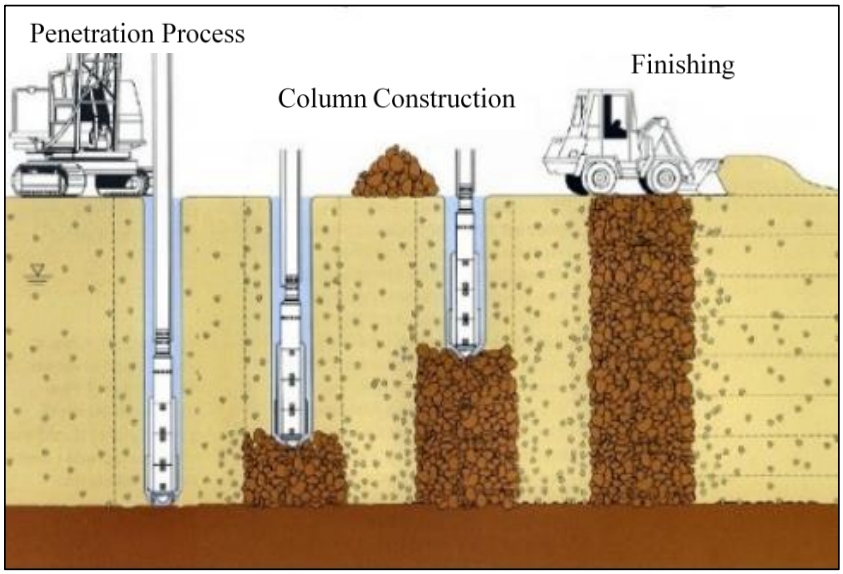

(a)

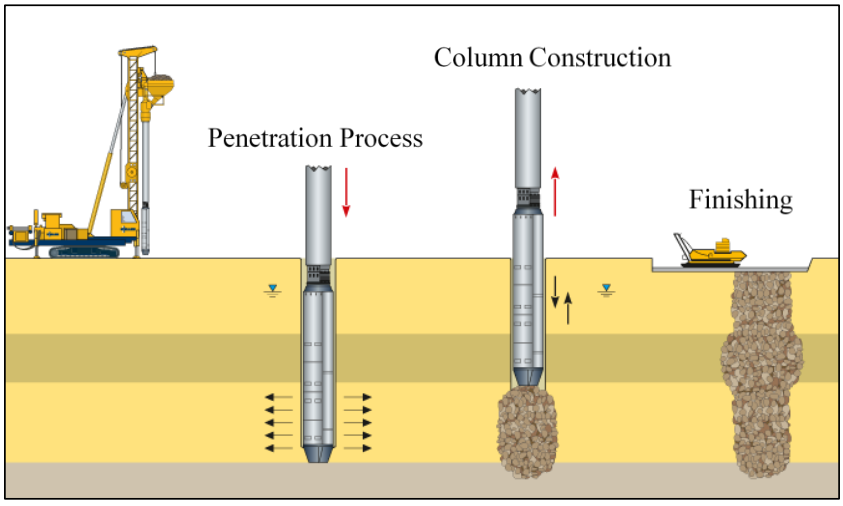

(b)

Fig. 2.2. Most common stone column installation methods. (a) dry-bottom feed method, and (b) wet-top feed method (after Raju and Sondermann 2005).

The direct costs associated with stone column construction include costs for aggregate material, installation equipment, labor, and mobilization (may be included separately). Other costs related with the installation control and quality assurance process (e.g., field testing and instrumentation) need to be added to the direct cost items. There are also other factors that can affect the costs of a specific stone column project such as project size and accessibility, weather and climate conditions, labor rates, availability of aggregate material, and soil conditions. The influence of these factors on the overall cost needs to be carefully identified and examined depending on the project characteristics. The direct costs for stone column construction are commonly measured in unit-prices per linear foot (LF) or square feet of column production. Typical unit-prices for aggregate column installation range from $15.00 to $60.00 per LF (Schaefer et al. 2017). Actual project costs from three state department of transportation (DOT) sources are summarized in Table 1.

Table 1. Examples of actual aggregate column projects *(*Data obtained from the second Strategic Highway Research Program SHRP2-R02).

Project Description	Quantity	Unit	Low unit- price	High unit-price	Average unit-price	Source
Stone columns (dry-bottom feed method)	6,467	LF	$39.62	$64.00	$53.62	New York DOT
Misc. stone columns	3,470	LF	$25.91	$27.43	$26.41	Missouri DOT
Stone columns	11,160	LF	$26.00	$40.00	$29.73	South Carolina DOT
	17,888	LF	$25.00	$34.00	$29.76	
	74,138	LF	$17.85	$19.36	$18.64	

2.3 Bearing capacity of single, isolated conventional stone columns

The behavior of vertically loaded aggregate column-foundation systems is not yet fully understood due to the complex interaction occurring between the surrounding soil, foundation and stone column, even though it has been extensively studied since the early '70s. Many methods ranging from simplified to complex have been developed to estimate the bearing capacity of single, isolated uncemented stone columns installed in soft clayey strata. These methods consist of analytical or semi-empirical methods (e.g., Greenwood 1970; Vesic 1972; Hughes et al. 1974, 1975; Stuedlein and Holtz 2013; and Bouassida and Frikha 2014), and empirical methods which are based on calibrations using field loading tests (e.g., Mitchell 1981; and Barksdale and Bachus 1983). These available methods are limited in their use and have not been satisfactory established and implemented in design codes, which has resulted in a lack of guidance for estimating the bearing capacity of single uncemented stone columns. The empirical and semi-empirical methods proposed by Mitchell (1981) and Hughes and Withers (1974), respectively, remain as the most useful approaches for estimating the bearing capacity of single stone columns and also widespread uncemented stone columns.

An initial methodology to estimate the ultimate bearing capacity of single stone columns (Eq.1) was proposed by Greenwood (1970) based on the classical plasticity theory assuming that plane-strain conditions at plastic equilibrium of the column aggregate are valid.

$$q_{\mathrm{ult}} = \sigma_1 = \sigma_3 \cdot K_p = \sigma_3 \cdot \frac{(1 + \sin \phi_{\mathrm{sc}})}{(1 - \sin \phi_{\mathrm{sc}})} \tag{1}$$

where K_p is the coefficient of passive earth pressure, ϕ_{sc} is the internal friction angle of the column aggregate, σ_3 is the confining pressure, and q_{ult} is the ultimate effective bearing pressure.

Hughes et al. (1974) conducted small-scale laboratory experiments to investigate the behavior of single stone columns. In this particular study, it was found that the failure mechanism of a single, isolated, uncemented aggregate column is primarily controlled by the horizontal confinement or reaction that the native soil can provide at the top part of the column known as the bulging zone. This lateral confinement is governed by the undrained shear strength of the surrounding soil. Based on the conditions of their experimental study, the authors reported that when the column L_{sc}/D_{sc} ratio is greater than four, bulging is the predominant failure mechanism controlling the global behavior of single, isolated uncemented stone columns.

Utilizing the cavity expansion elasto-plastic theory developed by Gibson and Anderson (1961) and considering undrained conditions, Hughes and Withers (1974) presented Eq. (2) to determine the ultimate lateral pressure developed by the surrounding soil as the column bulges

$$\sigma_{3ult} = \left[\sigma_{ro} + \left\{1 + \ln\left(\frac{E_c}{2 \cdot s_u \cdot (1+\nu)}\right)\right\} \cdot s_u \right] \quad (2)$$

where σ_{3ult} is the ultimate undrained confining pressure, σ_{ro} is the initial total horizontal stress, E_c is the modulus of elasticity of the surrounding soil, s_u is the undrained shear strength of the lateral soil at the bulging zone, and ν is the native soil Poisson's ratio. Based on experimental data obtained from field testing, Hughes et al. (1975) suggested that Eq. (3) can be simplified to:

$$\sigma_{3ult} = \sigma'_{3ult} = [\sigma'_{ro} + 4 \cdot s_u] \quad (3)$$

Assuming critical state conditions for the aggregate within the bulging zone, Hughes et al. (1975) recommended that the ultimate effective bearing pressure that can be applied on a single aggregate column can be computed by using Eq. (4):

$$q_{\mathrm{ult}} = \sigma'_{1\mathrm{ult}} = \sigma'_{3\mathrm{ult}} \cdot K_p = [\sigma'_{\mathrm{ro}} + 4 \cdot s_u] \cdot \frac{(1 + \sin \phi_{\mathrm{sc}})}{(1 - \sin \phi_{\mathrm{sc}})} \quad (4)$$

where K_p is the coefficient of passive earth pressure generated by the stone column, and ϕ_{sc} is the internal friction angle of the column aggregate. This equation remains as the one of the most useful for estimating the bearing capacity of single, isolated uncemented stone columns.

Vesic (1972) proposed that the ultimate lateral confining pressure could be estimated based on an elasto-plastic cylindrical cavity expansion solution considering the internal friction angle and cohesion of the surrounding soil and defined as:

$$\sigma_3 = c \cdot \mathrm{F'_c} + q \cdot \mathrm{F'_q} \quad (5)$$

where c is the matrix soil cohesion, q is the isotropic mean stress at the corresponding failure depth [q=(σ_1+σ_2+σ_3/3)], and F'$_c$ and F'$_q$ are known as the cavity expansion factors. These factors depend on the friction angle of surrounding soil (ϕ_c), the rigidity index (I_r) and the average volumetric strain (δ) and are defined as:

$$\mathrm{F'_c} = (\mathrm{F'_q} - 1) \cdot \cot \phi_{\mathrm{c}} \quad (6)$$

$$\mathrm{F'_q} = (1 + \sin \phi_{\mathrm{c}}) \cdot \left[\left(\frac{\mathrm{I_r}}{1 + \mathrm{I_r} \cdot \delta \cdot \sec \phi_{\mathrm{c}}}\right) \cdot \sec \phi_{\mathrm{c}}\right]^{\frac{\sin \phi_{\mathrm{c}}}{1+\sin \phi_{\mathrm{c}}}} \quad (7)$$

$$I_r = \frac{E_c}{2 \cdot (1 + \nu) \cdot (c + q \cdot \tan \phi_c)} \quad (8)$$

For undrained conditions (ϕ_c=0) and ignoring any reduction in the rigidity index during plastic deformation, Eq. (5) provides identical results to Eq. (2). The ultimate effective bearing pressure that can be applied on the column can be estimated by Eq. (9) using the same principle of failure mode previously mentioned for Eq. (4).

$$q_{ult} = \sigma_1 = \sigma_3 \cdot K_p = \left[c \cdot F'_c + q \cdot F'_q\right] \cdot \frac{(1 + \sin \phi_{sc})}{(1 - \sin \phi_{sc})} \quad (9)$$

Based on both field data and the semi-empirical method proposed by Hughes et al. (1974), Mitchell (1981) recommended that the bearing capacity of a single, isolated aggregate column under undrained soil conditions be estimated as:

$$q_{ult} = Nc_{sc} \cdot s_u \quad (10)$$

where Nc_{sc} is the bearing capacity factor for the stone column (a value of 25 was suggested by Mitchell 1981), and s_u is the representative undrained shear strength of the surrounding soil within the bulging depth.

In 1983, Barksdale and Bachus presented a very useful two-volume manual that summarized the main concepts and recommendations for designing and constructing stone columns. Fig. 2.3 illustrates the three different failure mechanisms for a single stone column fully embedded in a homogeneous weak layer presented by Barksdale et al. (1983). For these

three failure modes, the column is only loaded over the surface of its cross section, which could be a representation of a plate loading test scenario. The authors mentioned that regardless of the tip column condition (end bearing or free floating) stone columns with slenderness ratios greater than 3 fail in bulging as shown Fig. 2.3(a). However, when the L_{sc}/D_{sc} ratio is less than three, and the tip column condition is rigid, short columns fail in general or global shear at the surface as illustrated in Fig. 2.3(b). On the other hand, for short-floating columns, either punching or shear failure could occur as presented in Fig. 2.3(c). For estimating the bearing capacity of a single aggregate column which fails in bulging, Barksdale et al. (1983) recommended using the Mitchell (1981) method with Nc_{sc} values ranging from 18 to 22. These values are suggested based on back calculations from plate loading tests considering the stiffness of the surrounding soil (i.e., matrix soil). A value for Nc_{sc} of 18 is recommended when the matrix soil has low stiffness, whereas a value of 22 is suggested for soils with relative high stiffness. Barksdale et al. (1983) also proposed that the elasticity modulus in the equation proposed by Hughes et al. (1974) could be calculated as $11s_u$. However, Stuedlein et al. (2013) pointed out that this value produces estimations that are too conservative for bearing capacity.

In 2013, Stuedlein and Holtz conducted a statistical evaluation of the existing methods for estimating the bearing capacity of spread foundations placed on a clayey soil reinforced with aggregate columns. Stuedlein et al. (2013) reported that there is a notable variation in the performance of the existing methods (previously described) for estimating the bearing capacity of single uncemented stone columns with respect to the responses obtained from the full-scale experimental program conducted by Stuedlein (2008). Therefore, in order to advance these current available approaches, Stuedlein and Holtz (2013) empirically adapted the Mitchell (1981) method and the semi-empirical method proposed by Hughes et al. (1975) based on the field

database presented by Stuedlein (2008). Using back calculations, the bearing capacity factor of the stone column (Nc_{sc}) and the ultimate lateral pressure (σ_{3ult}) were defined as functions of the undrained shear strength as presented in Eq. (11) and Eq. (12).

$$Nc_{sc} = \exp(-0.0096 \cdot s_u + 3.5) \tag{11}$$

$$\sigma_{3ult} = [\sigma_{ro} + \{8.52 - 1.45 \cdot \ln(s_u)\} \cdot s_u] \tag{12}$$

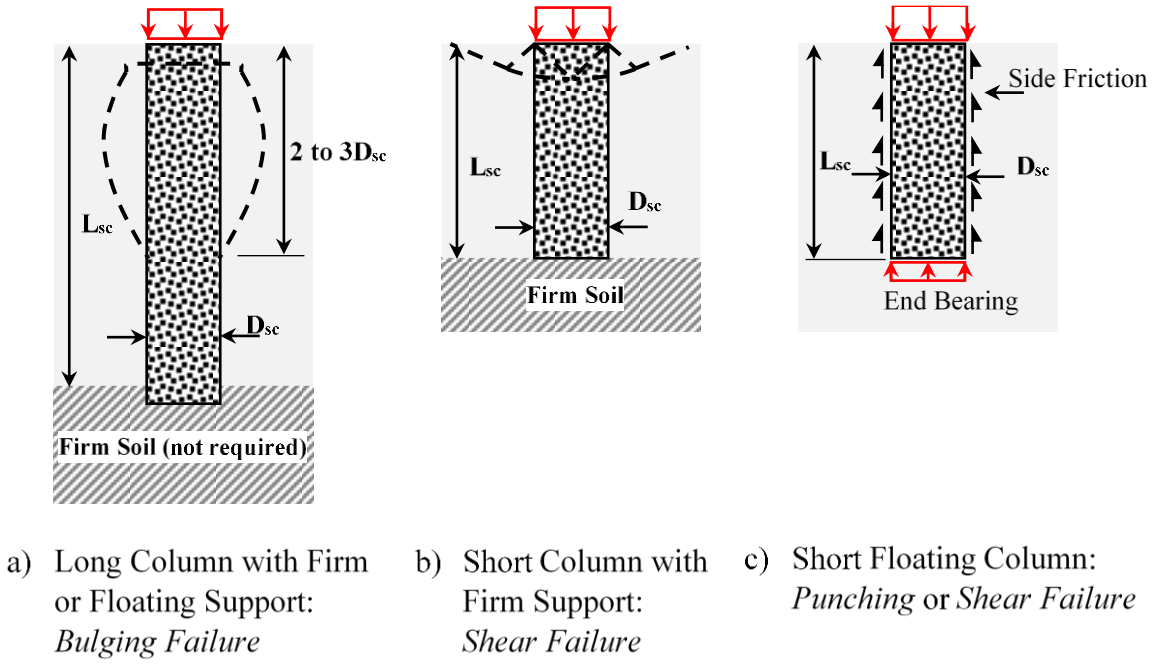

a) Long Column with Firm or Floating Support: *Bulging Failure*

b) Short Column with Firm Support: *Shear Failure*

c) Short Floating Column: *Punching* or *Shear Failure*

Fig. 2.3. Failure mechanisms of a single, isolated stone column in a homogeneous soft layer (modified from Barksdale and Bachus 1983).

Eqs. (13) and (14) were proposed by Stuedlein et al. (2013) to determine the bearing capacity of a single stone column installed in a clayey soil including the modifications made to the Mitchell (1981) and Hughes et al. (1975) methods, respectively.

$$q_{\mathrm{ult}} = \mathrm{Nc}_{\mathrm{sc}} \cdot s_u \cdot A_r + \lambda_{\mathrm{c}} \cdot \mathrm{d}_{\mathrm{c}} \cdot \mathrm{N}_{\mathrm{c}} \cdot s_u \cdot (1 - A_r) \quad (13)$$

$$q_{\mathrm{ult}} = [\sigma_{\mathrm{ro}} + \{8.52 - 1.45 \cdot \ln(s_u)\} \cdot s_u] \frac{(1 + \sin \phi_{\mathrm{sc}})}{(1 - \sin \phi_{\mathrm{sc}})} + \lambda_{\mathrm{c}} \cdot \mathrm{d}_{\mathrm{c}} \cdot \mathrm{N}_{\mathrm{c}} \cdot s_u \cdot (1 - A_r) \quad (14)$$

In these equations A_r represents the area replacement ratio, which is defined as fraction of the total tributary loaded area substituted by the stone column within the unit-cell. λ_c, and d_c are the shape and embedment correction factors for circular, square or rectangular foundations, and N_c is the bearing capacity factor based on the Meyerhof (1965) method (taken as $2+\pi$ for $\phi_c=0$).

Fig. 2.4 and Table 2 present the results of the statistical evaluation of the existing (e.g., Eq.1, 4, 9 and 10) and modified (e.g., Eq.13 and 14) bearing capacity methods for single stone columns. The performance of existing methods showed a widespread level of bearing capacity estimation variability, with bias (i.e., the ratio of observed to estimated bearing capacity) of the methods (previously described) ranging from 0.76 (Hughes et al. 1975) to 2.49 (Greenwood 1970), with a range in COVs in bias from 22 to 30%, respectively (Stuedlein et al. 2013). This variability in the results generates a lack of confidence in these existing methods and may lead stone column designers to select unsuitable factors of safety for bearing capacity of single stone columns. Even though the equations proposed by Stuedlein et al. (2013) include more variables that could likely result in a more accurate estimation of the bearing capacity of a single, isolated aggregate column, their use is restricted to field project conditions within the range of the field database (e.g., geometry, material properties) used to calibrate these modified equations (Stuedlein et al. 2013).

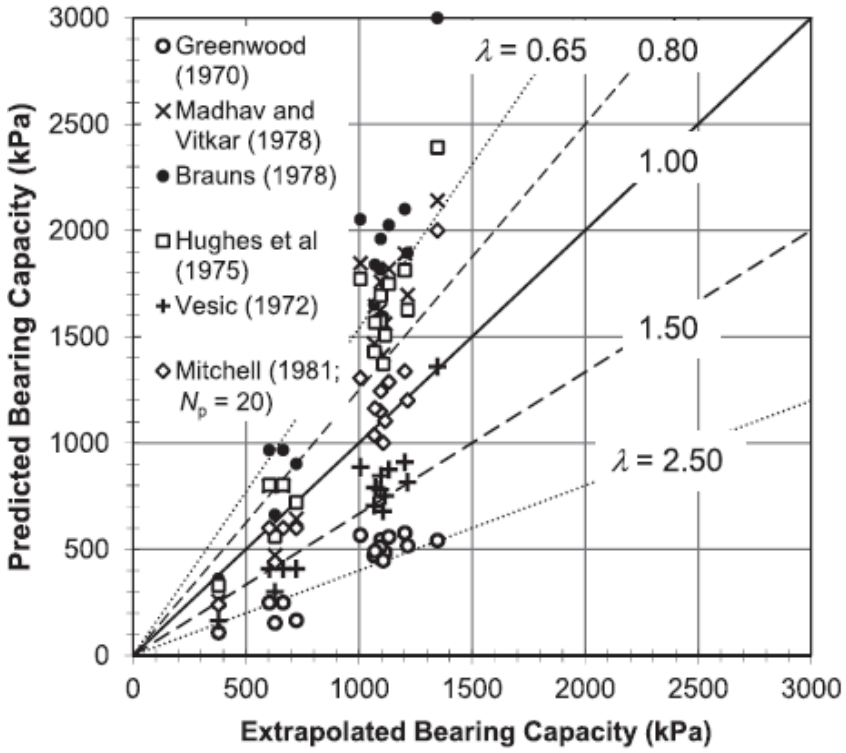

Fig. 2.4. Comparison of estimated ultimate bearing capacity to that estimated using existing methods for single stone columns (after Stuedlein et al. 2013).

In 2014, based on the existing cavity expansion theory, Bouassida and Frikha (2014) proposed Eq. (17) to determine the ultimate bearing pressure that can be applied on a single stone column installed in a weak cohesive soil. This equation was calibrated with a field database obtained from 25 plate loading tests performed on single, isolated aggregate columns, and it considers the effect of the angle of dilatancy of the column aggregate on the bearing pressure capacity of the column.

$$k = \frac{(1 - \sin \psi)}{(1 + \sin \psi)} \tag{15}$$

$$\alpha = -0.1812 \cdot \mathrm{k} + 0.1408 \tag{16}$$

$$q_{\mathrm{ult}} = \left[\sigma_{\mathrm{ro}} + \left\{1 + \frac{2}{1+\mathrm{k}} \cdot \ln\left(\frac{\mathrm{E_c}}{3 \cdot (\alpha)^{\mathrm{k}-1} \cdot s_u}\right)\right\} \cdot s_u\right] \frac{(1+\sin\phi_{\mathrm{sc}})}{(1-\sin\phi_{\mathrm{sc}})} \tag{17}$$

where ψ is the dilation angle of the column aggregate, and α and k are calibrated parameters established by Bouassida et al. (2014). The rest of the variables have been previously defined.

Table 2. Comparison of statistical results of existing and modified bearing capacity models (Table from Stuedlein et al. 2013).

Method	Bias, l		Mean absolute error
	Mean	COV (%)	[kPa]
Greenwood (1970)	2.49	29.7	533
Vesic (1972)	1.48	25.9	231
Hughes et al. (1975)	0.76	22.2	234
Mitchell (1981), Nc_{sc}=15	0.76	24.2	197
Mitchell (1981), Nc_{sc}=20	1.01	24.2	76
Mitchell (1981), Nc_{sc}=25	1.27	24.2	228
Modified Hughes et al. (1975)	1.01	9.5	40
Modified Mitchell (1981)	1.01	6.5	37

2.4 Bearing capacity of single, isolated cemented stone columns

In a column-foundation system, the column and its surrounding soil act as a composite system, where the stiffer aggregate column carries a higher percentage of the applied bearing pressure compared to the native adjacent soil (Barksdale et al. 1983). Larger modular ratios between the column and the native soil result in higher stress concentrations in the column, reducing the overall settlement of the system. Therefore, the stiffness of the aggregate column plays an important role in the bearing pressure-displacement response (q-δ) of a single, isolated stone column. When the aggregate column stiffness is not enough to meet the serviceability limit state design requirements for a specific project, the applicability of conventional stone columns as a soil improvement alternative is restricted unless techniques to reinforce the columns are implemented. For very poor strata (e.g., peat, organic material, and sensitive silts and clays for which strength may be reduced by the column installation procedure), the implementation of conventional stone columns is also questionable because of the early formation of bulging failures resulting from insufficient lateral support from the native soil (Barksdale et al. 1983). Several techniques have been developed to increase the effectiveness of conventional stone columns by providing extra lateral support or confinement to the column, enhancing the column granular material stiffness and strength, or combining these two options. Two examples of these techniques are: geotextile-encased stone columns and cemented stone columns (Golait and Padade 2016). Golait et al. (2016) reported that the construction of cemented aggregate columns does not result in significant additional cost or construction difficulties when compared to the use of regular uncemented granular material. As such, they have the advantage of being much easier to implement, and thus, are the focus of this study.

Cemented aggregate columns are less dependent on the lateral confinement provided by the surrounding soil and can provide stiffer q-δ responses in very weak soil deposits and disturbed soil zones when compared to uncemented aggregate columns (Barksdale et al. 1983; Stuedlein 2008, Golait et al. 2016). Typically, only a small percentage (between 3 to 5% by aggregate weight) of a binder (e.g., cement, fly ash, lime) is mixed with the conventional aggregate to produce a lightly-cemented granular mixture. An increase in the aggregate stiffness and strength is expected to be developed as a result of the cement-aggregate bonds generated at the particle contact areas as illustrated in Fig. 2.5(a). As the percentage of cement used in the mixture increases, the stiffness of the cemented granular material also increases so that it tends to behave more as a semi-rigid or rigid porous material (Fig. 2.5b). Therefore, the q-δ response of a single cemented stone column would be more similar to that of a conventional vertically loaded pile (Golait et al. 2016). While cemented columns offer a more cost-effective alternative for soil improvement, very little information regarding their design or performance has been found in the literature. A direct relationship between cement content and resulting stone column behavior has not been established to aid designers in estimating the bearing capacity of cemented columns.

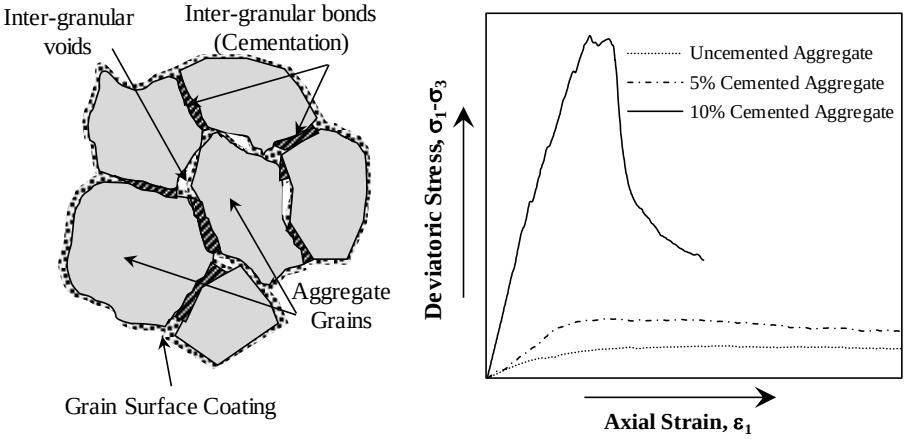

Fig. 2.5. (a) Schematic of cemented aggregate material, and (b) variation of stress-axial strain response of cemented aggregate as a function of cement content.

Golait and Padade (2016) conducted an analytical study of a single, isolated cemented stone column conceptualizing the load transfer mechanism of the column as an idealization of an axially loaded pile. The total cemented column-foundation system resistance (Q_f) is computed as the summation of the foundation bearing capacity contribution (R_s), the column side friction (R_f) and end bearing resistance (R_t) as expressed in Eq. (18) and illustrated in Fig. 2.6.

$$Q_f = R_s + R_f + R_t \tag{18}$$

The bearing resistance beneath the rigid circular foundation (Eq. 19) is computed assuming a local shear failure mode acting within a depth equal to the foundation diameter (*B*). The shaft resistance (Eq. 20) and the tip resistance (Eq. 21) are calculated as the following based on the assumption that there is enough relative displacement generated between the column and the surrounding soil to fully develop both shaft and toe resistances:

$$R_s = 4.04 s_u \times (A - A_{sc}) \tag{19}$$

$$R_f = (\pi \times \alpha \times D_{sc} \times L_{sc}) s_u \tag{20}$$

$$R_t = \left[10.35 - 0.45\left(\frac{L_{sc}}{D_{sc}}\right)\right] A_{sc} \times s_u \tag{21}$$

where A and A_{sc} are the circular foundation and column cross section areas, respectively, s_u is the undrained shear strength of the surrounding clayey soil, α is the adhesion factor, which is assumed as 0.95 for clayey soils with s_u values less than 25 kPa, and L_{sc} is the column length,

which shall be less than 23 times the diameter of the column (D_{sc}). The bearing capacity of a cemented column-foundation system can be estimated using Eq. (22).

$$q_{ult} = \left[\{4.04 \times (1 - A_r)\} + \left\{4 \times \alpha \times A_r \times \frac{L_{sc}}{D_{sc}}\right\} + \left\{10.35 - 0.45\left(\frac{L_{sc}}{D_{sc}}\right)\right\} A_r\right] s_u \qquad (22)$$

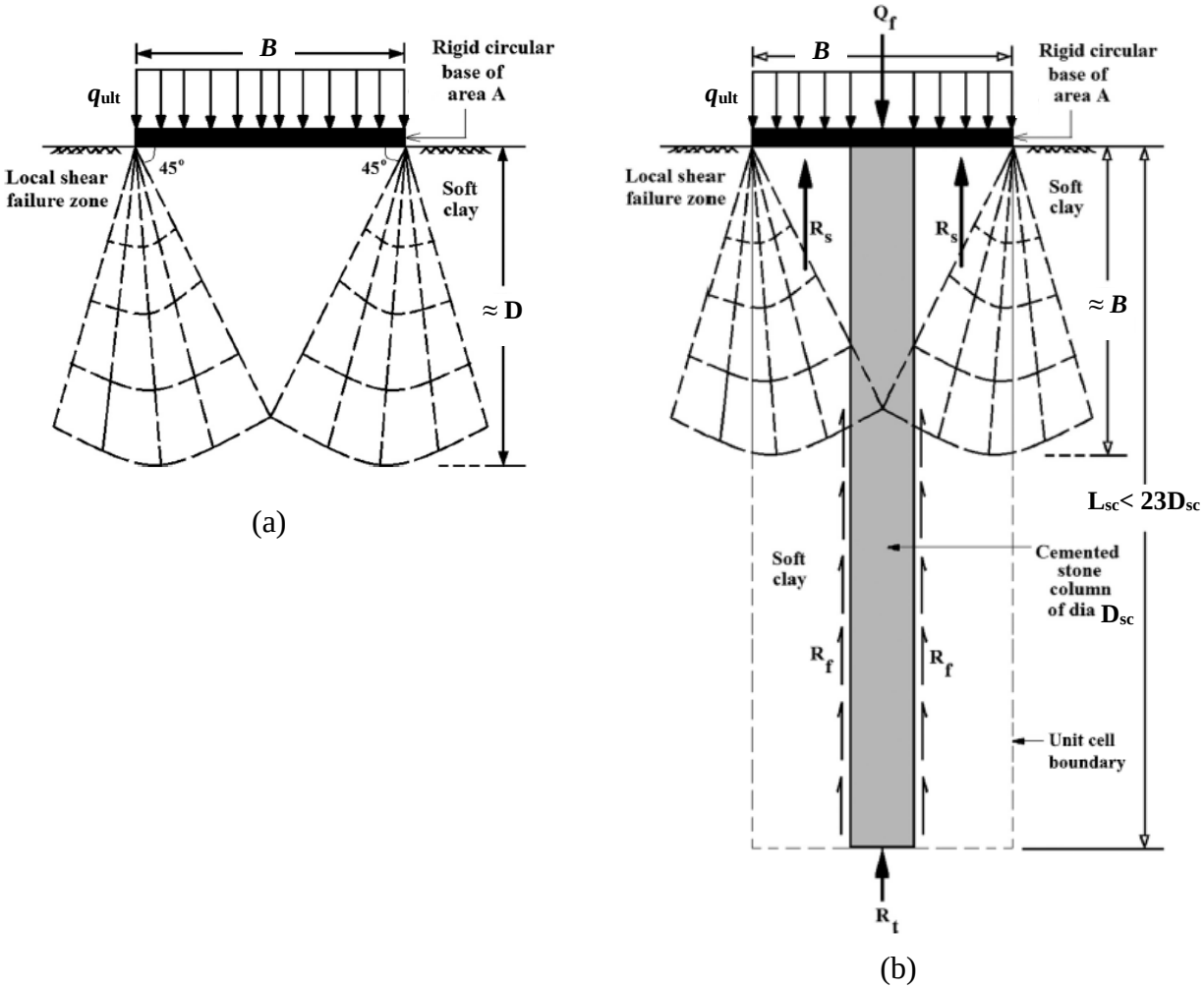

Fig. 2.6. Failure mechanism of a single cemented stone column. (a) untreated soft clay failure mode, and (b) single cemented stone column failure mode (after Golait and Padade 2016).

Golait and Padade (2016) validated their proposed analytical solution for estimating the bearing capacity of cemented stone columns by conducting scaled laboratory experiments. The authors reported excellent agreement between the analytical and the experimental results, with percentage error less than 10%. Additionally, a significant increase in the effectiveness of the cemented stone columns tested was observed when compared to not only the conventional stone columns, but also to other techniques for reinforcing stone columns. For example, for a L_{sc}/D_{sc} ratio of 10, Golait and Padade (2016) reported bearing capacity improvement factors (F_b) ranging from 2 to 4 for area replacement ratios varying from 0.10 to 0.30, respectively. This analytical and experimental research is one of the few studies conducted on cemented granular columns, making it a useful contribution; however, there are several limitations. First, its validation is based on small-scale representations of cemented stone columns, and its application is restricted for soft soils with s_u less than 25 kPa. There is no guidance for stone columns installed in medium stiff cohesive soils with s_u values ranging from 30 kPa to 45 kPa. Furthermore, all the laboratory tests were conducted for long-cemented stone columns with L_{sc}/D_{sc} ratios greater than 10. The authors reported that F_b linearly increases as the L_{sc}/D_{sc} ratio varies from 10 to 20. This implies that for short columns, F_b decreases; however, no bearing capacity improvement factors were reported for columns with slenderness ratios less than 10, which results in a gap in the knowledge, making it unclear how effective relative short-cemented stone columns may be.

Based on results obtained from full-scale load tests conducted on small foundations supported on single, isolated cemented stone columns with L_{sc}/D_{sc} ratios of six, Stuedlein (2008) reported bearing pressure improvement factors ranging from 2.5 to 3.2 compared to conventional stone columns. More details of the experimental programs conducted by Stuedlein (2008) and Golait et al. (2016) are presented and discussed in the next chapter.

2.5 Bearing capacity of uncemented stone column groups

The behavior of grouped uncemented stone columns is more complex and not well understood compared to the behavior of single, isolated uncemented aggregate columns. Difficulties emerge with the load transfer and interaction between the columns and the surrounding soil, as well as the nonlinear stress-strain responses of the elements comprising the column-foundation system. The bearing capacity of a large group of stone columns is typically computed as the summation of the capacities of the single columns in the group (Zhang et al. 2013). The capacity of a representative single stone column within the group is calculated based on the assumption of bulging failure mechanism (softer cohesive soils with $s_{u,}$ ranging from 20 kPa to 30 kPa) and the implementation of the unit-cell concept (widespread loading conditions). Then, this individual-representative capacity is multiplied by the total number of columns forming the group to obtain the total bearing capacity of the group. In a unit-cell model, the domain is represented by a cylindrical cell of an equivalent diameter (D_e), with no lateral movement and shear stress transfer on the cell boundaries as illustrated in Fig. 2.7. The equivalent unit-cell diameter is computed based on the stone column installation configuration, and center to center spacing between columns (S). For a square pattern, D_e is calculated as 1.05 S, whereas it is estimated as 1.13 S for an equilateral triangular pattern (Barksdale and Bachus 1983). As previously discussed, the average stress in the granular column is higher compared to the native surrounding soil within a unit-cell model because of its higher stiffness. Therefore, the relationship between the average stress in the column (σ_{sc}) and soil (σ_s) can be expressed in terms of a stress concentration factor (n) as presented in Eq. (23).

$$n = \frac{\sigma_{sc}}{\sigma_s} \tag{23}$$

Assuming that the applicability of the unit-cell is valid and static equilibrium is satisfied, the total average stress acting in the unit cell (Eq. 24), stone column (Eq. 25), and adjacent soil (Eq. 26), respectively, as a result of the applied bearing pressure at a given depth can be expressed as:

$$\sigma_{\text{avg}} = \sigma_{sc} \times A_r + \sigma_s \times (1 - A_r) \tag{24}$$

$$\sigma_{\text{sc}} = \left[\frac{n}{1 + (n-1) \times A_r}\right] \times \sigma_{\text{avg}} = \mu_{sc} \times \sigma_{\text{avg}} \tag{25}$$

$$\sigma_s = \left[\frac{1}{1 + (n-1) \times A_r}\right] \times \sigma_{\textbf{avg}} = \mu_c \times \sigma_{\text{avg}} \tag{26}$$

where σ_{avg} is the total average stress acting over the unit-cell tributary area, A_r is the area replacement ratio within the unit-cell, and μ_{sc} and μ_c are the ratio of stresses in the granular column and adjacent soil to σ_{avg}, respectively.

The methods developed using the unit-cell concept (Priebe 1976; Goughnour and Bayuk 1979a; Balaam and Booker 1981; Barksdale and Bachus 1983; Poorooshasb and Meyerhof 1997; Hughes et al. 1975) do not consider the effect of the column-group interaction, which is an important parameter for the design of isolated foundations supported on small stone column groups (Hanna et al. 2013). These methods are typically used due to their simplicity and acceptable estimations of the bearing capacity of widespread-large stone column groups.

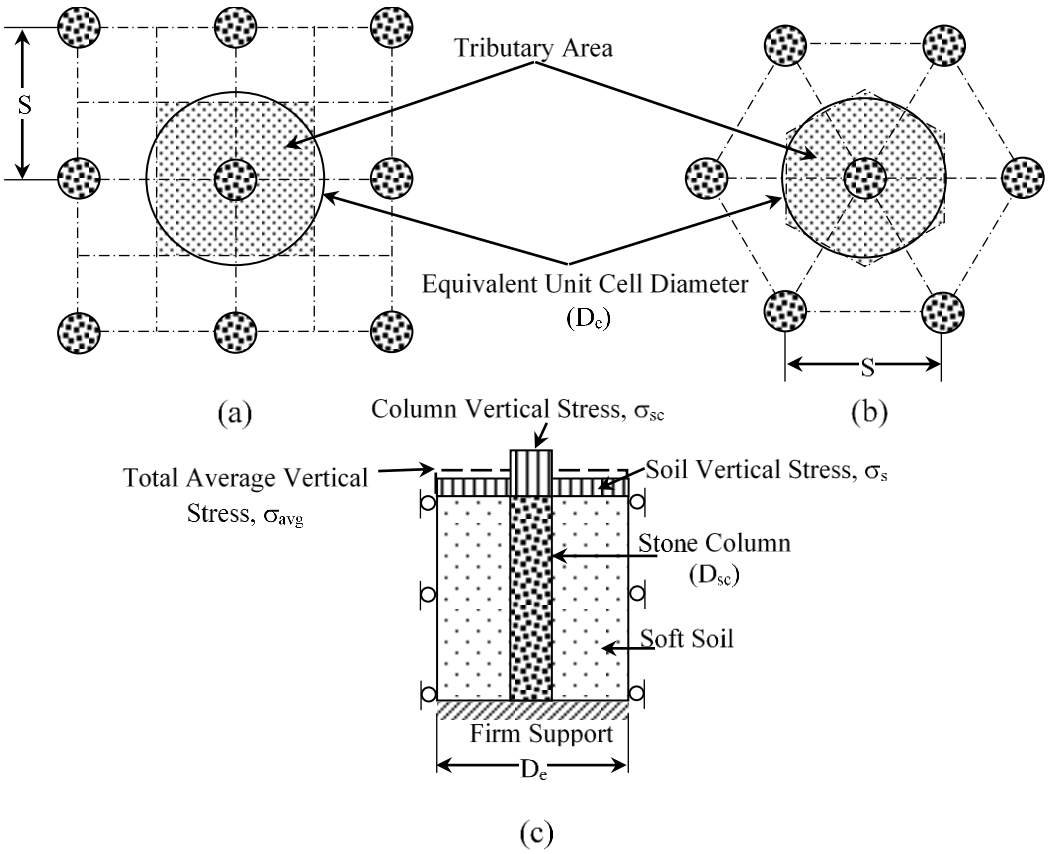

Fig. 2.7. Idealization of unit-cell concept for group stone columns. (a) square pattern, (b) triangular pattern, and (c) unit-cell model and boundary conditions (modified from Barksdale and Bachus, 1983).

For rigid foundations supported on small stone column groups, the relative position of an aggregate column with respect to the adjacent columns and foundation center seems to govern the behavior of the column within the group. The columns located along the edges of the foundation are not restricted to laterally expand into the in-situ soft soil likely exhibiting a bulging failure mode analogous to single, isolated aggregate columns. The columns located closer to the center of the foundation are presumably subjected to higher confining pressures and stress ratios that likely generate diagonal shear failure modes (Stuedlein, 2008). This has been investigated through laboratory experimental studies that have revealed that the failure mechanism of a small stone column group-foundation system is mostly controlled by a conical

shape of general shear failure instead of bulging of the individual columns as shown in Fig. 2.8 (Hu et al. 1997, Wehr 1999, and Wood et al. 2000). Based on a numerical investigation, Hanna et al. (2013) also observed that for area replacement ratios (A_r) greater than 10%, the analyzed stone column group-foundation systems failed in shear failure modes (global, local or punching) rather than individual column bulging failure. These authors reported that small aggregate column groups with high A_r values failed in a global shear failure mode, whereas for low A_r values, local or punching shear failure was observed.

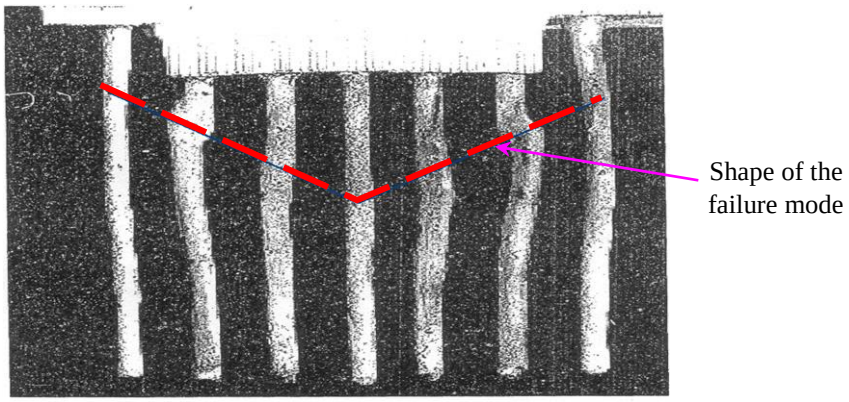

Fig. 2.8. Global shear failure mode of the small-scale stone column group investigated by Wood et al. (2000).

Barksdale and Bachus (1983) provided guidance for estimating the ultimate bearing capacity (q_{ult}) of foundations supported on stone column groups based on the soil strength. For softer soils (e.g. s_u less than 30 kPa), Barksdale et al. (1983) recommended estimating q_{ult} for wide-spread column scenarios using the empirical method proposed by Mitchell (1981). For firm cohesive soils (e.g. s_u greater than 30 kPa) where no local bulging failure mechanism of single columns within the group is expected to develop, Barksdale et al. (1983) suggested using average strength parameters of the composite soil-column system to approximately estimate q_{ult} of a

square-rigid foundation resting on a small stone column group. The ultimate bearing resistance beneath the rigid-square foundation, q_{ult}, is computed using Eq. 30 assuming a global wedge shear failure mode acting within a depth equal to the foundation width (B) times the angle β forming the failure plane with the foundation as illustrated in Fig. 2.9.

$$\beta = 45° + \frac{\phi_{\text{avg}}}{2} \tag{27}$$

$$\phi_{\text{avg}} = \tan^{-1}(\mu_{sc} \times A_r \times \tan \phi_{sc}) \tag{28}$$

$$s_{u_{\text{avg}}} = (1 - A_r) \times s_u \tag{29}$$

$$q_{ult} = \sigma_3 \times \tan^2(\beta) + 2 \times s_{u_{\text{avg}}} \times \tan(\beta) \tag{30}$$

where ϕ_{avg} and $s_{u_{\text{avg}}}$ are the average strength parameters of the stone column reinforced cohesive soil acting along the failure plane beneath the rigid foundation, ϕ_{avg} is the shear contribution due to the aggregate column friction angle (ϕ_{sc}), $s_{u_{\text{avg}}}$ is the average undrained shear resistance of the in-situ cohesive soil, and σ_3 is the average ultimate lateral pressure provided on the failure wedge by the native soil. For square foundations, Barksdale and Bachus (1983) recommended estimating σ_3 using the Vesic cavity expansion theory for cylinders discussed above. It is noted that no full-scale numerical simulations validating this approach and comparing the differences in the bearing pressure-displacement responses of external and

internal columns within a small stone column group using a unit-cell model were found in the literature.

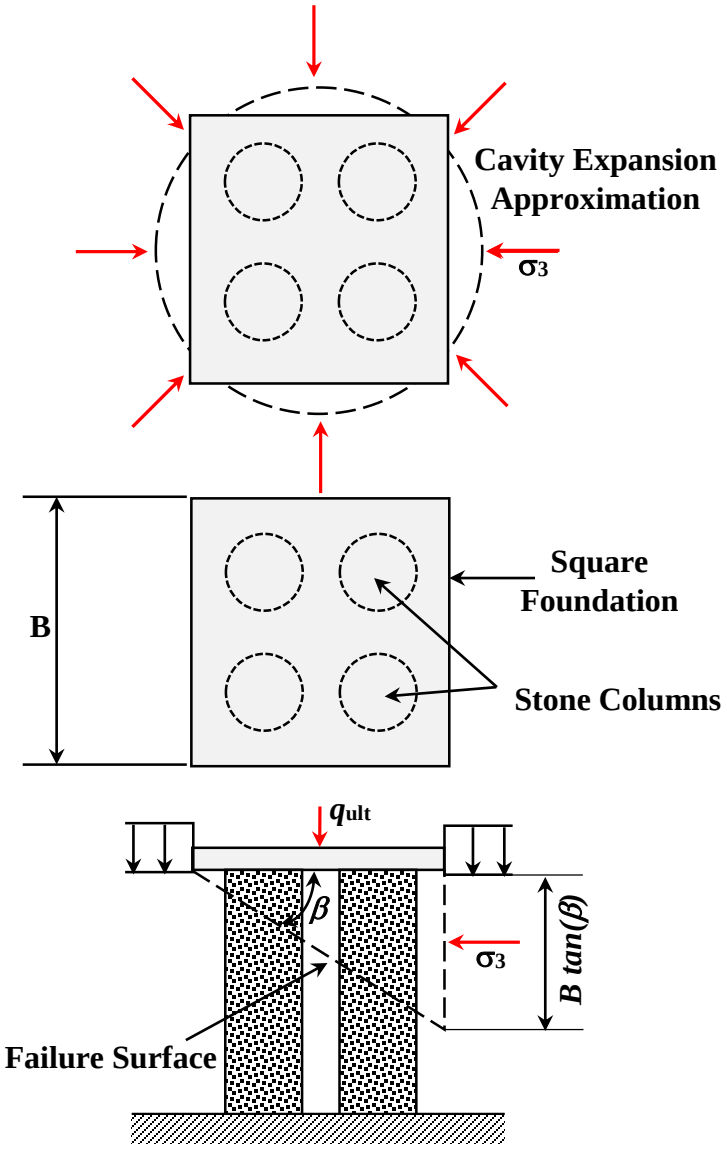

Fig. 2.9. Square foundation on stone column group analysis (modified from Barksdale and Bachus 1983).

2.6 Numerical modeling of stone columns

Many continuous numerical models have been developed to investigate the behavior of stone columns (e.g., Balaam et al. 1977, Poorooshasb and Meyerhof 1997, Han and Ye 2001, Elshazly et al. 2008, Ambily and Gandhi 2007, McCabe et al. 2009, and Hanna et al. 2013). The first finite element method (FEM) model used to analyze stone columns was conducted by Balaam et al. (1977). The authors treated the model domain considering the unit-cell idealization and reported a significant effect of the column stiffness on the bearing-pressure response of their model. A more recent FEM study of single and group stone columns was conducted by Ambily and Gandhi (2007). These authors reported that the most critical parameters affecting the stone column design are the aggregate column stiffness and applied load distribution within the surrounding soil and the column. It was also reported that the unit-cell framework provides a good representation of the behavior of an internal column within a group if the adjacent columns are simultaneously loaded. Hanna et al. (2013) also conducted a FEM investigation to identify the failure modes and estimate the bearing capacities of a raft supported on a single stone column and a group of stone columns. The numerical results showed that as the aggregate friction angle and modulus ratio between the column and the native soil increase, there is substantial improvement in the capacity of the stone column-foundation system. Even though numerical continuum approaches have been used extensively to simulate conventional granular columns (e.g., Balaam et al. 1977, Mitchell and Huber 1985, Ambily and Gandhi 2007, Hanna et al. 2013, McCabe et al. 2016, Ammari et al. 2018), similar approaches have not been used to examine cemented stone columns.

The column shearing resistance and stiffness depend on aggregate features such as particle shape, gradation, and aggregate-matrix soil interaction. The previously mentioned

analytical, empirical and numerical approaches have significantly contributed to the macroscopic understanding of the global behavior of stone columns. However, the use of these continuous approaches to simulate stone columns might be less suitable because they cannot properly capture the internal interaction occurring between the aggregate particles comprising a stone column (Ngo et al. 2016). Therefore, it is beneficial to use a numerical tool capable of providing a better representation of this aggregate particle interaction. This can be attained by using the discrete element method (DEM), which is a numerical approach used to simulate the behavior of discontinuous media (e.g., granular material).

Several numerical investigations using DEM have examined different factors affecting the performance of stone columns (e.g., Indraratna et al. 2015, Siahaan et al. 2015, Tan and Chen 2018). Indraratna et al. (2015) analyzed the bearing pressure-displacement response of a small-scale single stone column using a coupled numerical model. This model employed DEM to simulate the behavior of the aggregate column, whereas the surrounding soft clay was modeled using continuous finite difference method (FDM), as illustrated in Fig. 2.10. Even though the results of this coupled model were in good agreement with the experimental data, the use of monitored nodes for coupling the DEM-FDM model makes this numerical framework difficult to implement. Additionally, this study used a 2D analysis which requires a conversion from an axisymmetric domain to an equivalent plane strain model. Another limitation of this numerical approach is that the granular material was modeled using circular particles instead of more realistic crushed aggregate shapes, which could be improved to obtain better representation of the aggregate behavior.

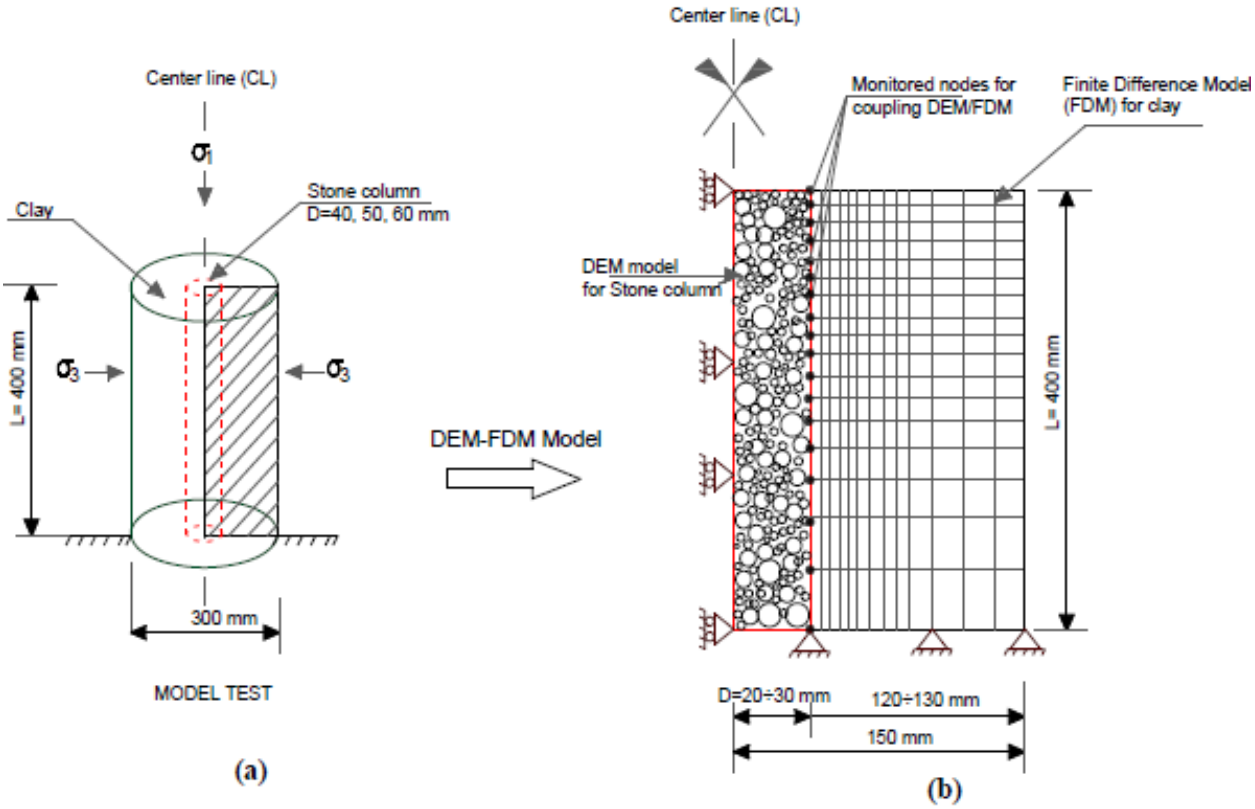

Fig. 2.10. Coupled DEM-FDM model conceptualization. (a) axisymmetric unit-cell, and (b) 2D-plane strain model geometry and meshing (after Indraratna et al. 2015).

A 3D DEM simulation was performed by Siahaan et al. (2015) to investigate the influence of particle size distribution on the bearing pressure-displacement performance of single stone columns. Clumped spheres were used to replicate basalt particle shapes, and an equivalent force-methodology (stress-controlled particles) was implemented at the cylindrical interface between the column and the soft soil to facilitate vertical and horizontal load transmission from the column to the soil as presented in Fig. 2.11. The results of this numerical investigation indicated that slight variations on the aggregate gradation affect the initial stiffness of the bearing pressure-displacement response of the columns, with well-graded gradations showing a tendency to result in a stiffer response at small displacements. Siahaan et al. (2015) mentioned that stone columns are mostly comprised of angular particles rather than rounded particles; therefore, the

use of clump spheres in a stone column model needs to be well calibrated in order to obtain a good representation of the micromechanical behavior of inter-particle interaction.

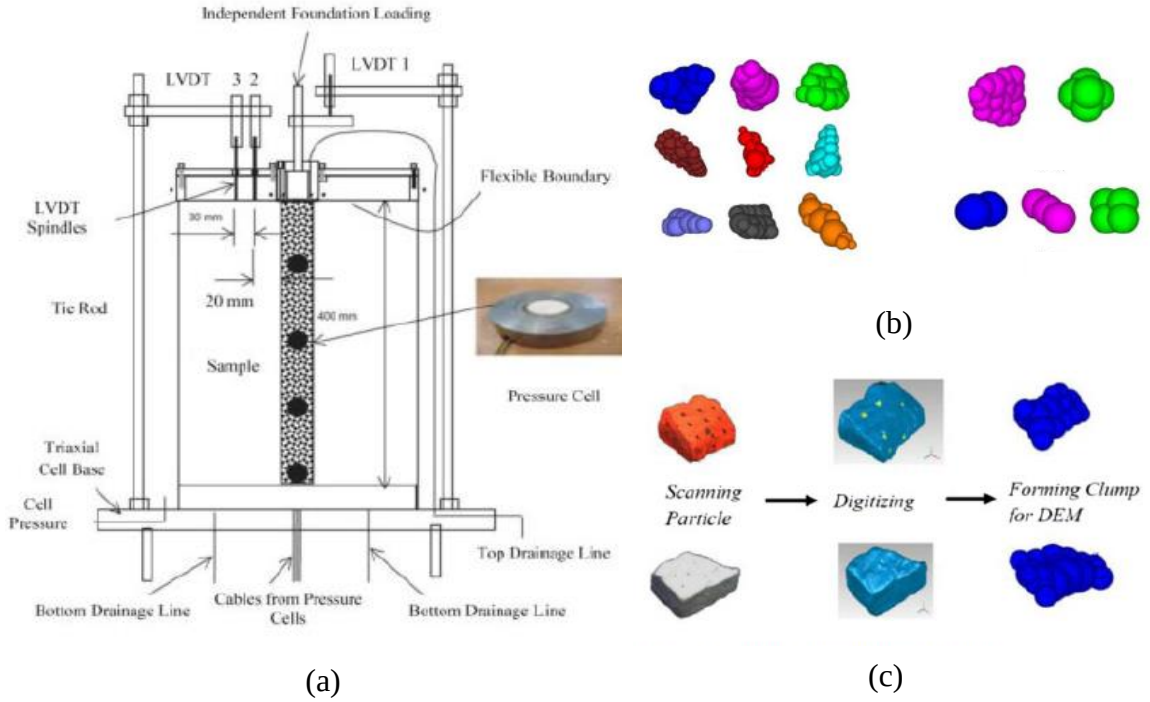

Fig. 2.11. Laboratory experiment and particle shapes used in the DEM simulations. (a) experimental test setup used by Sivakumar et al. (2011), (b) representation of basalt particle shapes used in the DEM Model, and (c) process to convert real particle shapes to simplified clump particles for the DEM model (after Siahaan et al. 2015).

Tan and Chen (2018) conducted a two-dimensional numerical investigation on a single stone column in a clayey stratum using a coupled DEM-FDM model similar to the framework proposed by Indraratna et al. 2015. Tan and Chen used the Universal Distinct Element Code (UDEC), which is a 2D-DEM program mainly developed to represent the behavior of discontinuous materials (e.g., jointed rock mass, aggregate columns) exposed to either static or dynamic forces. In UDEC, the distinct blocks behave as either rigid or deformable elements, which also allows simulating continuous materials. Tan and Chen (2018) simulated the column

granular material in UDEC as convex-shaped discrete rigid blocks (polygons) randomly generated based on the Voronoi tessellation, whereas the adjacent clayey soil was simulated as continuous Mohr-Coulomb material using deformable blocks as illustrated in Fig. 2.12. The advantage of this procedure implemented in UDEC is that the complex interaction between the aggregate column and surrounding soil can be simulated in a single model without needing monitored nodes for coupling the DEM-FDM model. The numerical results coincided well with the laboratory experimental data indicating the potential of this proposed modeling procedure for further numerical investigations to continue advancing the understanding of the behavior of stone column-foundation systems. However, this modeling framework presents a significant limitation in terms of the aggregate void ratio and relative density modeling. By using the Voronoi block system, the stone column is generated in a zero-porosity packing arrangement, which represents a much denser compaction condition than in stone columns. Additionally, it is typical in DEM models that the micro-mechanical contact parameters are different that those obtained from laboratory testing (Tan et al. 2015, 2016). Therefore, proper calibrations are needed in order to ensure that the modeling contact parameters reproduce the behavior of the granular material. The authors also highlighted that the three-dimensional behavior of a stone column could only be approximately simulated using 2D-rigid disks and plain strain model. Hence, a full-scale 3D-DEM model could improve understanding of the complex behavior of stone columns.

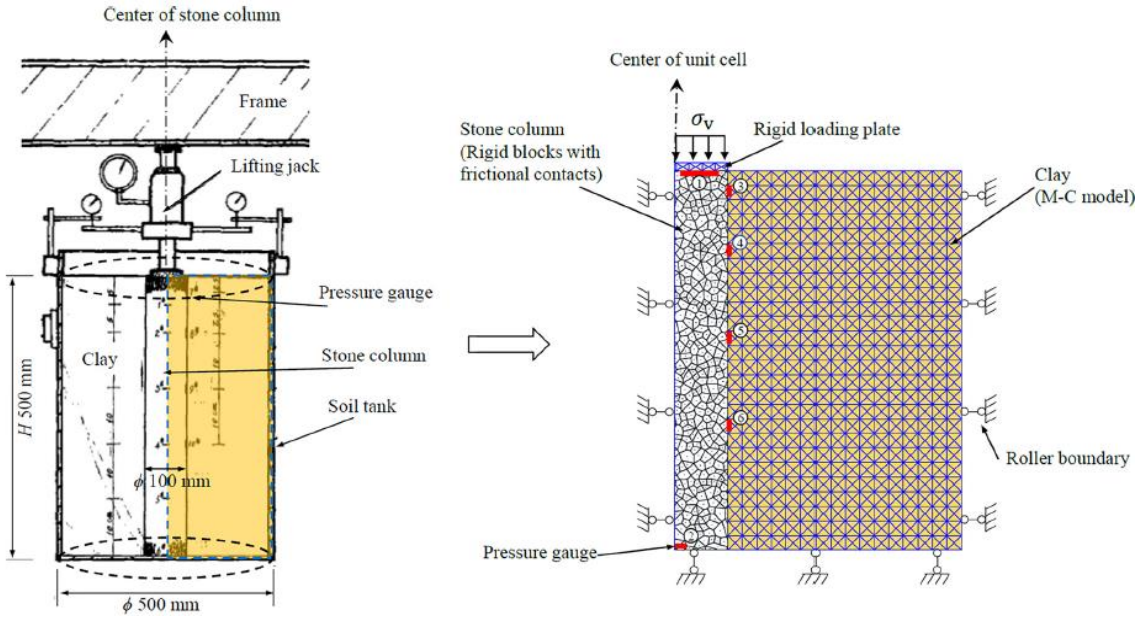

Fig. 2.12. Model conceptualization from the experimental to the numerical model. a) experimental test setup used by Meng and Shen (1987), and b) two dimensional DEM-FDM model in UDEC (after Tan and Chen 2018).

2.7 Summary of literature review and main areas for investigation

Despite the fact that the use of stone columns as a soil improvement option has significantly increased in the last few decades, there are still some uncertainties regarding their internal and global behavior that have not been fully captured by analytical and numerical continuous approaches. In reference to the literature, three main areas need to be investigated further in an effort to improve the design of isolated foundations supported on stone columns. These are:

1. *Lack of reliability and validation of the existing design methods for spread foundations resting on single, isolated conventional stone columns.*

Previous efforts to assess the load transfer mechanisms have treated the bulging failure mechanism of single, isolated columns as analogues to the expansion of a cylindrical cavity, using results of pressuremeter testing or idealized elasto-plastic constitutive responses to represent the native soil and aggregate. However, the soil constituents comprising the stone column system exhibit nonlinear, pressure-dependent stress-strain characteristics, a critical shortcoming in the methods. Additionally, the load transfer between the column and the surrounding soil is progressive in nature and depends on the exceedance of local shear stresses and redistribution of normal and shear stresses that are governed by the magnitude of the imposed displacements and the loading boundary conditions (Stuedlein 2010). Furthermore, the accuracy of these methods has not been validated in full-scale footing loading test experiments, largely due to the difficulty in observing and measuring load transfer of stone column-reinforced soil (Stuedlein and Holtz 2008).

2. *Lack of available information regarding the performance of cemented stone columns.*

The applicability of conventional stone columns is generally restricted for low-strength clayey soils (i.e. $s_u < 20$ kPa) because of the insufficient lateral confinement that these types of soils can provide to the aggregate columns, which can result in the occurrence of premature bulging failure (Barksdale and Bachus 1983). The use of cemented aggregate has been considered as one of the solutions to improve the efficiency of conventional stone columns installed in very soft soils. However, cemented aggregate columns have not widely been implemented because there are still uncertainties regarding their global performance under different loading and field conditions in comparison with conventional stone columns. Furthermore, there is a lack of information regarding material parameters (e.g., Young's Modulus, friction angle, cohesion) needed for design and numerical modeling.

3. *Lack of methods for predicting the bearing capacity and settlement of foundations supported on small stone column groups.*

Typically, stone columns installed in wide spread group configurations are designed using methods developed considering the unit-cell concept. However, the application of this approach to design footings resting on small stone column groups is questionable because it does not provide an appropriate representation of the global three-dimensional failure mode (conical shear failure) and does not take into account the group effect. However, a lack of convincing information comparing the design and performance of small stone column groups with or without considering the unit-cell concept was found in the literature review. Additionally, the use of the method proposed by Barksdale and Bachus (1983) is restricted for some soil types and foundation shapes.

CHAPTER 3. DESCRIPTION OF EXPERIMENTAL DATABASE

Experimental calibration or verification of the 3D-DEM models is important in order to provide confidence in the numerical findings. This calibration was developed based on the experimental studies conducted on the full-scale stone columns (Stuedlein 2008; and Stuedlein et al. 2012a) and small-scale cemented stone columns (Golait et al. 2016).

3.1 Overview of Full-scale Experimental Program by Stuedlein et al. (2012a)

Stuedlein (2008) and Stuedlein and Holtz (2012a) described a comprehensive footing loading test program designed to investigate the effect of aggregate column installation method, aggregate gradation, and column length on the bearing pressure-displacement performance. This information was used to form a basis for validation of the numerical approach and evaluation of various design variables described herein.

3.1.1 Description of the Test Site Location and Geology

The test site was located in Baytown, TX, at an approximate distance of 50 km east of Houston. The strata at the test site is known as the Beaumont clay formation, and it is primarily composed of an overconsolidated, tan and brownish red clay with sporadic thin seams of silty sand or silt. The initial depositional process of the Beaumont clay formation occurred on areas subjected to flooding during the first Wisconsin glacial stage approximately 100,000–50,000 years ago (Stuedlein et al. 2010, 2012a). After deposition, the clay formation surface was exposed to a net lowering of the sea level of the nearby Gulf of Mexico of approximately 125 m during the late Wisconsin glacial stage, which induced desiccation in the Beaumont clay formation. This desiccation subsequently produced the development of fissures and joints in the

Beaumont formation originating coefficients of lateral earth pressure for at-rest condition close to passive earth pressure (Stuedlein et al. 2012a; O'Neill and Yoon 1995).

3.1.2 Geotechnical Characterization of the Test Site

The characterization of the subsurface conditions at the test site location was conducted by a series of in-situ tests in combination with laboratory testing. The field exploration program was developed using five mud rotary borings (designated B-1−B-5; Stuedlein and Holtz 2010) and nine cone penetration tests (designated CPT-1−CPT-3, CPT-F1− CPT-F6; Stuedlein and Holtz 2010) distributed over the test site as illustrated in Fig. 3.1. Two of the five mud rotary borings were used for standard penetration tests (SPTs) while the rest were used for thin-walled tube sampling. Based on the results obtained from the CPT soundings, SPT blow counts, and thin-walled tube sampling, a representation of the subsurface profile was developed along section A-A', as illustrated in Fig. 3.2 (Stuedlein and Holtz 2012b). The subsurface consisted of a desiccated clay crust layer 0.6 m thick, overlying an approximately 3 m thick upper layer of medium stiff to stiff, low to medium plasticity Beaumont Clay, underlain by a layer of stiff to very stiff medium to high plasticity clay. The upper and lower clay layers were separated by a thin, loose to medium dense layer of sandy silt to silty sand. Table 3 summarizes the results obtained from the in-situ test program. Soil samples obtained from the test site using thin-walled tubes were used to perform consolidated isotropic undrained (CIU) triaxial strength tests using the SHANSEP laboratory testing protocol (4 tests) and recompression procedure (8 tests), as detailed in Stuedlein (2008). Fig. 3.3 shows the CIU triaxial strength test results for the desiccated clay at different overconsolidation ratios (OCRs). The stress-strain responses of the soil specimens prepared using the recompression technique are presented in Fig. 3.3a, whereas

Fig. 3.3b shows the stress path and principal stress ratios as function of the axial strain for samples prepared using SHANSEP.

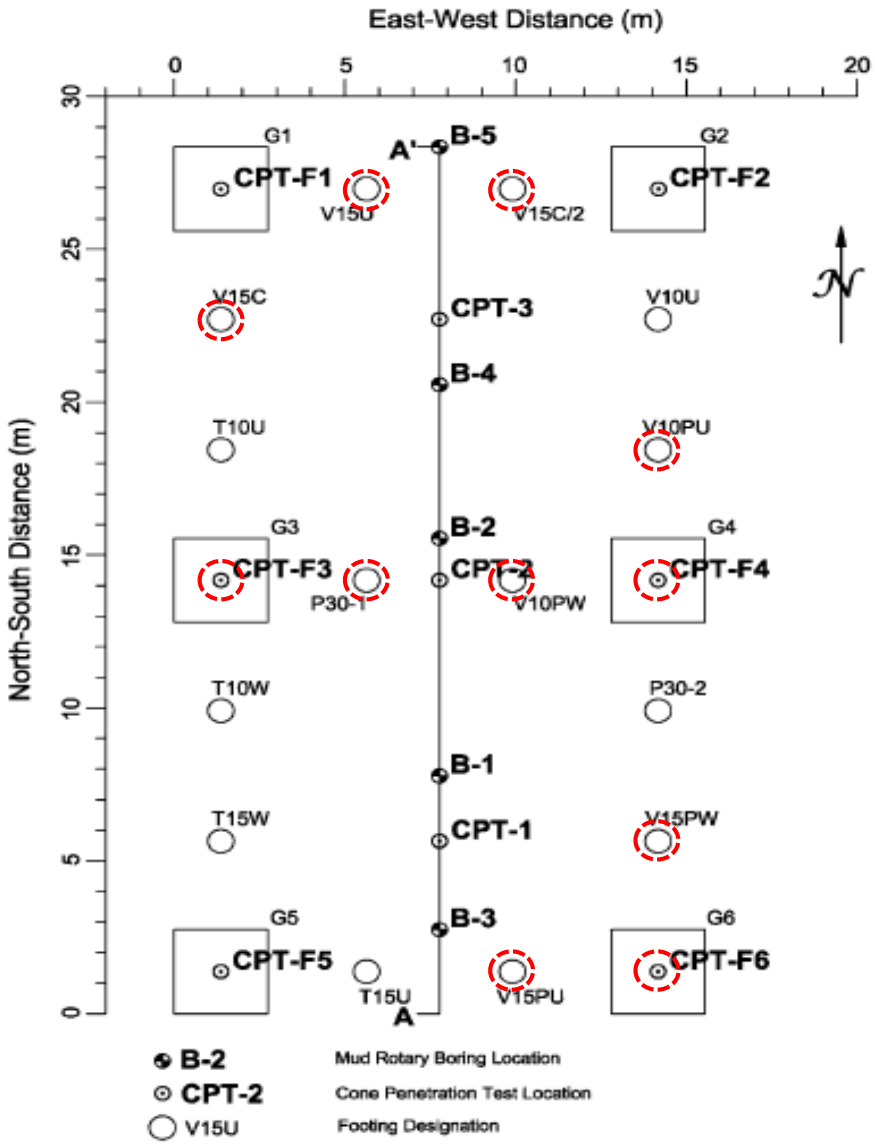

The red-dashed circles indicate the foundations selected to calibrate the DEM simulations.

Fig. 3.1. Plan view of the experimental program and exploration plan of the test site (after Stuedlein and Holtz 2012b).

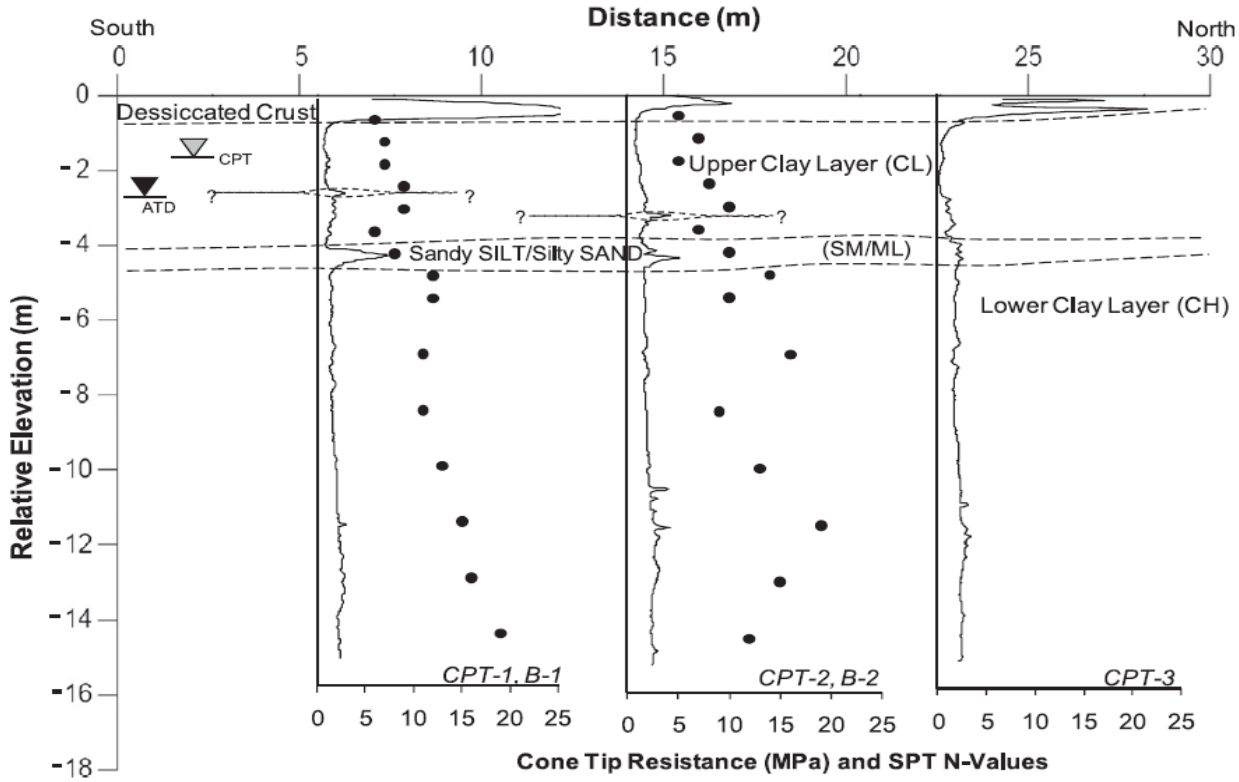

Fig. 3.2. Subsurface profile was developed along section A-A'(after Stuedlein and Holtz 2012b).

Table 3. Summary of results obtained from the in-situ test experimental program.

Soil type	USCS	Consistency	Thickness [m]	SPT, Nm			CPT, q_t [MPa]		
				Min	Mean	Max	Min	Mean	Max
Desiccated crust	CL	Very Stiff	0.6	---	---	---	0.94	7.45	21.6
Upper clay layer	CL	Medium stiff	3.2	5	7	10	0.06	1.35	4.19
Silty sand/ sandy silt	SM/ML	Loose	0.8	6	8	10	0.79	2.94	8.20
Lower clay layer	CH	Stiff to very stiff	---	9	14	19	1.27	2.05	4.21

qt= corrected tip resistance. Table modified from Stuedlein and Holtz (2012b).

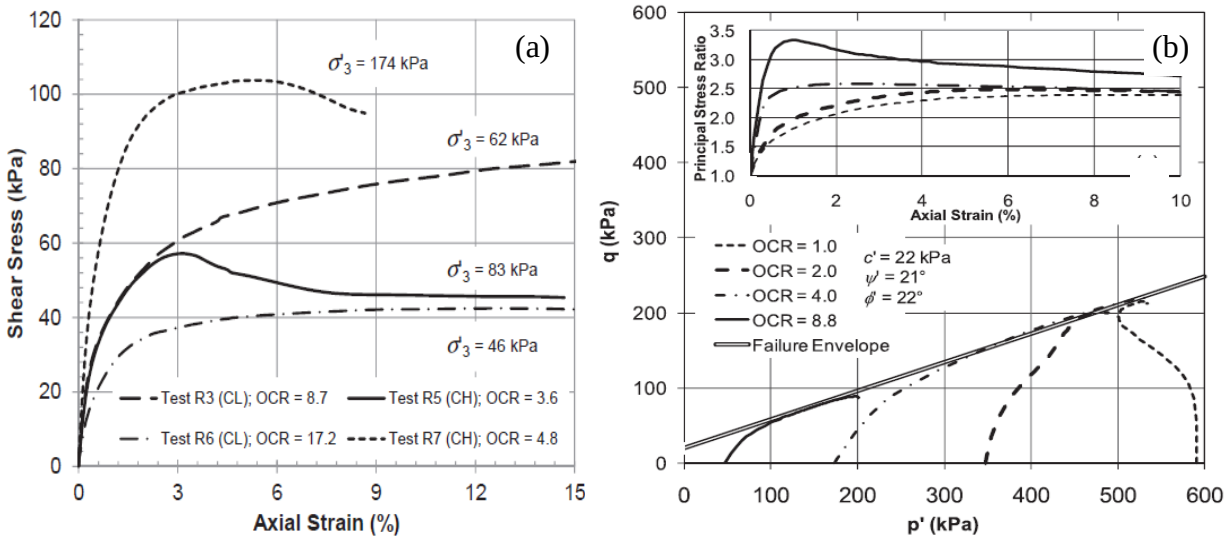

Fig. 3.3. Results from the CIU triaxial strength tests for the overconsolidated clay at different overconsolidation ratios. (a) stress-strain responses using the recompression technique, and (b) stress path and principal stress ratios as function of the axial strain for SHANSEP (after Stuedlein and Young 2012; Stuedlein and Holtz 2012b).

Stuedlein et al. (2012b) followed the procedure proposed by Mahar and O'Neill (1983) to develop the normalized undrained shear strength (s_u/σ'_v) multiplied by the liquid limit (LL) as a function of OCR's (SHANSEP curve) for the test site, as illustrated in Fig. 3.4. The CPT results in conjunction with SHANSEP curve, correlations, and a geostatistical model of the 3D spatial (Stuedlein et al. 2012c) were used to estimate field geotechnical material properties (e.g., preconsolidation stress, σ'_p, overconsolidation ratios, OCRs, undrained shear strength, s_u, lateral earth pressure coefficient at-rest, K_o) at the test site. Eq. 31 (Chen and Mayne 1996), Eq. 32, Eq. 33 (Mahar and O'Neill 1983, Stuedlein et al. 2012b), and Eq. 34 (Kulhawy and Mayne 1990) were used to develop the subsurface soil profiles for σ'_p, OCRs, s_u, and K_o, respectively, at each desired location within the test site (Fig. 3.5).

$$\sigma'_p = 0.305 \times (q_t - \sigma_{vo}) \tag{31}$$

$$OCR = \frac{\sigma'_p}{\sigma'_{vo}} \tag{32}$$

$$s_u = \left(\frac{s_u}{\sigma'_{vo}}\right)_{NC} \times \sigma'_{vo} \times OCR^m = 0.364 \times \sigma'_{vo} \times OCR^{0.706} \tag{33}$$

$$K_o = \left[\frac{\left(\frac{s_u}{\sigma'_{vo}}\right)_{OC}}{\left(\frac{s_u}{\sigma'_{vo}}\right)_{NC}}\right]^{0.6} \tag{34}$$

where σ_{vo} and σ'_{vo} are the total and effective vertical stresses, and *m* is fitting parameter of the SHASHEP curve.

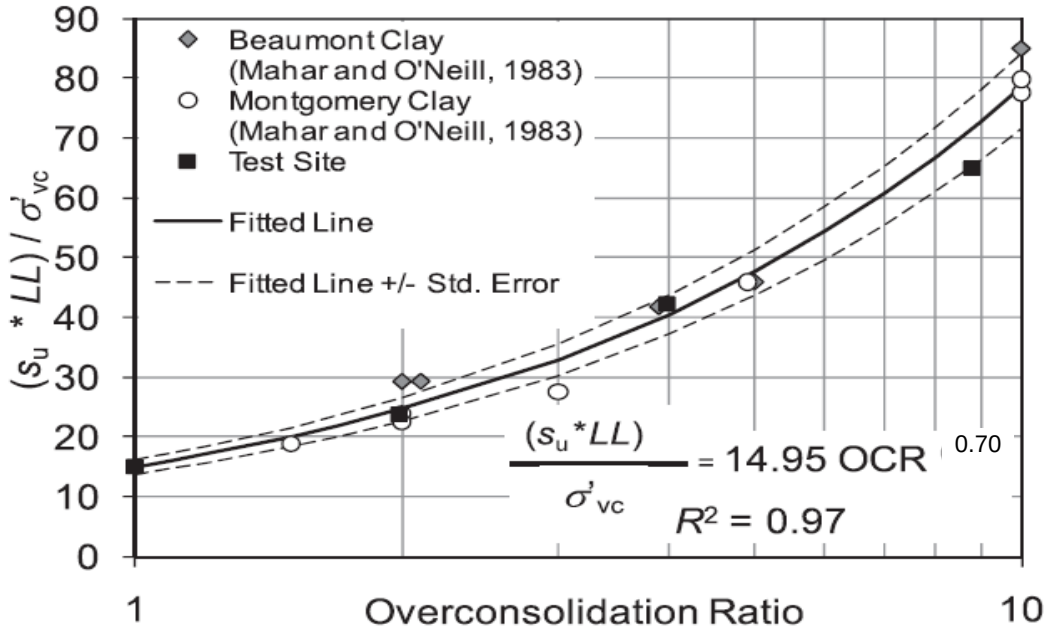

Fig. 3.4. Fitted SHANSEP curve for Beaumont clay (after Stuedlein and Holtz 2012b).

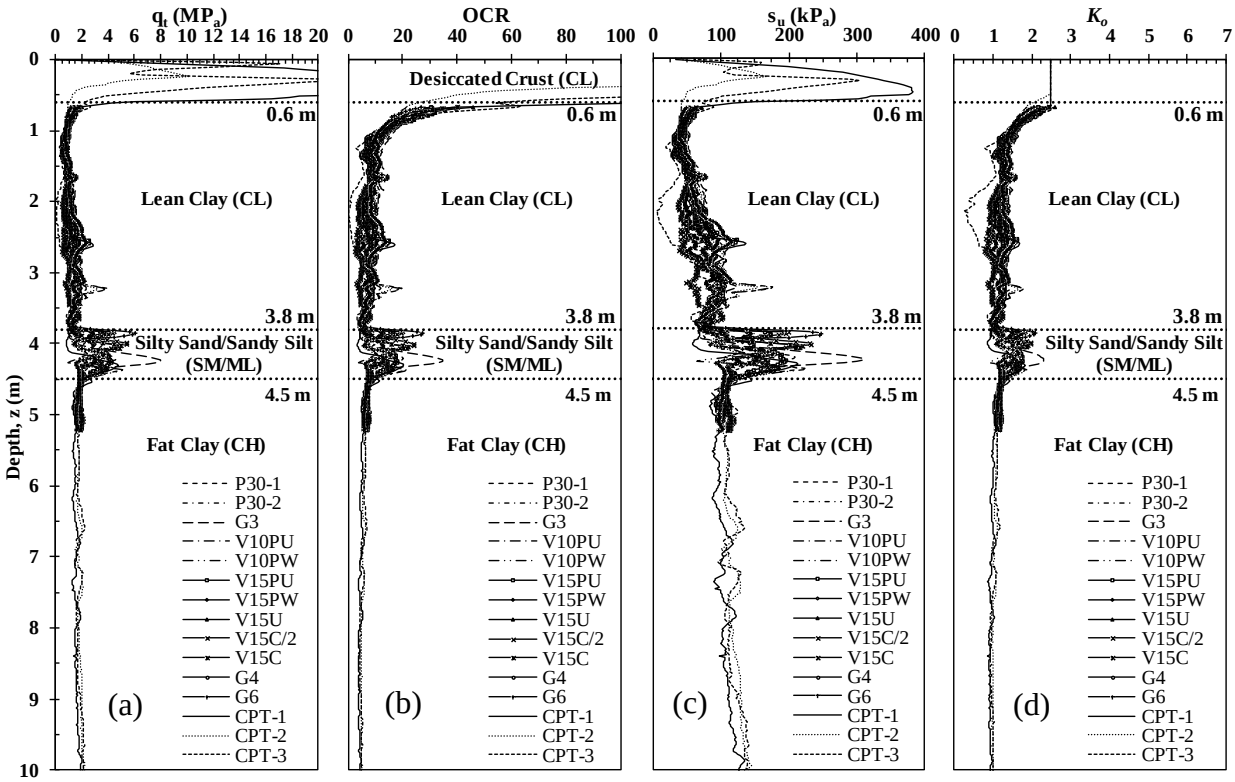

Fig. 3.5. Subsurface property profiles. (a) corrected tip resistance, q_t, (b) overconsolidation ratio, OCR, (c) undrained shear strength, s_u, and (d) coefficient of earth pressure at-rest, K_o (data provided by Dr. Stuedlein).

3.1.3 General Details of the Full-Scale Testing Program

Twenty full-scale loading tests on unreinforced and stone column-reinforced soil were conducted, including 14 tests on small circular concrete footings (0.76 m diameter, *B*) and six on large square concrete footings (2.74 m width, *B*), as detailed in Table 4. The tests were performed to evaluate the effect of densification method (those investigated in the proposed work are vibrated, designated by V), depth of treatment (3.05 and 4.57 m, designated as 10 and 15 feet), predrilling prior to densification (designated by P), and aggregate gradation (U or W, representing uniform- and well-graded aggregate, respectively). The diameter, D_{sc}, of the test columns ranged from 0.74 to 0.76 m, resulting in area replacement ratios, A_r, ranging from 95 to

100% for the small footings, whereas A_r was approximately 30% for the large footings. The slenderness ratio, L_{sc}/D_{sc}, evaluated was either four or six for both small and large footings, as shown in Table 4. Two small baseline footings (designated P30-1 and P30-2; Stuedlein and Holtz 2010), overlying unreinforced ground, were tested with the same configuration to evaluate repeatability and were found to produce nearly identical results. The small footings overlying the unreinforced (baseline condition) and stone column-reinforced soil were embedded 0.61 m below grade. Also, a large baseline footing (designated G3; Stuedlein and Holtz 2010) was tested on the unimproved ground, and its response was found to be similar to the other two small baseline footings in terms of the mobilized shear strength as a function of the normalized displacement as presented in Fig. 3.9. The large square footings (0.27 m thick) were not embedded into the desiccated crust layer, and a square-stiffened steel structure (3.05 m square) was centrically placed over them in order to provide a rigid foundation condition.

Two of those load tests were conducted on footings (embedded 0.61 m below grade) supported on single, isolated stone columns constructed using cement-coated aggregate. One of these columns (V15C/2U, Stuedlein and Holtz 2012a) was constructed with cemented aggregate in the upper half, and uncemented aggregate in the bottom half (designated here as V15U-PCSC). The other column (V15CU, Stuedlein and Holtz 2012a) was entirely constructed with cemented aggregate (referred to here as V15U-FCSC). Views of the setup of the small footings and large footings are presented in Fig. 3.6 and Fig. 3.7, respectively.

Table 4. Foundation and stone column geometries for full-scale DEM models

Element	Footing/ Column, B/D_{sc} [m]	Number of Columns	Length, L_{sc} [m]	L_{sc}/D_{sc} ratio ---	Area Replacement Ratio, A_r [%]
V10PW	0.76/0.76	1	3.05	4	100
V15PW	0.76/0.76	1	4.57	6	100
V10PU	0.76/0.74	1	3.05	4	95
V15PU	0.76/0.74	1	4.57	6	95
V15U-UCSC	0.76/0.74	1	4.57	6	95
V15U-FCSC	0.76/0.76	1	4.57	6	100
V15U-PCSC	0.76/0.74	1	4.57	6	95
V10PU-5 (G4)	2.74/0.74	5	3.05	4	30
V15PU-5 (G6)	2.74/0.74	5	4.57	6	30
P30-1 (Baseline)	0.76	---	---	---	---
G3 (Baseline)	2.74	---	---	---	---

B=footing size, D_{sc}=stone column diameter, L_{sc}=stone column length.

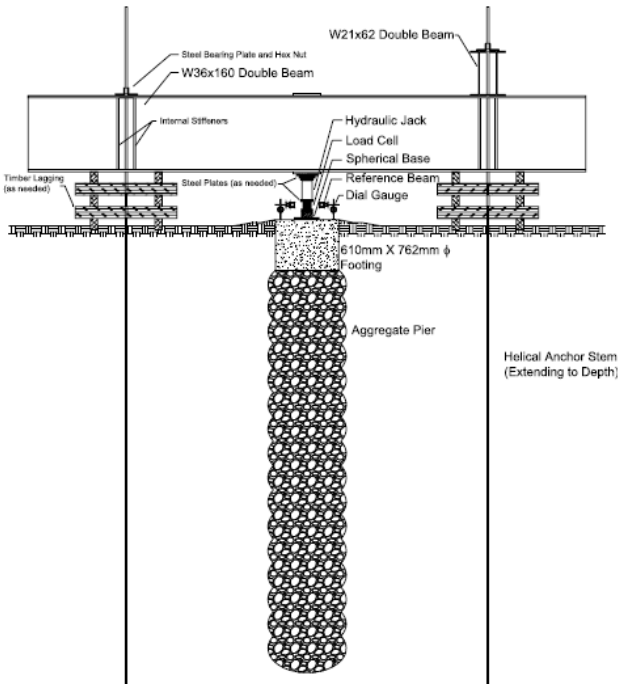

Fig. 3.6. Sketch of the small footing setup on single stone column (after Stuedlein et al. 2012b).

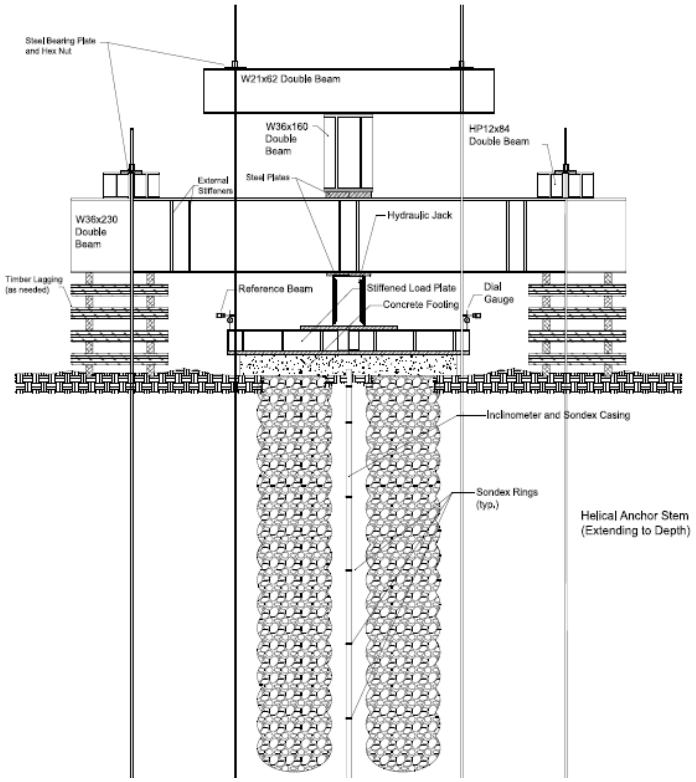

Fig. 3.7. Sketch of the large footing setup on a small stone column group (after Stuedlein et al. 2012b).

3.1.4 Aggregate Material Used in Stone Column Construction

The granular material used within stone columns is generally, crushed gravel (typically limestone) or waste rock. The selection of the aggregate gradation, typically made by the geotechnical specialty contractor, depends on the installation method, column length and diameter, and groundwater table, but the particle size generally varies from 6 mm to 50 mm (Barksdale and Bachus 1983). The aggregate used to construct the stone columns in Stuedlein and Holtz (2012b) was a uniformly-graded crushed gravel (#57 limestone gradation, GP, C_u = 2.3, C_c = 1.2, D_{50} = 13.5 mm) and a well-graded, angular, silty sand and gravel mixture (21b limestone gradation, GW-GM, C_u = 250, C_c = 2.5, D_{50} = 6.1 mm), as illustrated in Fig. 3.8a,b. For the cemented columns, this aggregate was mixed in the front-end loader bucket at a cement to aggregate ratio of 5 to 6 % of the total dry aggregate weight (Fig. 3.8c). The bottom feed method was used to place the aggregate into the ground during stone column installation (Stuedlein, 2008).

(a)

(b)

(c)

Fig. 3.8. Illustrations of aggregates used to construct stone columns. (a) uniformly-graded aggregate-#57 limestone, (b) well-graded aggregate-21b limestone, (c) cemented uniformly-graded aggregate (after Duncan et al. 2007; Newton 2014).

3.1.5 Bearing Pressure-Displacement Responses of Small and Large Footings on Unreinforced and Stone Column-Reinforced Soil

The variation of the mobilized undrained shear strength as a function of the normalized vertical displacement is illustrated in Fig. 3.9. The mobilized shear strength curves computed for the small and large baseline footings (P30-1, P30-2, and G3) exhibited almost an identical tendency, which indicates a very consistent response of the untreated ground at the test site.

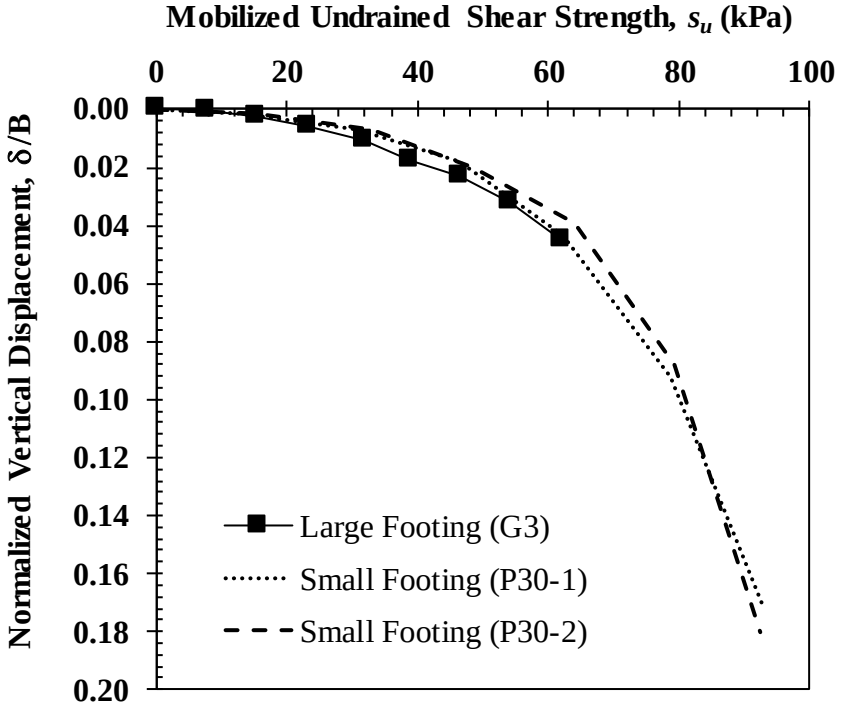

Fig. 3.9. Mobilized undrained shear strength-normalized vertical displacement response of untreated clayey soil (after Stuedlein, 2008).

Fig. 3.10 presents the bearing pressure-displacement, or q-δ, curves, for the baseline footing and aggregate column-reinforced footings described in Table 4. The footings overlying V10PW and V15PW share a near-identical response, despite differences in the column length, whereas the corresponding columns with uniformly-graded aggregate (i.e., V10PU, V15PU)

show significant differences. While some differences in the q-δ response can be attributed to differences in column length or soil strength (through column location in the spatially-variable soils at the test site; Stuedlein et al. 2012c) there is no consistent trend observed in the responses. Stuedlein et al. (2012a) reported that the longer stone columns constructed with uniformly-graded aggregate exhibited greater initial stiffness than the shorter columns, whereas the column length did not appear to affect the q-δ response of the well-graded columns. These findings leave questions regarding the role of aggregate column length, gradation, and strength and stiffness of the surrounding soil on the bearing pressure response of footings supported on stone columns. These questions are explored using numerical modeling in the remaining sections of this dissertation due to ability to systematically vary and compare these factors in the DEM simulations.

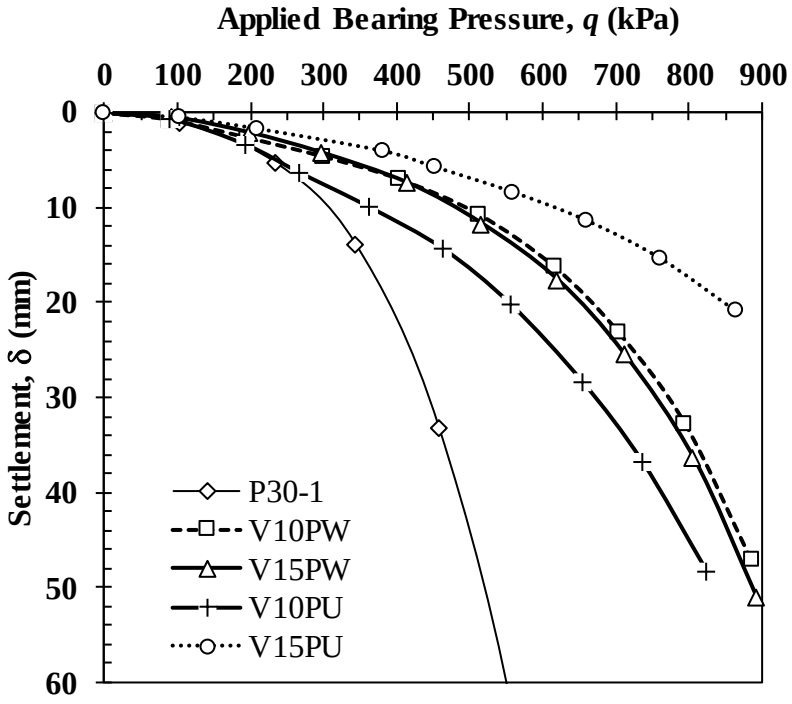

Fig. 3.10. Bearing pressure-displacement curves for selected well-graded and uniformly-graded stone columns (after Stuedlein and Holtz 2012a).

The q-δ responses for the cemented stone columns, V15U-PCSC and V15U-FCSC, and the uncemented stone column, V15U-UCSC, are presented in Fig. 3.11. The q-δ responses for the cemented stone columns were considerably stiffer than the uncemented column. For a settlement value of 20 mm, the bearing pressure improvement ratio of columns V15U-FCSC and V15U-PCSC to column V15U-UCSC is approximately 2.6 and 3.5, respectively, indicating a substantial increase in the bearing pressure performance and reduction on the foundation settlement. It is important to highlight that V15U-PCSC, constructed with the cemented aggregate in only the upper half of the column, exhibited a stiffer q-δ response than V15U-FCSC, which cannot be explained only by the cement inclusion in the aggregate mixture. Experimental or field observations are not able to explain these differences, and further investigation using numerical models is needed.

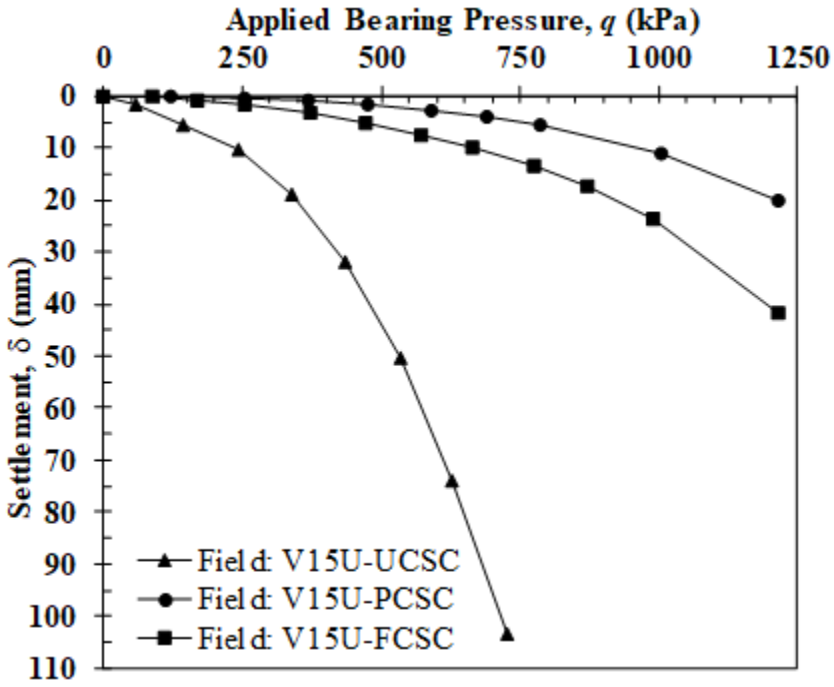

Fig. 3.11. Bearing pressure-displacement curves for selected uniformly-graded-cemented stone columns (after Stuedlein and Holtz 2012a).

Fig. 3.12 illustrates the bearing pressure-displacement curves for the baseline footing (G3) and aggregate column-reinforced footings (G4 and G6). The large footings G4 and G6 were constructed over a group of five vibro-compacted aggregate columns that were installed using uniformly-graded uncemented aggregate to depths of 3.05 m and 4.57 m, respectively. The q-δ responses of G4 and G6 initially coincide with that corresponding to G3 up to approximately 90 kPa. However, beyond this value, both G4 and G6 exhibited stiffer responses than that of G3 with a reduction in the observed displacement (≈ 62 mm) at the final load increment of approximately 50% in comparison with G3 (≈ 123 mm). G4 exhibited a slightly stiffer q-δ response than G6 for q values greater than 200 kPa, which cannot be explained by the length difference, but it might be caused by the variation in the s_u profile at each footing location.

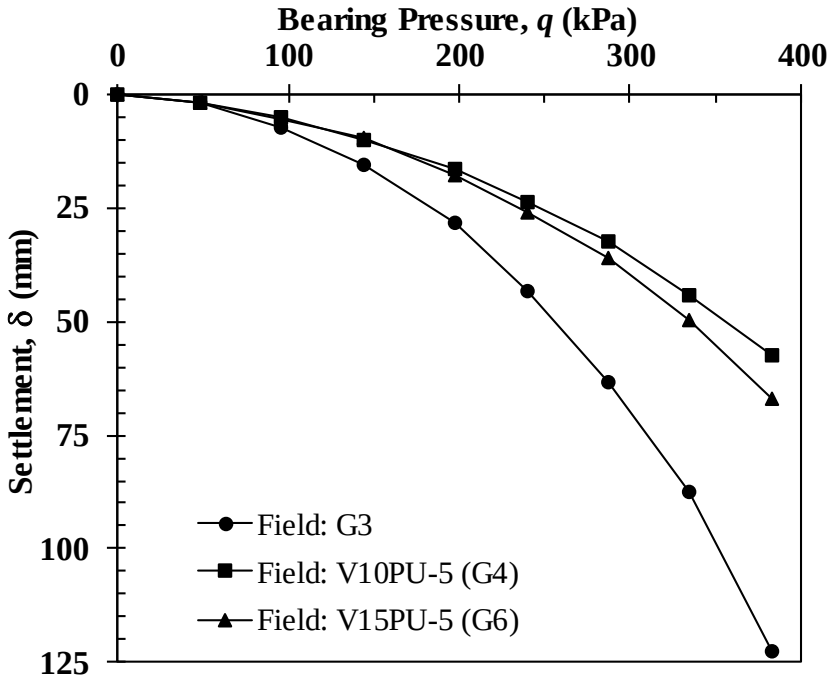

Fig. 3.12. Bearing pressure-displacement curves for selected uniformly-graded-uncemented stone column groups (after Stuedlein and Holtz 2012a).

3.2 Overview of Small-scale Experimental Investigation by Golait et al. (2016)

Golait and Padade (2016) conducted small-scale 1g laboratory experiments on single cemented stone columns to evaluate the performance and effectiveness of these type of columns in comparison with the conventional stone columns and other column-type soil improvement techniques. The experimental results were also used to validate the analytical procedure that the authors proposed for cemented aggregate column design using the unit-cell idealization.

The unit-cell idealization employed in the laboratory setup was intended to represent a stone column 4.0 m long and 0.40 m in diameter, installed in a triangular configuration with a center-to-center column spacing of 0.95 m. The authors selected a scale factor of 10 to reduce the prototype geometry to a small-scale model with the column length (L_{sc}= 40 cm), column diameter (D_{sc}= 4.0 cm), and until-cell diameter (B= 10 cm) as illustrated in Fig.3.13a. Based on this model geometry (Table 3), the column slenderness ratio (L_{sc}/D_{sc}) was 10, and the area replacement ratio (A_r) was approximately 16% (Table 5). A schematic of the experimental setup is presented in Fig. 3.13b, which included: a perforated mild-steel tank (diameter and height of 50 cm), a saturation tank, dial gauges for settlement measurements, and a rigid steel plate (loading ram, B= 10 cm) to apply a uniform pressure on top of the unit-cell (Golait et al. 2016).

Table 5. Foundation and stone column geometries for small-scale DEM models

Model	Element	Diameter B/D_{sc} [m]	Length, L_{sc} [m]	L_{sc}/D_{sc} ratio ---	Area replacement ratio, A_r [%]
Small-Scale (Golait et al. 2016)	UCSC, PCSC, and FCSC	0.1/0.04	0.40	10	16

B=footing diameter, D_{sc}=stone column diameter, L_{sc}=stone column length

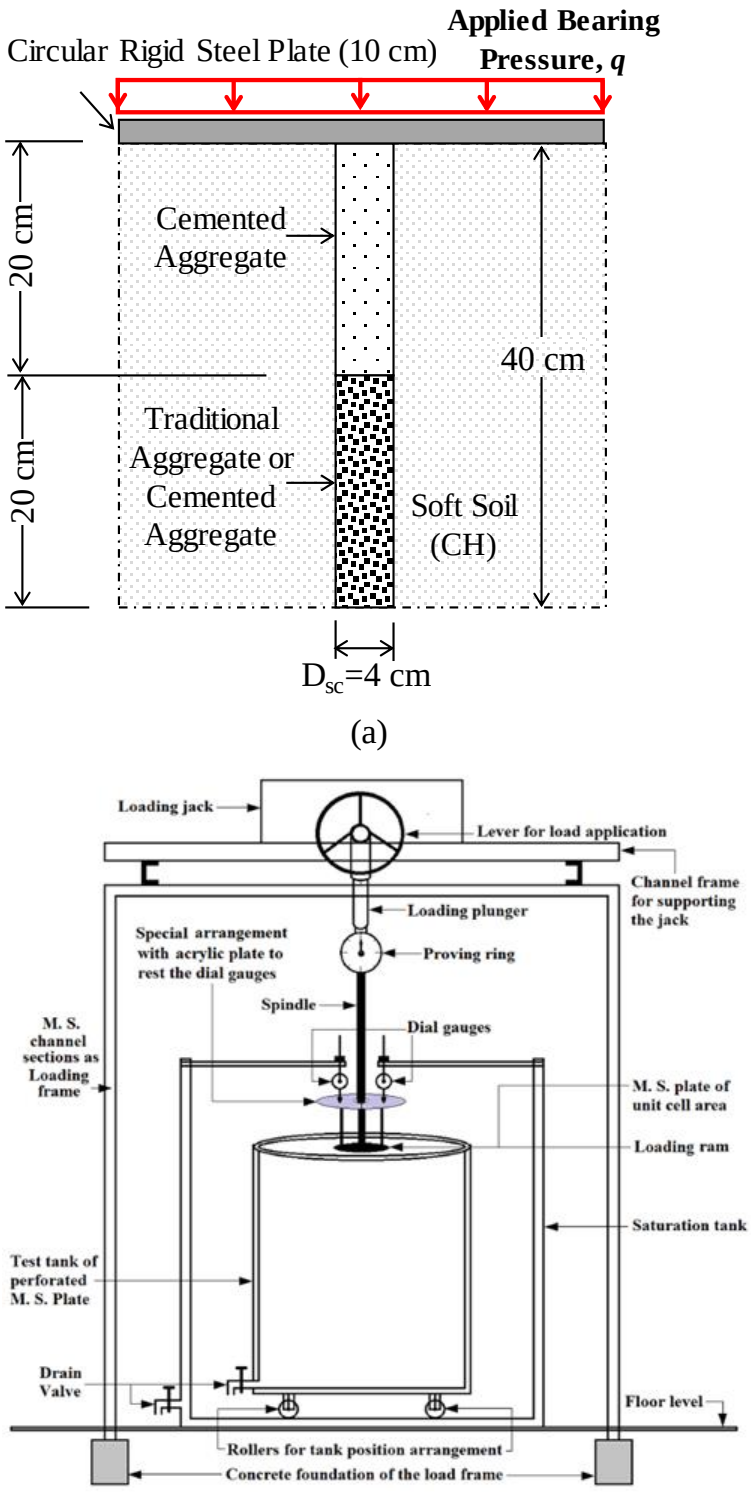

Fig. 3.13. (a) Schematic of the unit-cell idealization, and (b) laboratory setup for testing small-scale cemented stone columns (after Golait et al. 2016).

To examine the cementation effect within the bulging zone, a column (designated here as PCSC) was constructed with cemented granular material in the upper half, whereas the lower half of the column was constructed using uncemented granular material. Another column was constructed entirely of cemented granular material for comparison (referred to here as FCSC).

The granular material used to construct the PCSC and FCSC columns contained 60% coarse sand and 40% fine sand and was mixed with 2% cement and 6% fly ash for the cemented granular material. The granular materials were mixed at a water content of 5% and then were placed and compacted within a small-diameter "borehole" perforated into the clay layer (Golait et al. 2016).

The bearing pressure-displacement responses for the partially cemented stone column (PCSC) and fully cemented stone column (FCSC) are presented in Fig. 3.14, along with the q-δ curve corresponding to the unreinforced clayey soil (USS), and an uncemented stone column for comparison (UCSC). PCSC and FCSC exhibited a similar initial linear behavior, but for q values above 60 kPa, a nonlinear behavior was observed. Overall, FCSC exhibited a slightly stiffer q-δ response than PCSC. This is an opposite behavior of what was observed from the full-scale cemented stone columns tested by Stuedlein (2010) and Stuedlein and Holtz (2012a), indicating the need for further investigation using numerical models to improve understanding this behavior. Computed using the double tangent method, columns PCSC and FCSC provided an increase in the bearing capacity of 44% and 57%, respectively, with respect to UCSC. The bearing capacity improvement factors are approximately 2.3 and 2.5 for PCSC and FCSC, respectively, computed in terms of the bearing capacity of the unreinforced soil.

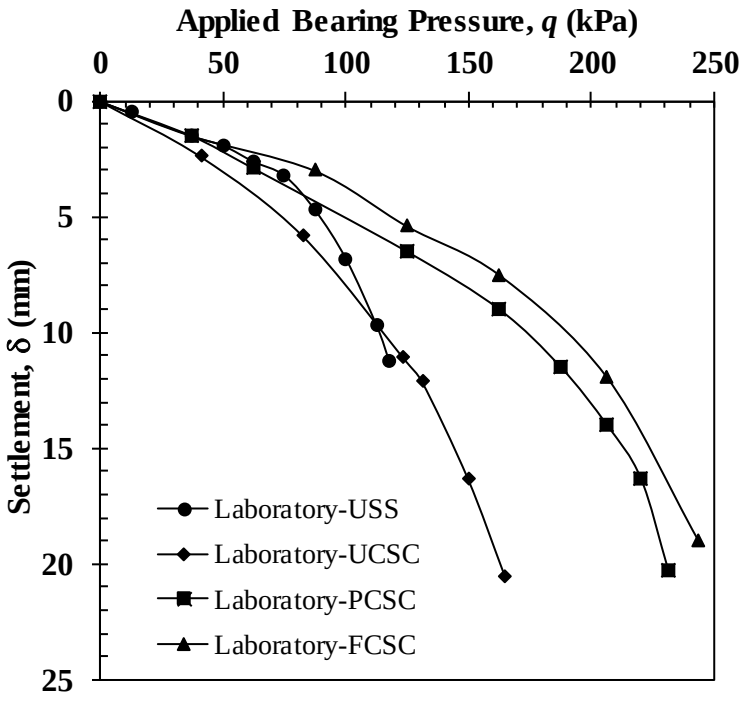

Fig. 3.14. Bearing pressure-displacement curves for selected small-scale cemented stone columns. USS refers to the unreinforced soil, and USCS, PCSC, and FCSC refer to uncemented, partially cemented, and fully cemented stone columns, respectively (after Golait et al. 2016).

CHAPTER 4. NUMERICAL FRAMEWORK AND METHODOLOGY

4.1 Summary of Previous DEM Simulations on Stone Columns

The behavior of stone columns has been investigated using numerical continuum mechanics to address questions of system or global response (e.g., Balaam et al. 1977, Mitchell and Huber 1985, Ambily and Gandhi 2007, Hanna et al. 2013, McCabe et al. 2016, Ammari et al. 2018). However, continuum approaches may be limited due to the difficulty of capturing internal interactions occurring between the aggregate particles comprising the stone column. The discrete element method (DEM) provides an alternative modeling approach capable of capturing these particle interactions, as well as the global response of particulate materials, and researchers have shown recent success in modeling stone column systems using coupled discrete-continuum approaches (Indraratna et al. 2015, Tan et al. 2018). Indraratna et al. (2015) simulated the bearing pressure-displacement response of a small-scale single stone column using a 2D coupled numerical model that linked discrete element analyses (comprised of disks) of the stone column to the surrounding soft clay, which was modeled as a continuum. Tan et al. (2018) conducted a similar study using coupled DEM-FDM approach implementing the Universal Distinct Element Code (UDEC) to simulate stone columns in clay. The granular material comprising the stone column was simulated using convex-shaped discrete-rigid polygon blocks randomly generated using a zero-porosity Voronoi tessellation packing scheme, whereas the surrounding clay soil was simulated as a continuum using deformable blocks with a Mohr-Coulomb failure criterion. Tan et al. (2018) reported good agreement between experimental results and the simulations; however, the calibration efforts necessary to approximate the experimental results using the suite of contact law parameters is computationally expensive and time-prohibitive, and the assumption of zero-porosity of the column material model deviates significantly from the physical frictional

phenomena giving rise to aggregate strength and stiffness. Additionally, 2D simulations of the actual 3D loading and geometry of discrete aggregate columns, as well as the effects of out-of-plane soil-aggregate interfaces, cannot capture potentially important and salient aspects of aggregate column performance (Tan et al. 2018). Siahaan et al. (2015) used 3D-DEM simulations to investigate the influence of particle size distribution on the q-δ response of single stone columns. Clumped spheres were used to replicate basalt aggregates whereas stress-controlled nodes along the cylindrical interface to simulate the interaction between the column to the surrounding soil. The use of stress-controlled nodes makes this numerical framework difficult to implement when the adjacent soil is nonhomogeneous. Slight variations of the aggregate gradation were shown to affect the initial q-δ response, with well-graded aggregates providing a stiffer response at small displacements.

4.2 Overview of Modeling Methodology

The computational platform 3DEC by Itasca Consulting Group, Inc. was used to conduct the 3D-DEM investigations herein. This platform has been used extensively to investigate the mechanical response of discontinuous media modeled as assemblies of discrete "blocks" of arbitrary 3D shapes. Individual 3D blocks can be modeled either as a rigid or deformable body in response to nodal static or dynamic forces (Itasca 2013). Rigid blocks are comprised of polygonal-plane faces, and their motion state is described in terms of three translational and three rotational degrees of freedom. The deformable blocks are internally discretized into finite difference tetrahedral zones with vertices that enable three translational degrees of freedom (Cundall 1988). The polyhedral blocks interact along specified discontinuities, which are treated as boundary conditions (e.g., block joints or contacts). The mechanical interaction between the discrete blocks is governed by the normal stiffness and tensile strength criterion in the direction

perpendicular to the sub-contact surface, and the tangential stiffness and shear strength criterion in the direction parallel to the sub-contact area (Itasca 2013). Once calculated for given time step, the sub-contact forces are used to compute the total force and moment at the centroid of each rigid block and its position is updated using the equations of motion. In the case of deformable blocks, the equations of motion defined for each block's grid-points are solved using an explicit time-domain integration scheme. The new stress state for the tetrahedral zones is then calculated using a stress-displacement contact law (Cundall 1988). Fig. 4.1a illustrates a schematic of a simple assembly of discrete rigid and deformable blocks generated in 3DEC, and a diagram of the calculation process for rigid and deformable blocks implemented in 3DEC is presented in Fig. 4.1b.

4.3 Block Zone Generation

Typical of all numerical techniques, the generation of block zones (analogous to mesh discretization) represents a critical aspect in the performance and efficiency of a DEM model in 3DEC. Deformable blocks can be discretized into tetrahedral zones in 3DEC using three different types of zoning techniques (e.g., regular tetrahedral zoning, high-order tetrahedral zoning, and six-sided polyhedra zoning- "quads"). A tetrahedral zone generation developed using either high-order zones or quad zones (referred to as mixed discretization) provide a more accurate solution than regular tetrahedral zones for simulations including large plastic deformations (Itasca 2013). Fig. 4.2 presents the q-δ responses of a rigid foundation on a soft soil simulated using these three types of tetrahedral zone generation techniques. It can be noticed that the q-δ curves for the high-order zoning and mixed discretization zoning are almost identical and in good agreement with Meyerhof's (1963) analytical solution (Fig. 4.2). The

mixed zone discretization technique was used in this study to discretize the blocks into deformable tetrahedrons.

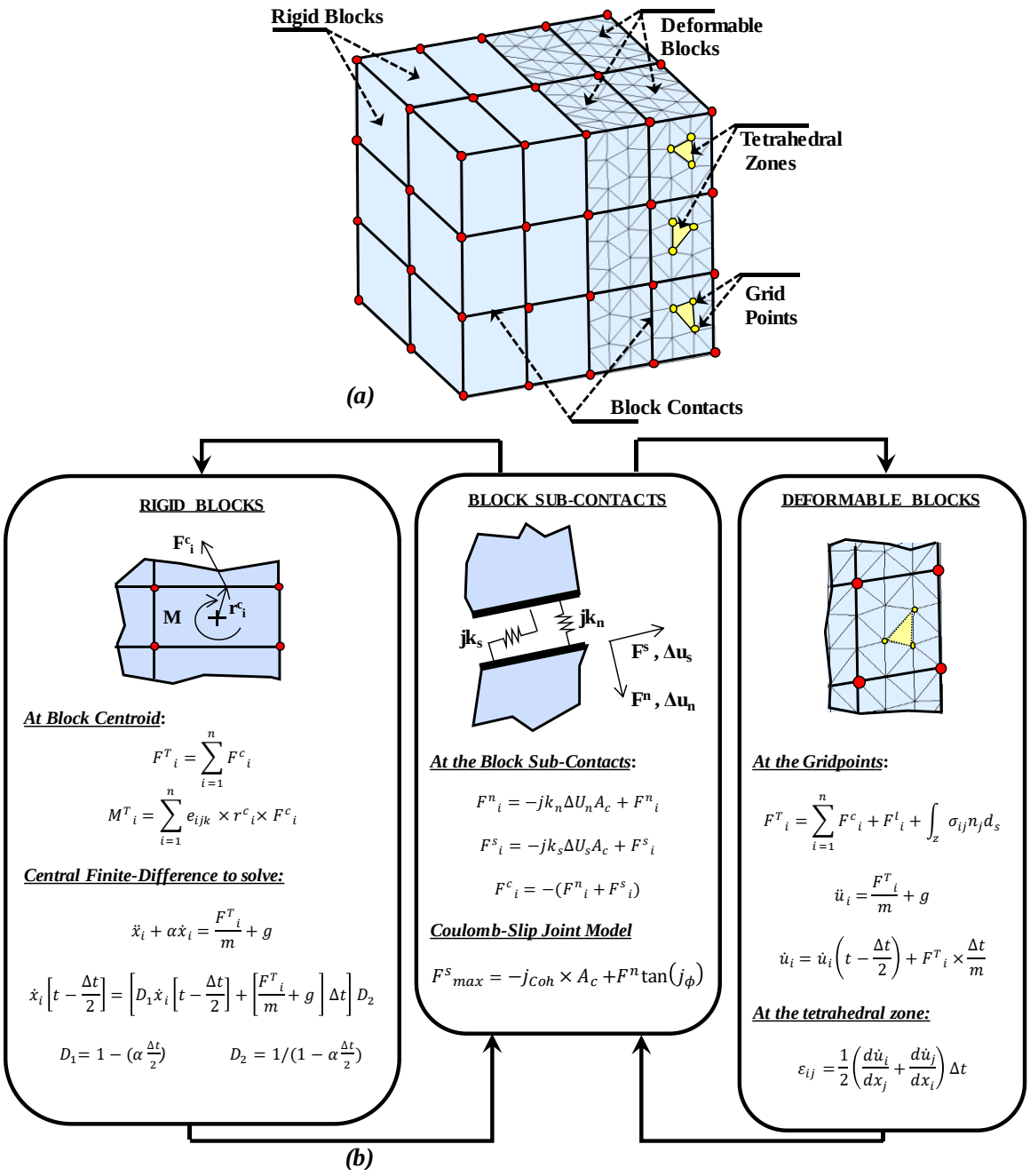

F=force, *M*=moment, *j*=joint properties, A_c=contact area, *u*=displacement, *m*=mass, Δt=time step, t=time, ε=strain, σ=stress, *g*=gravity, α=damping ratio, *T*=tension, $\ddot{x}, \ddot{u}$=acceleration, $\dot{x}, \dot{u}$=velocity, ω=rotation, *r*=moment arm

Fig. 4.1. Illustration of discrete blocks in 3DEC: (a) basic block discretization in 3DEC; (b) calculation cycle for rigid and deformable blocks in 3DEC Program (adapted from Itasca 2013 and Tran et al. 2018).

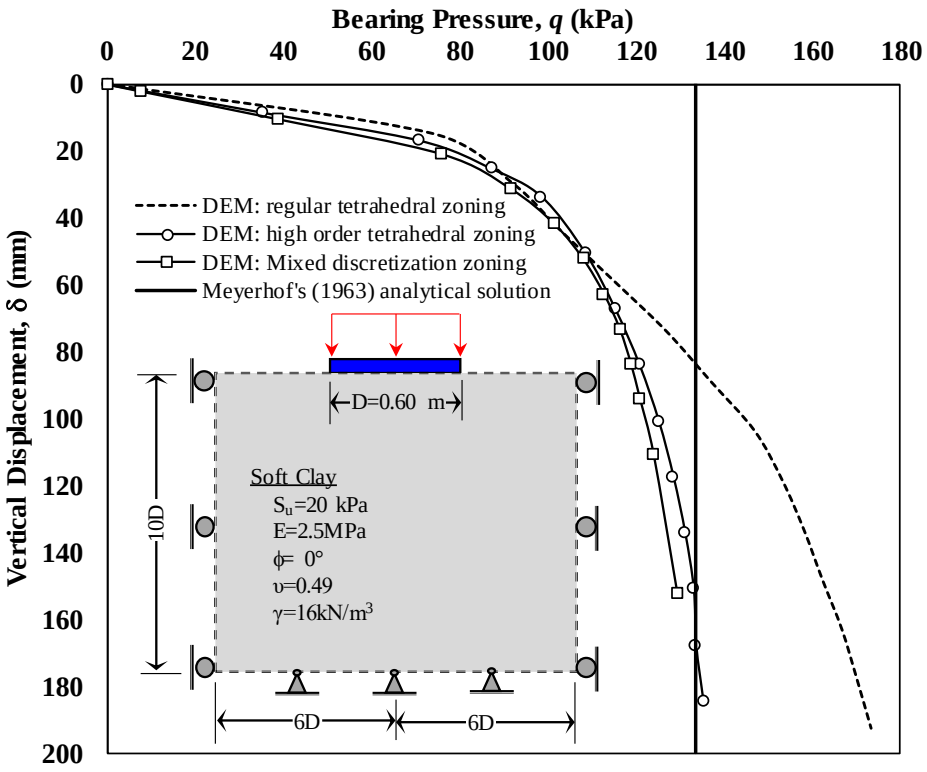

Fig. 4.2. Bearing pressure-displacement responses for rigid circular foundation using different tetrahedral zoning techniques in 3DEC.

Discrete-deformable blocks can be joined to create larger elements of arbitrary shape and thus simulate the mechanical response of a continuous material. Joined-deformable blocks were used to model the clay soil material surrounding the column, whereas mixed zone discretization was used to refine the blocks located near the aggregate columns to improve the accuracy of computed deformations, confining and shear stress distributions, and development of displacements along the soil-column interface. The aggregate material comprising the stone columns was also generated using block elements, which are discrete and deformable according to specified constitutive characteristics and unique to this study (Fig. 4.3). Although the block size distribution does not precisely replicate the aggregate gradations, the blocks were refined

and internally discretized into tetrahedrons to better capture the non-linear behavior of the aggregate.

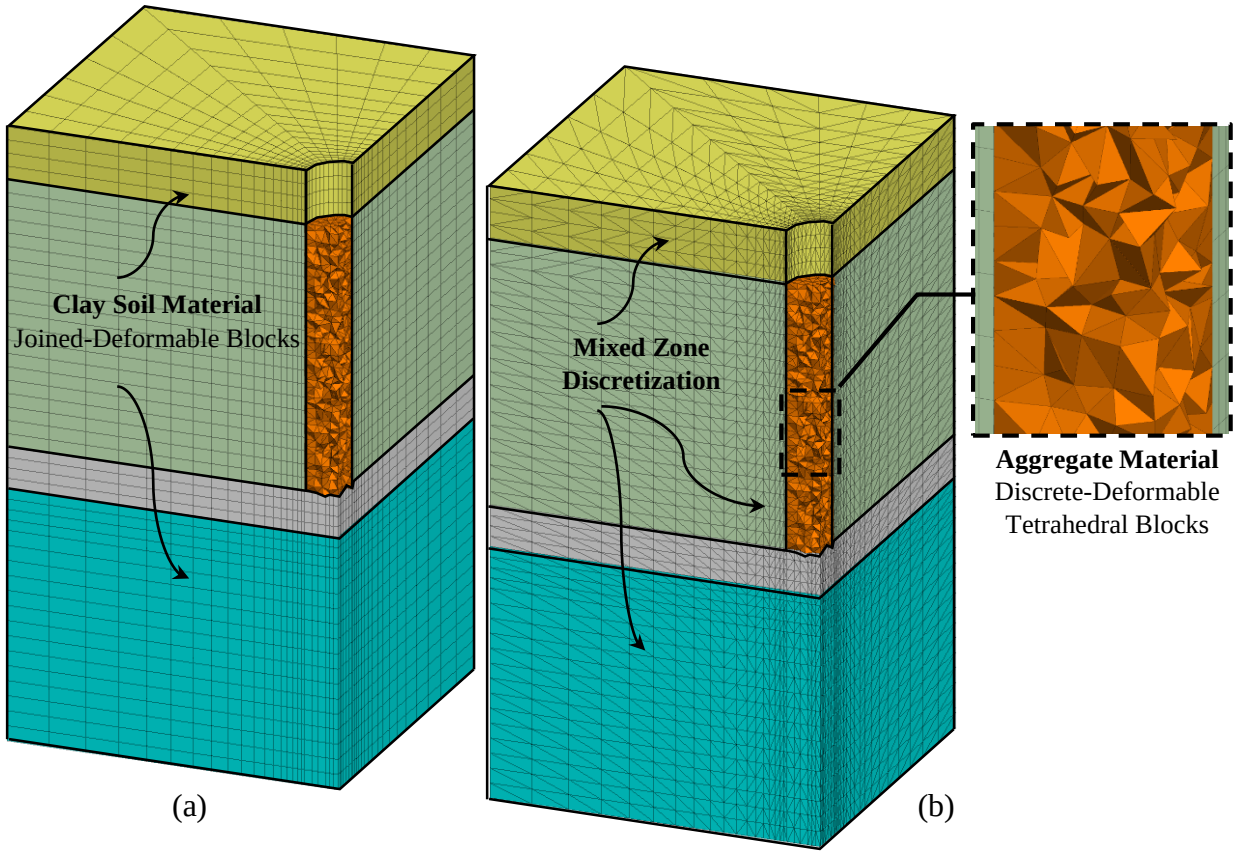

Fig. 4.3. Block generation and zone discretization generated in 3DEC for full-scale stone column simulations (only a quarter of the model is presented). (a) deformable block generation and (b) mixed zone discretization.

4.4 Numerical Modeling of Full-Scale Field Testing

4.4.1 Model Geometries and Boundary Conditions

The dimensions of the 3D-DEM models were selected based on the full-scale loading tests previously described (Table 4). For all the full-scale 3D-DEM simulations, global boundary conditions of the numerical mesh are specified in the usual manner, with vertical and lateral fixity applied to the bottommost blocks and lateral fixity applied to the sides of the mesh nodes.

The boundary conditions are located as far as possible from the model central axis to minimize their effects on the simulation results, and they are defined based on the foundation dimensions. Vertical displacement was uniformly applied on the rigid foundation to simulate the plate bearing testing. Fig. 4.4 shows the model boundary conditions and block mesh generated in 3DEC for small-footings supported on single, uncemented stone column simulations. The polyhedral faces are not shown for clarity. Similarly, Fig. 4.5 illustrates the model boundary conditions and geometries corresponding to the cemented stone column.

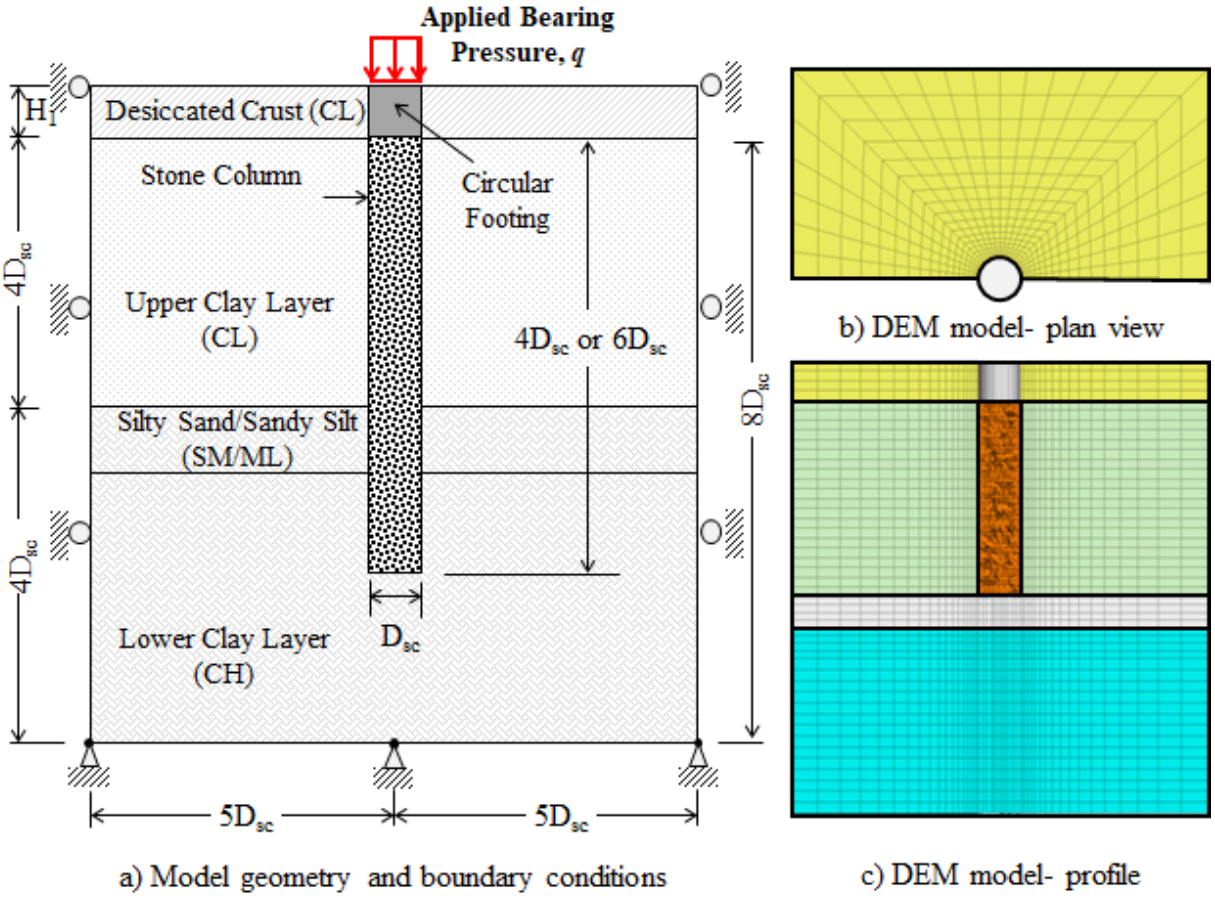

Fig. 4.4. Typical 3DEC mesh and model geometry used in the numerical simulations of small footings on single stone columns constructed with uncemented aggregate. (a) example soil layering for a pier with slenderness ratio of four, and six, (b) plan view of the mesh, and (c) side view of mesh through an isolated, single stone column.

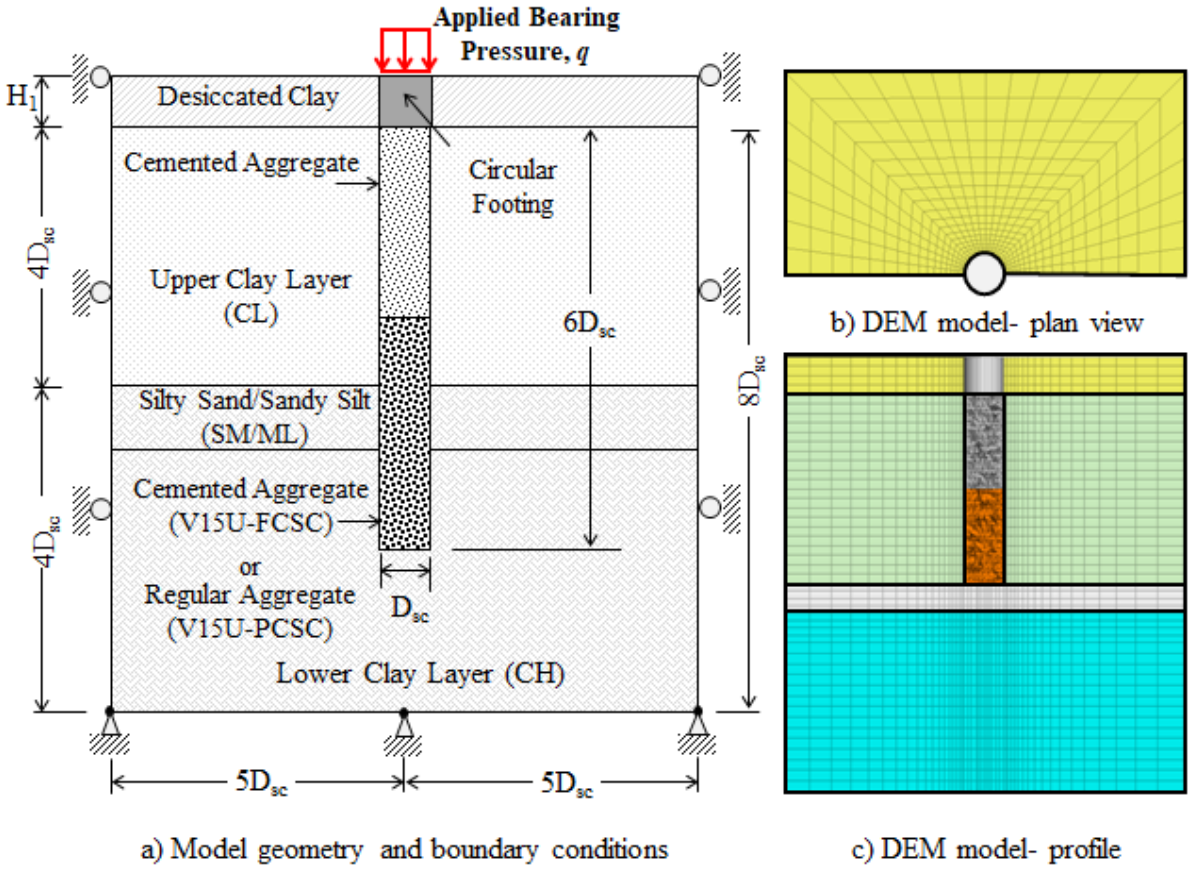

Fig. 4.5. Typical 3DEC mesh and model geometry used in the numerical simulations of small footing on a single stone column constructed with cemented aggregate. (a) example soil layering for a pier with slenderness ratio of six, (b) plan view of the mesh, and (c) side view of mesh through an isolated, single stone column.

The dimensions of the 3D-DEM simulations of large foundations supported on five stone columns were selected to replicate the field test conditions previously discussed. The model geometry, section of block mesh, simplified soil stratigraphy, and boundary conditions are illustrated in Fig. 4.6.

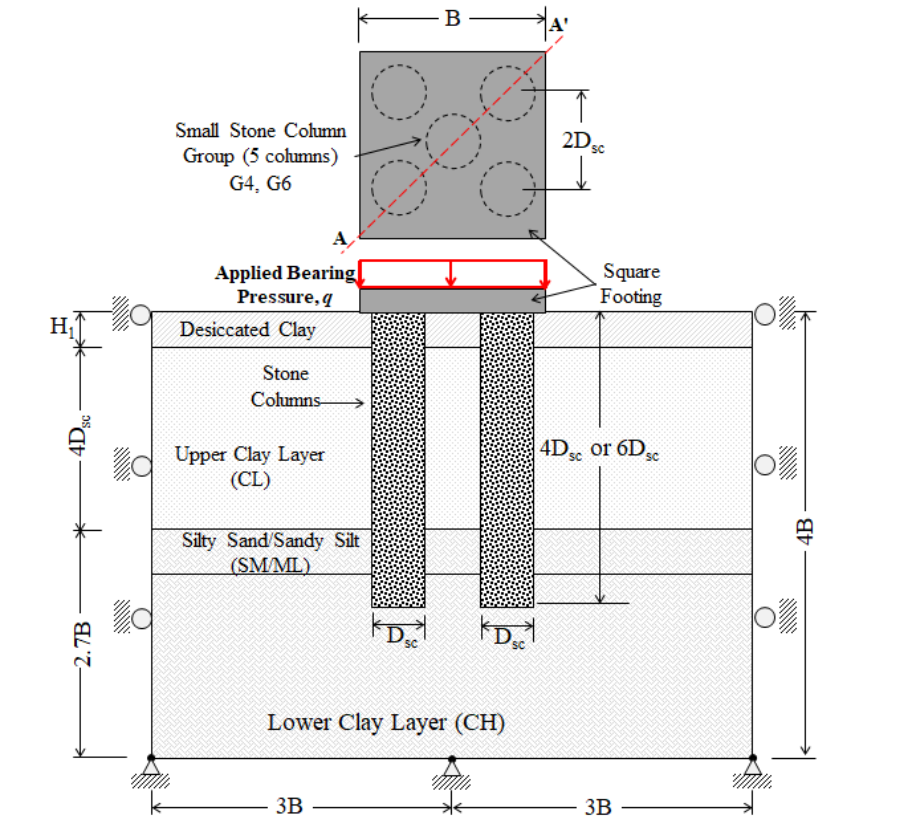

(a) Model geometry and boundary conditions

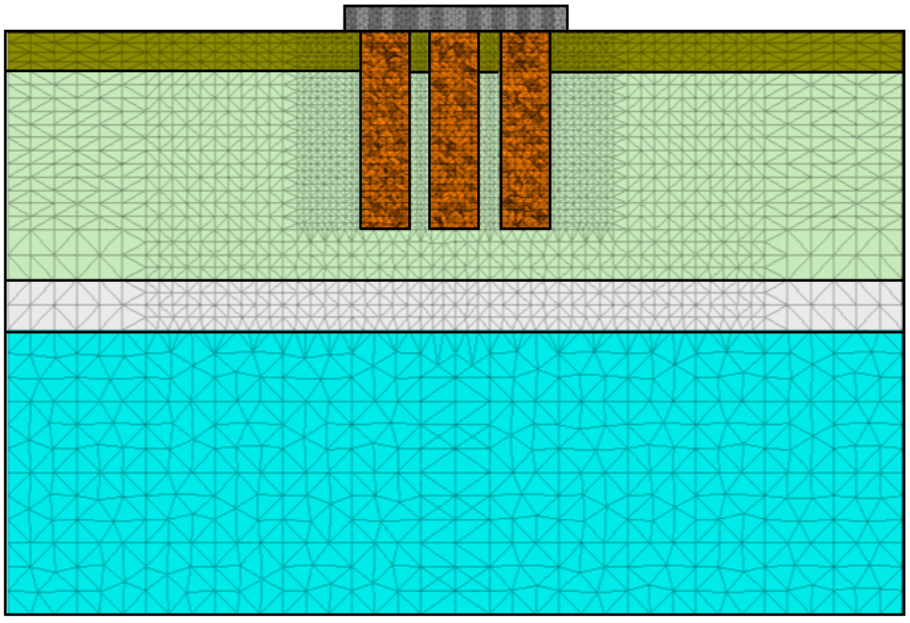

(b) DEM model along section A-A'

Fig. 4.6. 3DEC mesh and model geometry used in the numerical simulations of large footings on a small group of stone columns constructed with uncemented aggregate. (a) example soil layering for a pier with slenderness ratio of six, and (b) side view of mesh along section A-A'.

Variation in the geometry of field test conditions were conducted to simulate alternative geometric models for footings resting on five-column groups. Fig. 4.7 shows the geometric configurations for an equivalent diameter single stone column and unit-cell model, respectively.

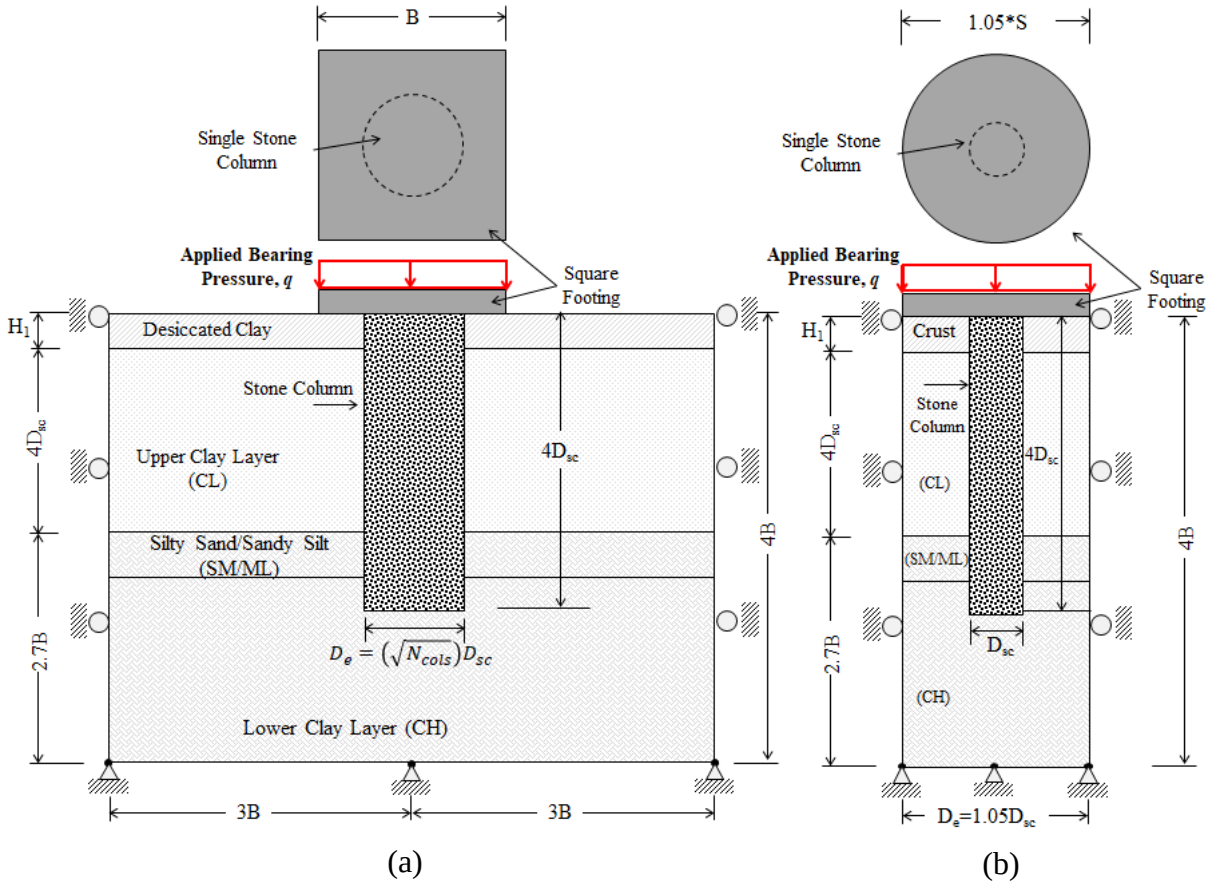

Fig. 4.7. Alternative geometric models for large footings on small group of stone columns. (a) equivalent column diameter and (b) unit-cell model.

4.4.2 Model Validation of the Native Soil (Overconsolidated Clay)

In order to select appropriate constitutive model parameters for the native soil, information reported from a variety of sources (largely from previous studies of the same test site) were used. The bearing pressure-displacement responses of the baseline small and large footings were then evaluated to validate the models. The native soils were modeled using the

linear elastic-perfectly plastic stress-strain response with the Mohr-Coulomb failure criterion and the nonlinear Duncan-Chang model (Duncan and Chang 1970). Duncan-Chang model assumes a hyperbolic stress-strain response where the deviatoric stress (σ_1-σ_3) is expressed as a function of the axial strain (ε) and initial undrained Young's modulus (E_{cu}), as presented in Eq. (35), with the failure criterion defined by the available undrained shear strength (Eq. 36) for undrained conditions (Stuedlein and Holtz 2010).

$$\sigma_1 - \sigma_3 = \frac{\varepsilon}{\frac{1}{E_u} + \frac{\varepsilon}{(\sigma'_1 - \sigma'_3)_{ult}}} \tag{35}$$

$$(\sigma'_1 - \sigma'_3)_{ult} = 2 \times s_u \tag{36}$$

Geotechnical properties (e.g., OCR, s_u, lateral earth pressure coefficient at-rest, K_o, undrained Young's modulus, E_u) for the clayey layers are selected based on the laboratory test data for samples retrieved from the test site reported by Stuedlein and Holtz (2010) in conjunction with CPT results, correlations, and a geostatistical model of the 3D spatial variability (Stuedlein et al. 2012c). Fig. 4.8 illustrates the variation of the undrained Young's modulus for the native soils with depth resulting from CIU triaxial strength tests at different confining pressures (Stuedlein and Holtz 2010), and the correlations proposed by Duncan and Buchignani (1987).

Profiles of s_u with depth for the selected footing loading tests (Table 2) are shown in Fig. 4.9, including the variability inferred from the calibrated geostatistical model. The s_u profile was subdivided into small sublayers (0.30 m thick) to more realistically represent the profile of s_u

within the bulging zone. Fig. 4.9b illustrates the comparison of the field s_u profile and the representative s_u profile that was used to simulate column V10PW (DEM models were developed using a representative s_u profile corresponding to each footing location).

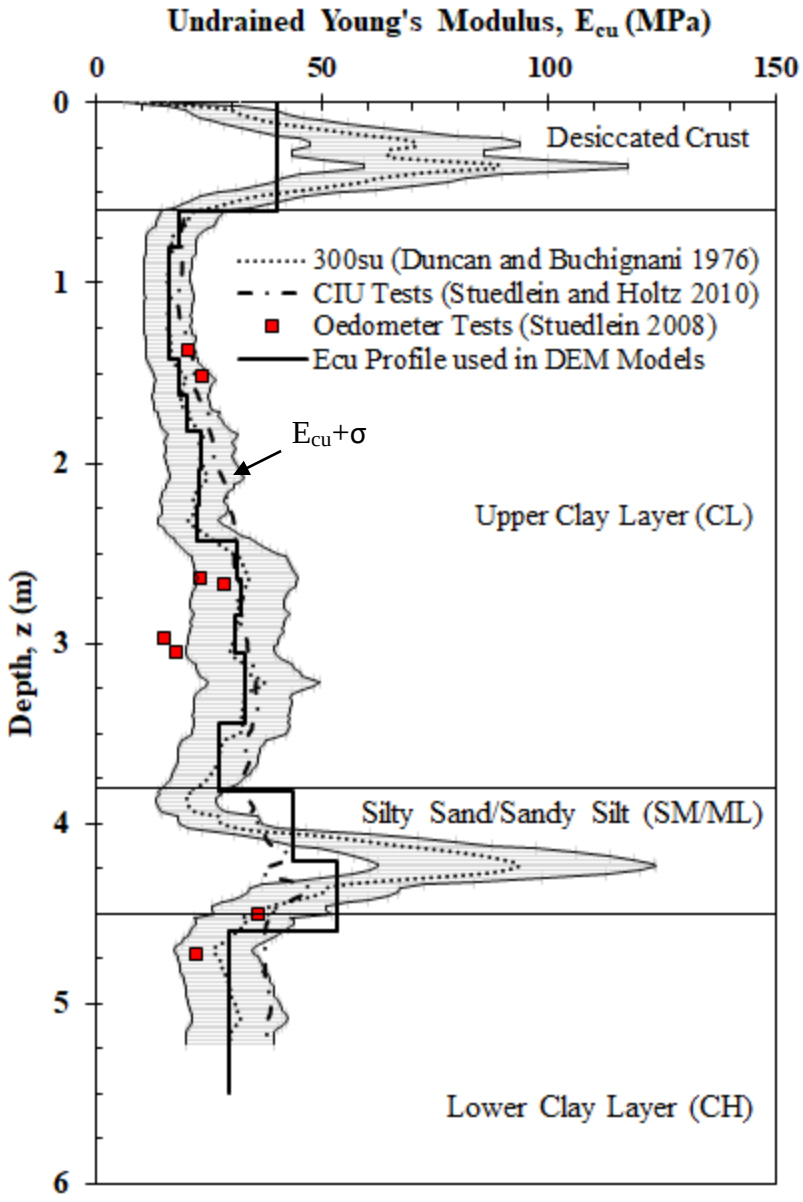

Fig. 4.8. Variation of the undrained Young's modulus for native soils with depth using laboratory testing results and correlations.

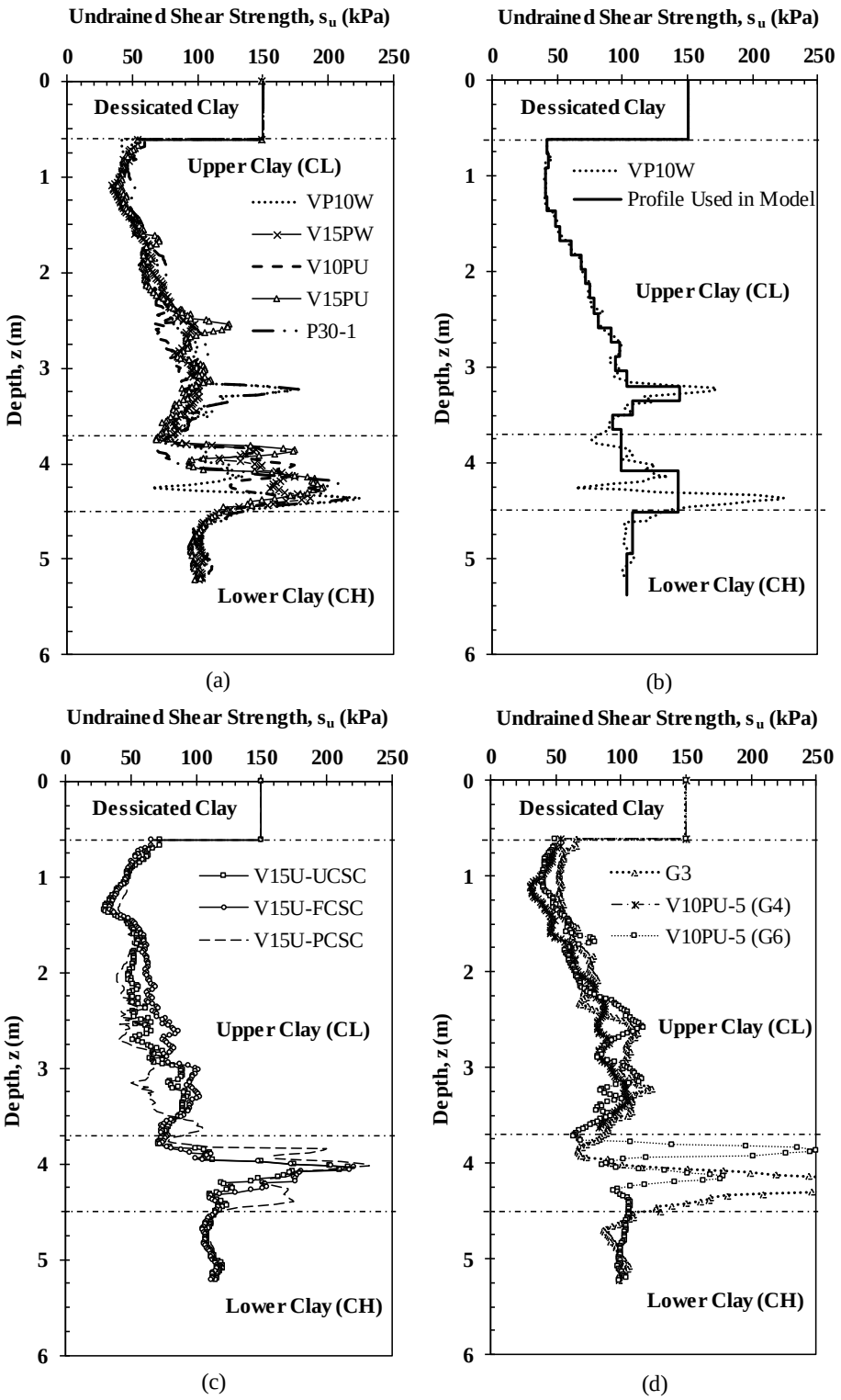

Fig. 4.9. Profiles of s_u for the (a) single-uncemented stone columns, (b) approximated s_u profile used in the model for stone column VP10W, (c) single-cemented stone columns, and (d) small-uncemented stone column groups (data from Stuedlein 2008).

A three-dimensional CIU triaxial test simulation (Fig. 3.3a; Test R6-CL; OCR=17.2; σ'_3=46 kPa) was developed to calibrate the constitutive response of the native soil by implementing the Duncan-Chang model (Eq.35-36) and using joined-deformable blocks. Fig. 4.10 indicates that the numerical stress-axial strain response is in a good agreement with the laboratory response; hence, validating the ability of the 3D DEM models to adequately capture the response of continuum materials (e.g., cohesive soils). However, it is important to highlight that the use of joined deformable blocks is more a finite difference method than DEM. 3D DEM simulations of the small, 0.76 m circular footing (P30-1) and large, 2.74 m square footing (G3) supported on unimproved ground were conducted to validate the selected constitutive model parameters for the native soil. Table 6 summarizes the constitutive model parameters used to simulate the native soils.

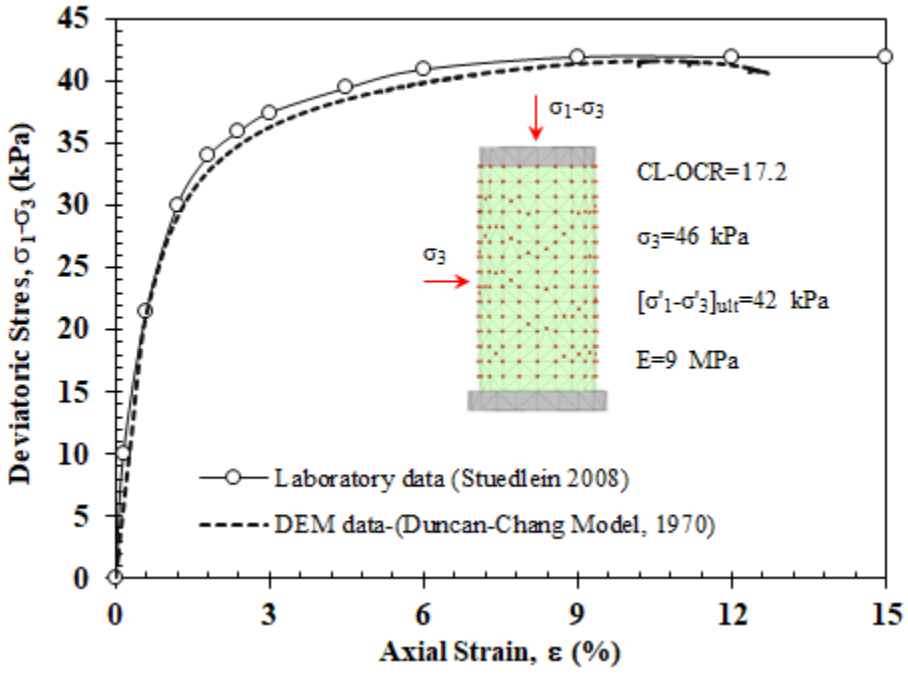

Fig. 4.10. Comparison of numerical and measured deviatoric stress-axial strain responses of CIU triaxial test at a confining pressure of 46 kPa.

The baseline footing (P30-1) was modeled using both the Mohr-Coulomb model and Duncan-Chang model for comparison, whereas the large baseline footing (G3) was only modeled using the hyperbolic model (Duncan and Chang 1970). The q-δ responses of the baseline footings simulated using the selected model parameters are compared with the observed responses corresponding to the footing (P30-1) in Fig. 4.11. The numerical results indicate good agreement with the field data for the range in displacements considered, thus validating the small footing DEM model and constitutive parameters used for the native soils.

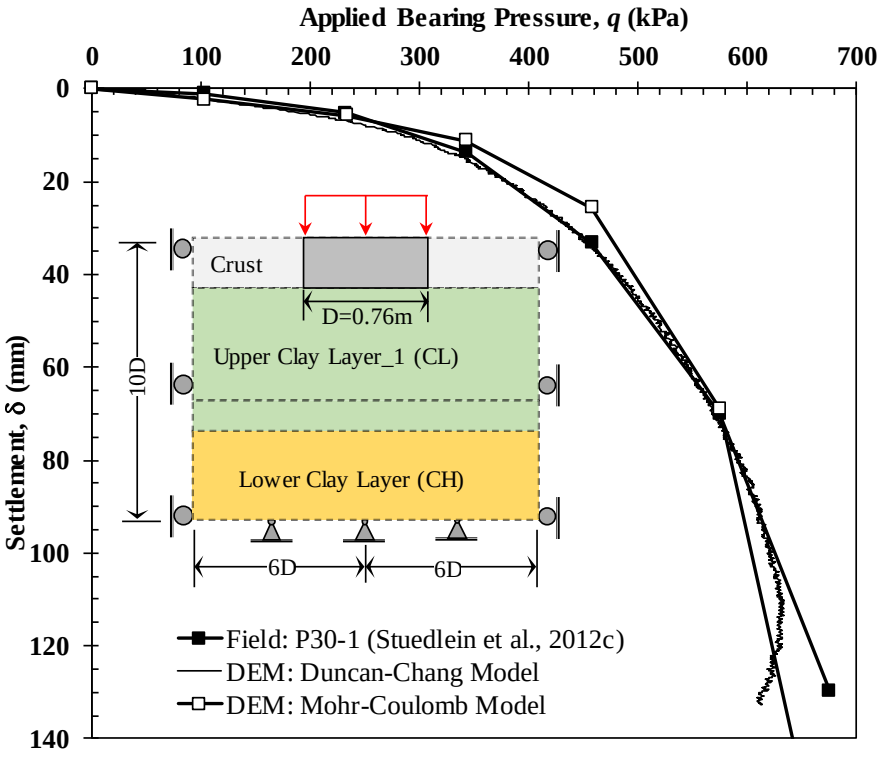

Fig. 4.11. Comparison of the bearing pressure-displacement curves for the small footing, P30-1.

During the field footing loading test, vertical displacements and rotations were monitored at three different locations on the foundation (i.e., dial gauges 1-3) in a triangular configuration for the large footing G3 (Stuedlein 2008). Then, the average vertical displacements at the

foundation center were estimated using a triangulation of the observed displacements and rotations at each gauge location as described by Stuedlein (2008). Additionally, Stuedlein (2008) reported that the q-δ point for the last load increment (i.e., 383 kPa) was extrapolated using the q-δ data recorded from the previous load increments due to a failure of the helical reaction anchors before completing the load application time (i.e., 64 min). Fig. 4.12 shows that the numerical and field q-δ responses for footing G3 agree well throughout the range of observed displacements at each gauge location, indicating a satisfactory validation of the constitutive parameters of the native soils.

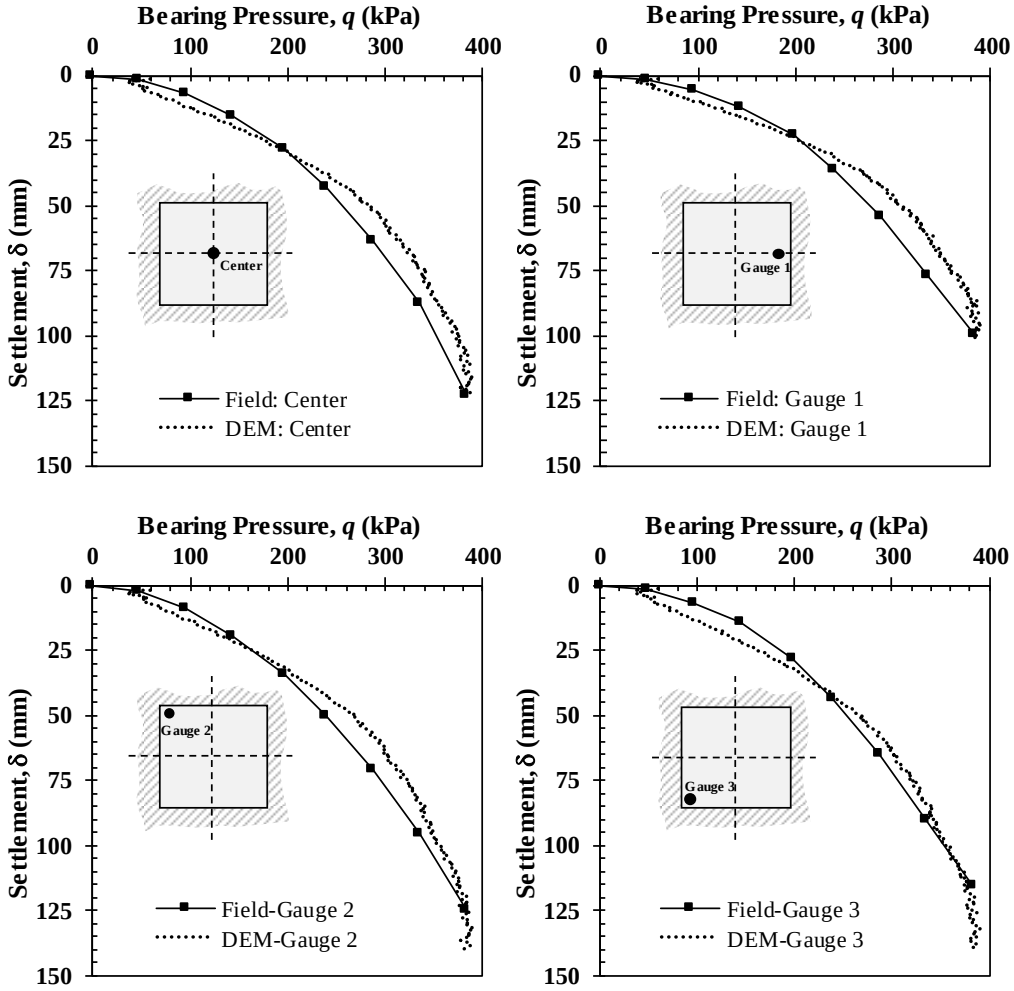

Fig. 4.12. Comparison of the bearing pressure-displacement curves for large footing G3.

Table 6. Summary of model parameters used in the DEM simulations for native soils.

Material	T [m]	γ [kN/m^3]	v ---	E_{cu} [MPa]	s_u [kPa]	PI [%]	OCR ---
Desiccated Crust (CL)	0.60	17	0.495	30-40	130-170	---	>20
Upper Clay (CL)	3.2	18	0.495	Fig. 4.8	Fig. 4.9	26	12
Lower Clay (CH)	---	19	0.495	Fig. 4.8	Fig. 4.9	42	6
Foundation (P30-1)	0.60	23.5	0.20	30000	---	---	---
Foundation (G3)	0.40	23.5	0.20	30000			

T=thickness, γ= total unit weight, ν= Poisson's ratio, E_{cu}= undrained Young's modulus, OCR= overconsolidation ratio, PI= plasticity index, s_u= undrained shear strength,

Lateral soil displacements adjacent to the large footing G3 were measured at depth intervals of approximately 0.305 m using a vertical inclinometer casing installed to a depth of 10.7 m below the ground surface and at an approximate distance of 0.20 m away from the edge of the footing (Stuedlein et al. 2010). Fig. 4.13 compares the estimated and observed profiles of lateral soil displacements with depth adjacent to the footing G3. However, it is clearly noticed that the DEM simulation overestimates the measured lateral displacements for all applied bearing pressure increments. The numerical results indicate a maximum lateral displacement of 29 mm at a depth 0.90 m, which is approximately 32% greater than the maximum observed lateral movement (i.e., 22 mm) at the same depth for q = 335 kPa. No comparisons were made between simulated and measured profiles for q = 383 kPa since no increase in the lateral displacement profile was observed for this last bearing pressure increment (Stuedlein 2008). Minimal lateral soil movements were observed for depths greater than the size of the foundation (B=2.74 m),

with negative lateral displacements for depths ranging from 1*B* to 2*B* likely generated by casing bending (Stuedlein 2008). However, the numerical results show that lateral movement is negligible for depths greater than 2*B.*

The variability with depth of the undrained Young's Modulus (Fig. 4.8) and coefficient of lateral earth pressure at-rest condition (Fig. 3.5d) at the site were investigated as a possible factor influencing the lateral soil displacement profile by considering the standard deviation (σ) in these both parameters. Figs. 4.14 and 4.15 present comparisons of the lateral displacement profiles incorporating the mean (E_{cu} and K_o) + σ with depth, respectively, indicating close agreement with the observed data. However, these incorporations of σ in E_{cu} and K_o, respectively, resulted in stiffer q-δ responses of G3 (Fig. 4.16).

The bentonite-cement grout stiffness and anisotropic behavior of the native soils are other possible factors affecting the inclinometer measurements but are more difficult to implement in the DEM models because of a lack of data to conduct a proper model calibration. As a result of the good agreement of the q-δ responses with the field data for both baseline footings (P30-1 and G3) , constitutive parameters for the native soils (Table 6) were considered calibrated despite the slight difference in the lateral displacements and were used for the surrounding soil in subsequent simulations considering the aggregate-reinforced soil.

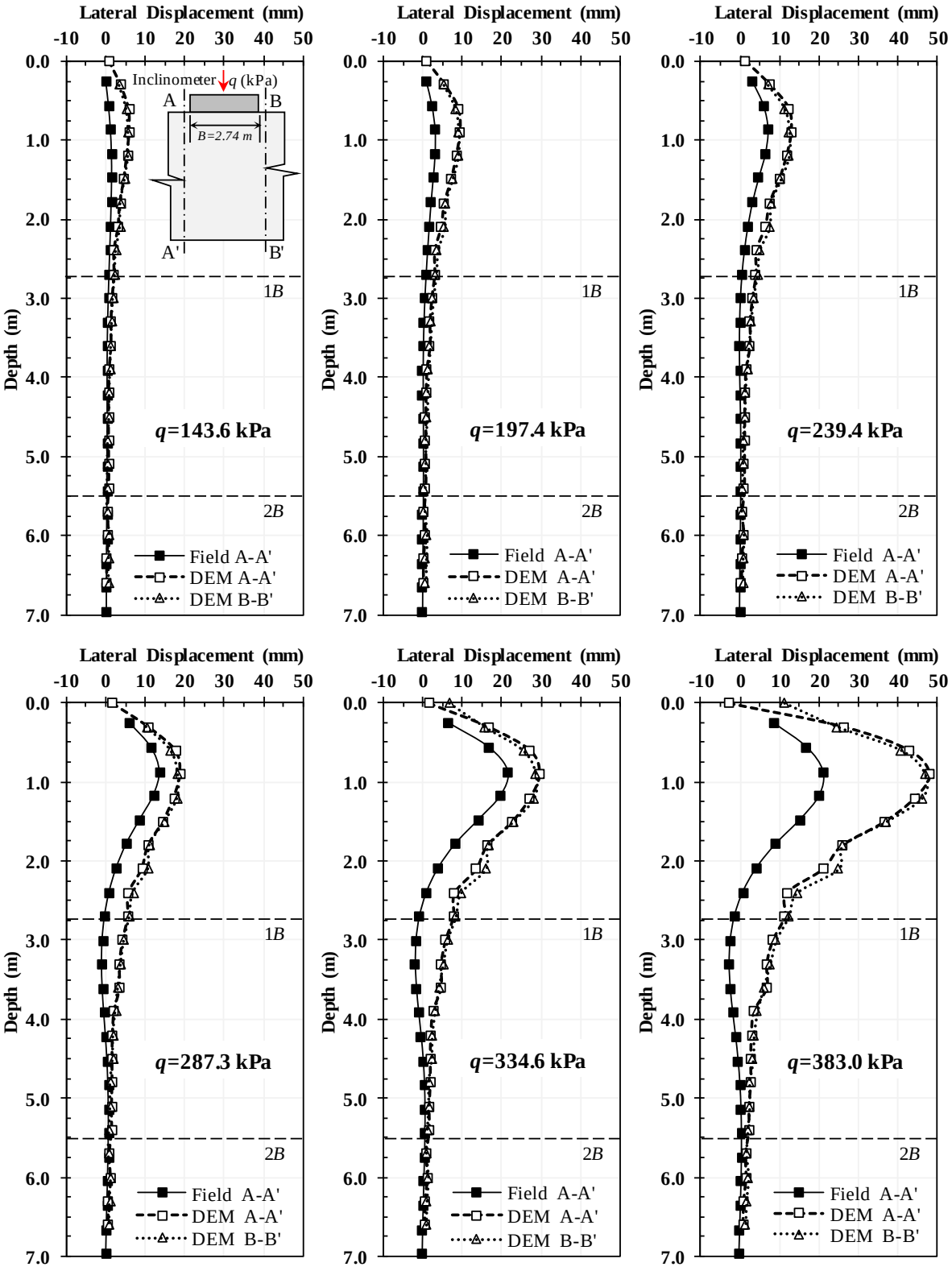

Fig. 4.13. Comparison of profiles of lateral soil movements adjacent to the large footing G3.

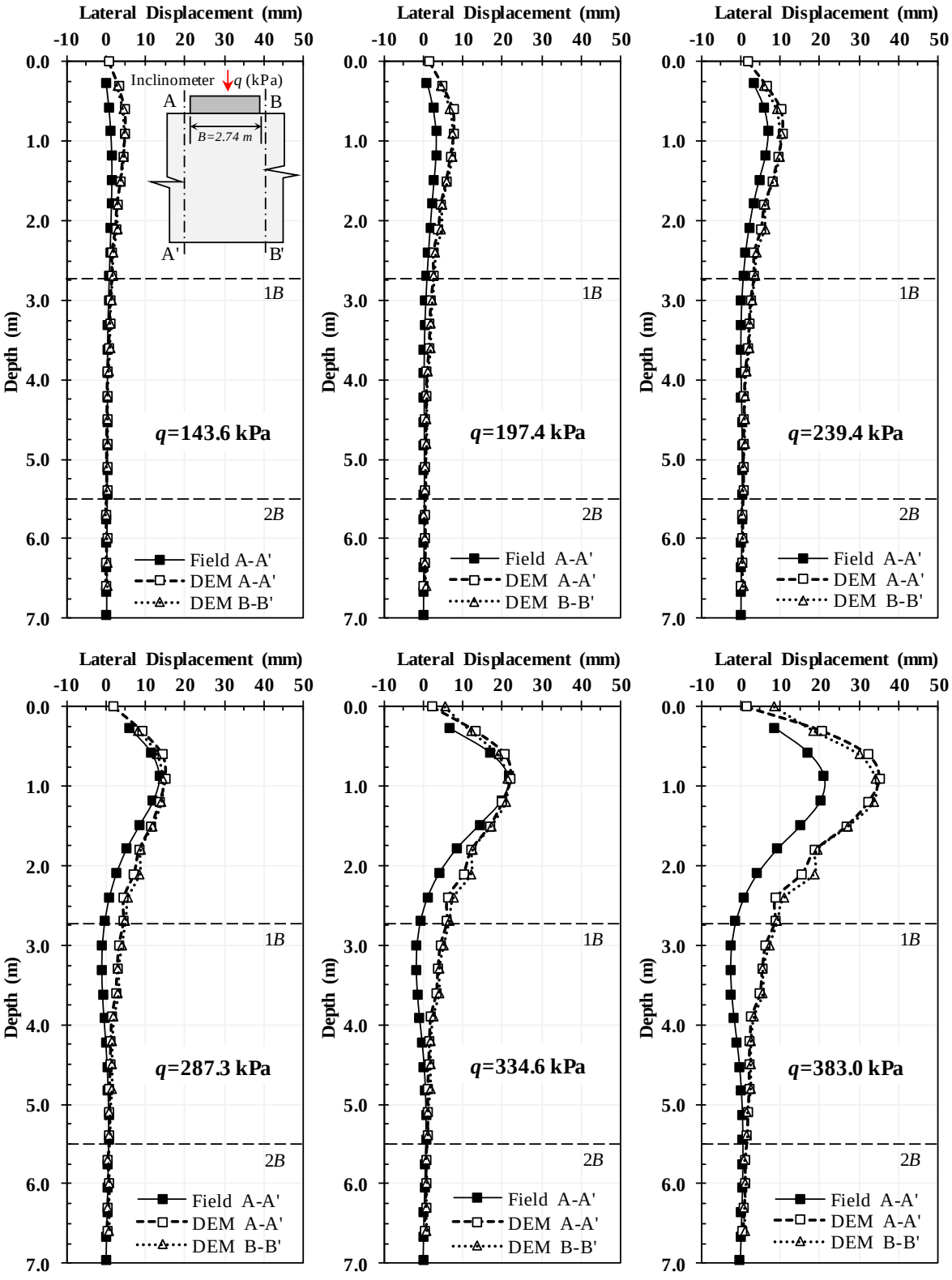

Fig. 4.14. Comparison of profiles of lateral soil movements adjacent to the large footing G3 considering the mean E_{cu} + σ.

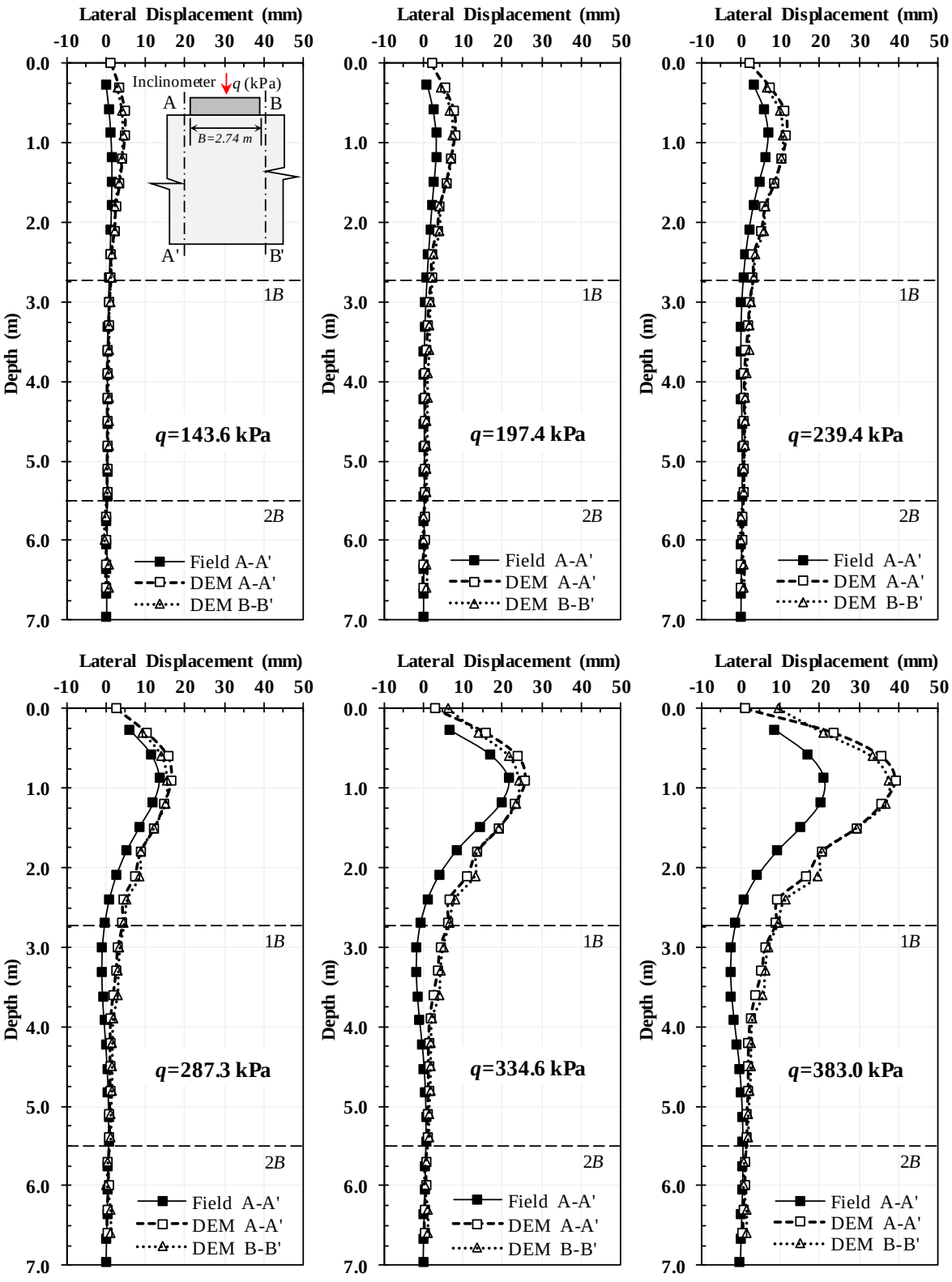

Fig. 4.15. Comparison of profiles of lateral soil movements adjacent to the large footing G3 considering the mean K_o + σ.

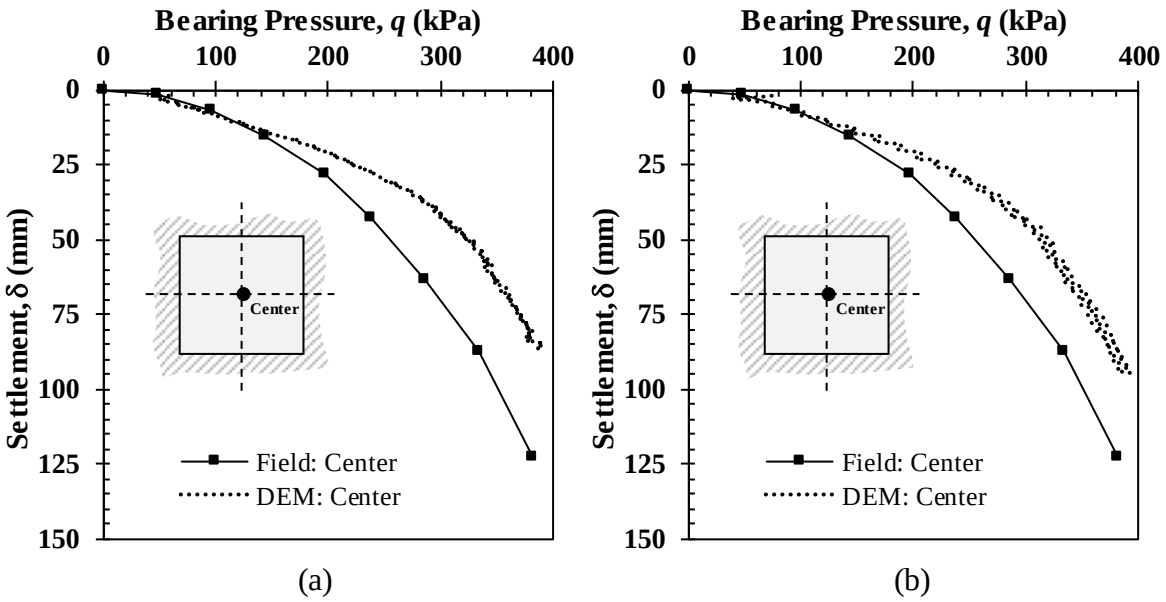

Fig. 4.16. Comparison of the bearing pressure-displacement responses for large footing G3 considering (a) the mean E_{cu} + σ, and (b) the mean K_o + σ.

4.4.3 Model Validation of the Stone Column Aggregates

Newton (2014) performed a laboratory investigation of the stiffness, strength, and stress-dilatancy characteristics of the uniformly-graded uncemented material used in the full-scale experimental program. The well-graded material shared similar angularity, gradation, and mineralogy as those reported by Duncan et al. (2007), and the variation of friction angle, dilation angle, and Young's modulus with confining stress for these aggregates were used herein for this material. A comparison of the aggregates evaluated using isotopically-consolidated triaxial compression tests reported by Duncan et al. (2007) and Newton (2014) is presented in Fig. 4.17, alongside those used in the construction of the stone columns. The relationships presented provide the mechanical response for the aggregates at relative densities similar to those expected in the constructed stone columns.

The strength, dilatancy, and stiffness of these granular materials, as represented by the peak internal friction angle, ϕ'_{sc}, dilation angle, ψ_{sc}, and Young's modulus, E_{sc}, respectively, vary considerably owing to the suppression of dilation with increases in radial confining pressure, σ'_r, as illustrated in Fig. 4.17.

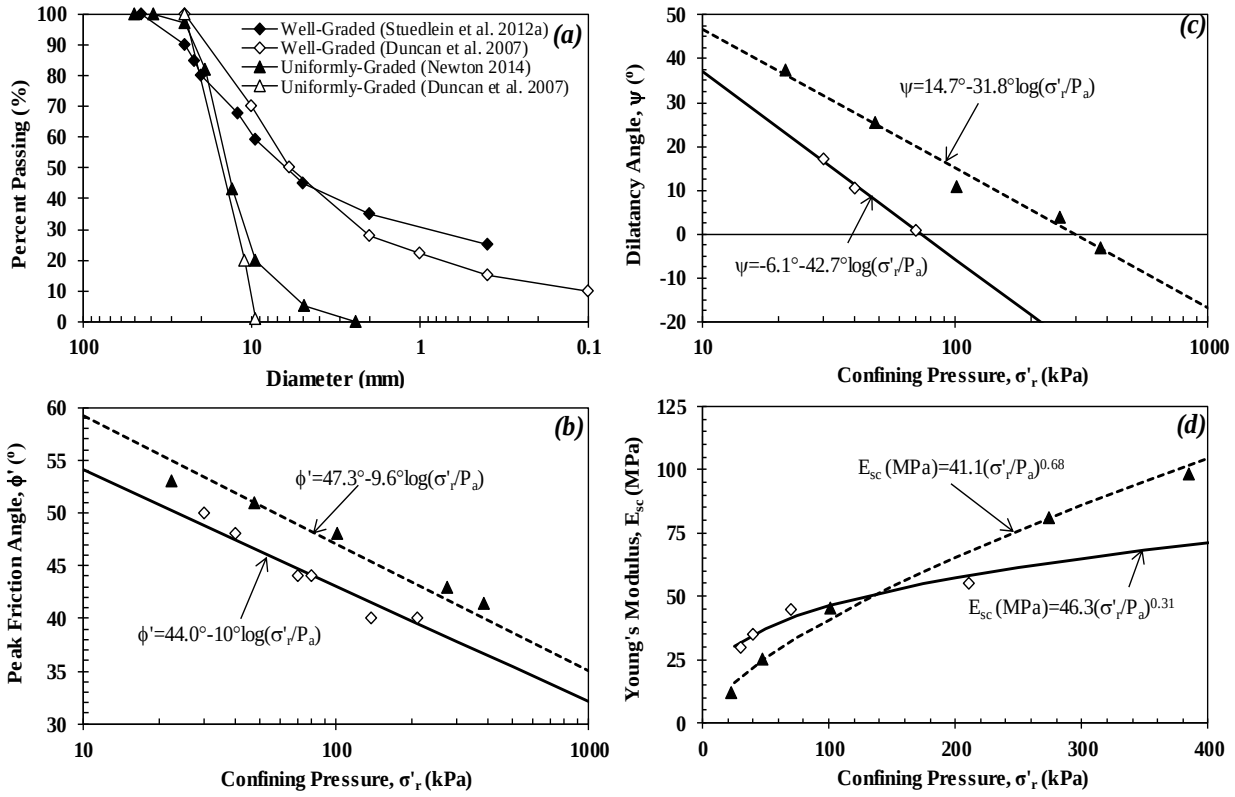

Fig. 4.17. Mechanical response of well-graded (D_r=66-86%) and uniformly-graded (D_r=67-72%) aggregates: (a) gradations commonly used in stone columns, (b) variation of peak friction angle with effective confining pressure, (c) variation of dilation angle with effective confining pressure, (d) variation of initial Young's Modulus with effective confining pressure (data from Duncan et al. 2007, Stuedlein et al. 2012a, and Newton 2014).

For ease of comparison and specification in the numerical models, the frictional response and stiffness of the well-graded aggregates with D_r ranging from 66 to 72% was represented using (Duncan et al. 2007),

$$\phi'_{sc}=44°-10° \log\left(\frac{\sigma'_r}{P_a}\right) \quad (37)$$

$$\psi_{sc}=-6.1°-42.7° \log\left(\frac{\sigma'_r}{P_a}\right) \quad \text{for } \psi_{sc}>0 \quad (38)$$

$$E_{sc}(\text{MPa})= 46.3\left(\frac{\sigma'_r}{P_a}\right)^{0.31} \quad (39)$$

and the frictional response and stiffness of the uniform-graded aggregates with D_r ranging from 66 to 86% was described using (Newton 2014)

$$\phi'_{sc}=47.3°-9.6° \log\left(\frac{\sigma'_r}{P_a}\right) \quad (40)$$

$$\psi_{sc}=14.7°-31.8° \log\left(\frac{\sigma'_r}{P_a}\right) \quad (41)$$

$$E_{sc}(\text{MPa})= 41.1\left(\frac{\sigma'_r}{P_a}\right)^{0.68} \quad (42)$$

where P_a is atmospheric pressure (101.3 kPa).

Newton (2014) also conducted a laboratory investigation on the aggregate used by Stuedlein (2008) to determine the main factors affecting the mechanical behavior of lightly-cemented granular material and typical strength parameters that could be used in the design of cemented stone columns. Cemented specimens were prepared using 5 and 10% Portland cement type I/II by dry aggregate weight with a 0.55 water-cement ratio (Newton, 2014). Based on the results from consolidated drained triaxial tests, Newton (2014) reported a significant improvement in the compressive strength and modulus of elasticity of the cemented aggregate specimens with respect to the uncemented aggregate specimens. It was also noted that the cemented aggregate specimens exhibited more strain-softening and reached their peak principal stress differences (i.e., peak deviatoric stress) at lower axial strains than the uncemented specimens at similar effective confining stress, as illustrated in Fig. 4.18. Newton (2014) also

mentioned that the axial strain at peak stress for the 5% cement specimens ranged between 2.8 to 4.1%, while for the 10% cement specimens, it ranged between 1.7 to 2.7%. Therefore, the axial strain values at peak (i.e., failure) are essential input parameters in order to define an appropriate constitutive material model that can numerically represent the mechanical behavior of cemented aggregate columns.

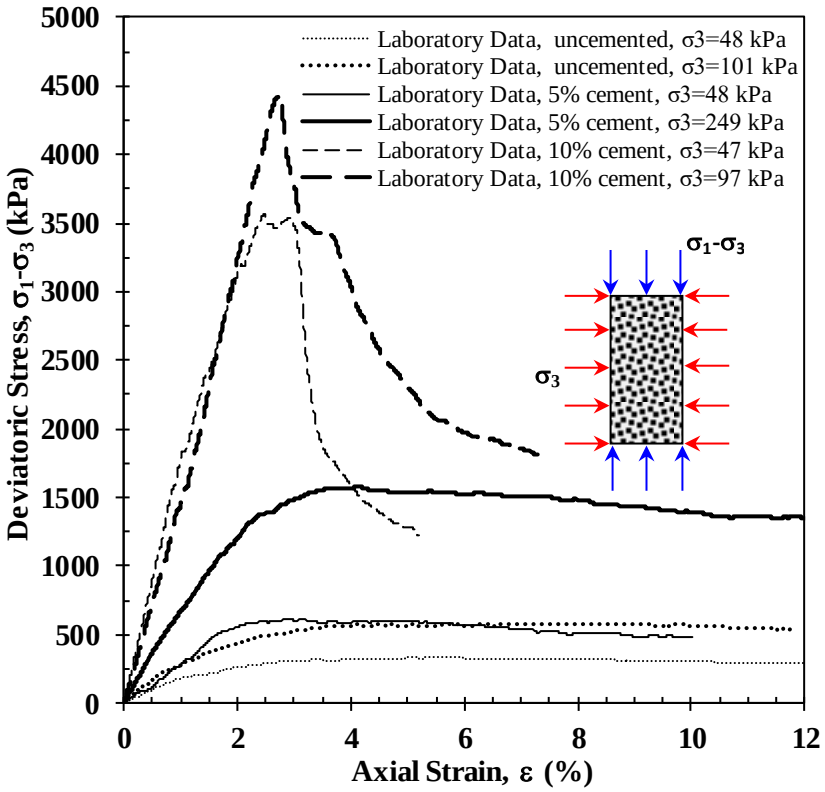

Fig. 4.18. Comparison of the deviatoric stress-axial strain responses for different confining stress conditions for uncemented and cemented specimens (data from Newton 2014).

Three-dimensional triaxial test simulations were conducted to calibrate the constitutive model used for the stone column aggregate. Discrete-deformable blocks were used to simulate the aggregate while joined-deformable blocks were used to simulate the latex membrane. Simulations were conducted at two different initial confining stresses and compared to laboratory

data from Duncan et al. (2007). Each discrete-deformable block comprising the aggregate material was modeled using the linear elastic-perfectly plastic stress-strain response with the Mohr-Coulomb failure criterion (provided in Fig. 4.17) rather than using rigid blocks, as in previous studies. Fig. 4.19 indicates that the stress-strain responses for both aggregate gradations are adequately captured by the DEM triaxial test simulations, thus validating the constitutive model and parameter selection for uncemented aggregate.

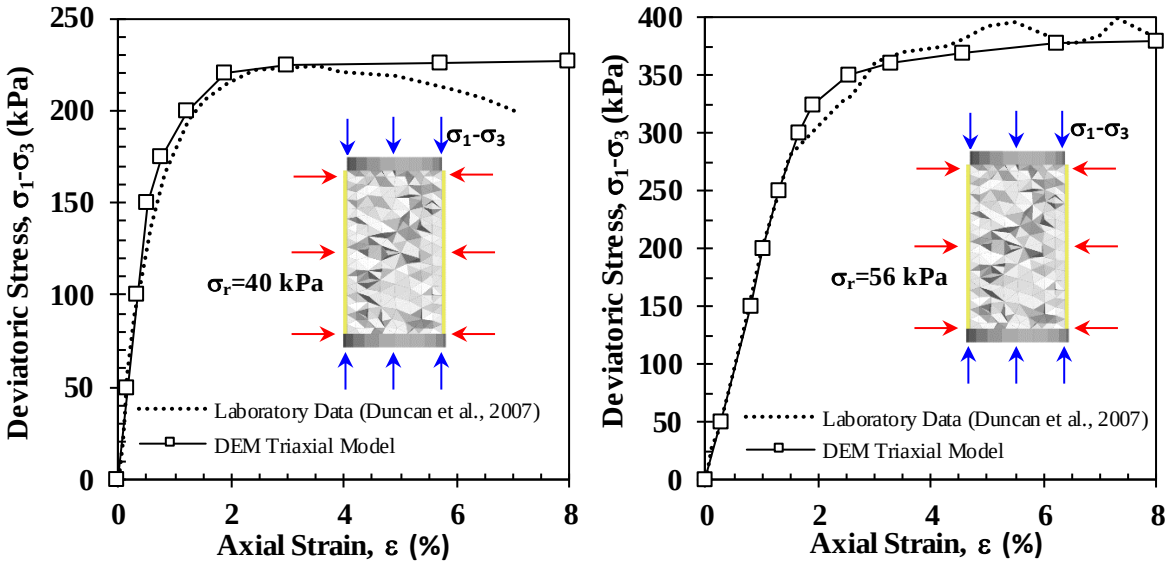

Fig. 4.19. Deviatoric stress-axial strain responses of the aggregate for different confining stress conditions (a) well-graded aggregate ($\sigma_r = 40\ kPa$), and (b) uniformly-graded aggregate ($\sigma_r = 56\ kPa$).

Three-dimensional triaxial test simulations were developed to calibrate and validate the constitutive response of the uncemented and cemented granular material (Fig. 4.20a) based on laboratory triaxial testing conducted by Newton (2014). Joined-deformable blocks were used to represent the latex membrane while discrete-deformable tetrahedral blocks were employed to simulate the aggregate. Strain-hardening/softening models were used to better represent the nonlinear response of the granular material. A strain-hardening/softening model can be

implemented in 3DEC by defining the variation of the material constitutive parameters (e.g., cohesion, friction angle, dilation) as a function the plastic shear strain (Itasca, 2013). A friction-hardening model was used to represent the uncemented aggregate response while the cemented aggregate was simulated by combining a cohesion-softening model with a friction-hardening/softening model as proposed by Vermeer and Borst (1984).

Figs. 4.20b and 4.20c show the model parameter functions (i.e., friction angle and cohesion versus plastic strain) used to simulate the uncemented aggregate and aggregate with 5 and 10% cement content in the triaxial test simulations. Simulations were conducted at two different confining pressures and compared to laboratory data reported in Newton (2014).

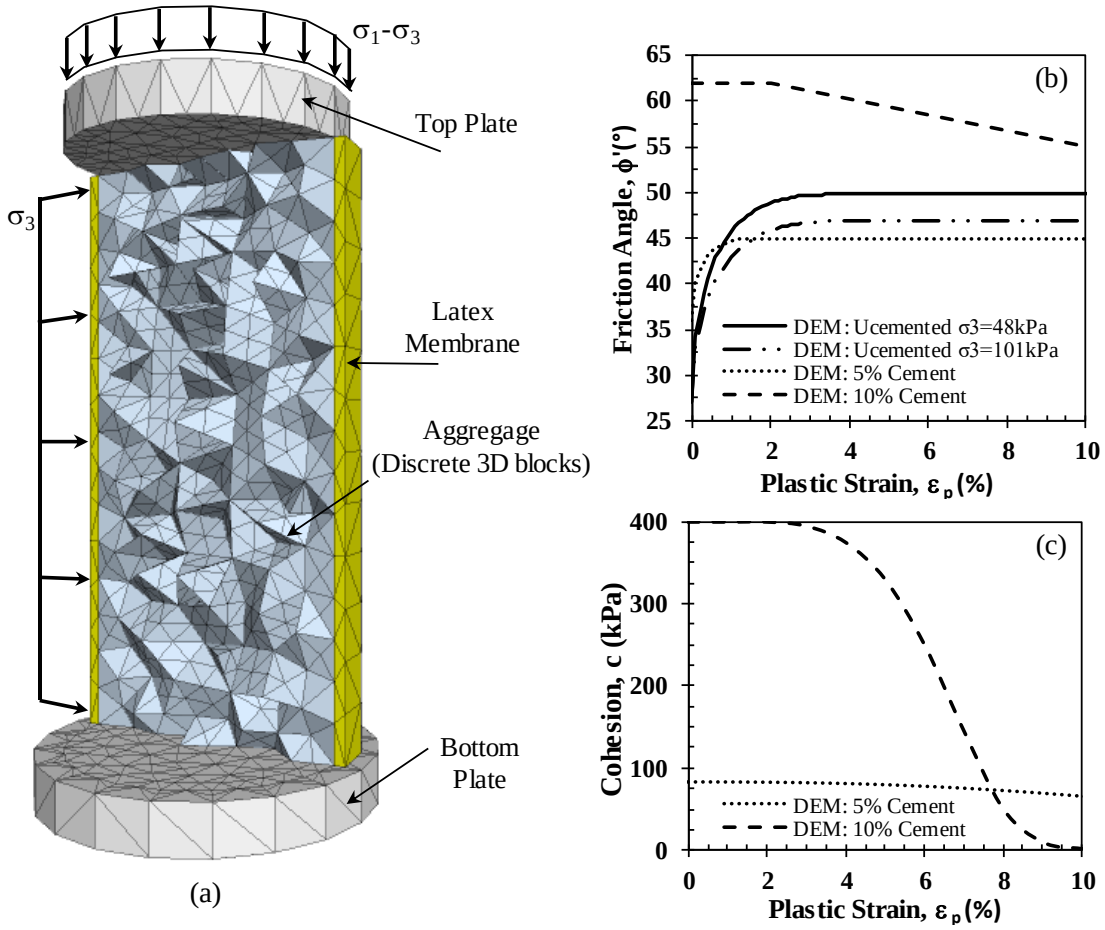

Fig. 4.20. (a) Illustration of the 3D-DEM triaxial simulations, (b) friction-softening/hardening models used in DEM simulations, and (c) cohesion-softening models used in DEM simulations.

Fig. 21a illustrates the deformed-shape of a triaxial simulation, whereas Figs. 21b, 21c, and 21d indicate that the constitutive responses for both uncemented and cemented aggregate are suitably captured by the DEM triaxial test simulations, thus validating the selected model parameters (Table 7).

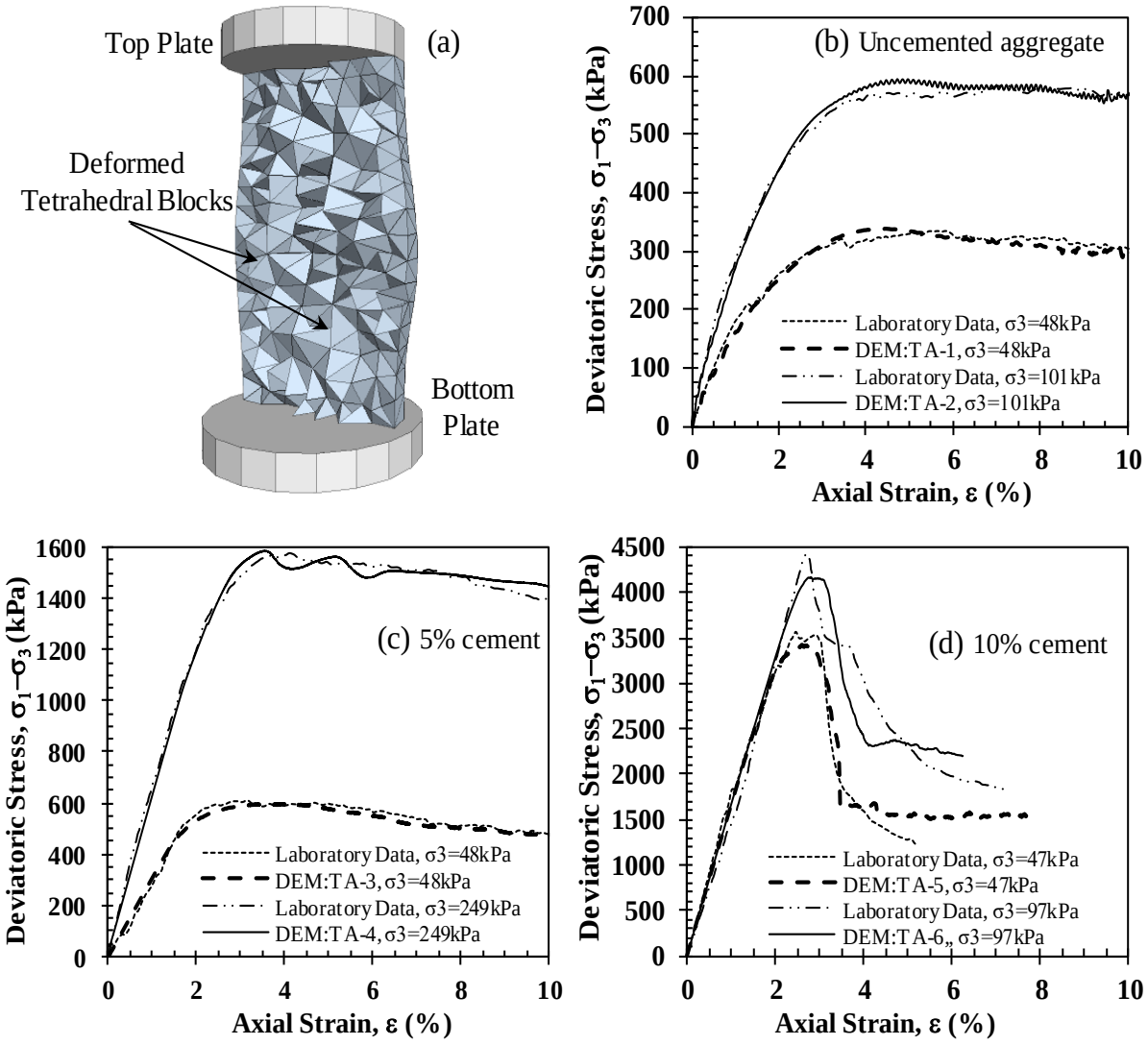

Fig. 4.21. Calibration of the aggregate response: (a) illustration of deformed shape of 3D DEM triaxial simulation, and (b, c and d) deviatoric stress-axial strain responses of the aggregates for different confining stress conditions (data from Newton 2014).

Table 7. Summary of constitutive model parameters used in the triaxial DEM simulations to calibrate the uncemented and cemented aggregates.

Model	Material	Block Material Properties					Joint Properties		
		γ	ν	E	c	ϕ'	J_{kn}, J_{ks}	J_{fri}	J_{coh}
		[kN/m^3]	---	[MPa]	[kPa]	[°]	[GPa/m^2]	[°]	[kPa]
Triaxial	Latex Membrane	14.7	0.49	1.8	---	---	---	---	---
	Top and Bottom Plate	4.9	0.20	20000	---	---	50	30	---
	DEM: TA-1, uncemented	17.9	0.30	41	---	Fig.4.20b	13	40	---
	DEM: TA-2, uncemented	17.9	0.30	25	----	Fig.4.20b	8	40	---
	DEM: TA-3, 5% cement	20.5	0.30	35	Fig.4.20c	Fig.4.20b	30	42	85
	DEM: TA-4, 5% cement	20.5	0.30	80	Fig.4.20c	Fig.4.20b	30	42	85
	DEM: TA-5, 10% cement	20.5	0.30	210	Fig.4.20c	Fig.4.20b	80	65	400
	DEM: TA-6, 10% cement	20.5	0.30	220	Fig.4.20c	Fig.4.20b	80	65	400

γ= total unit weight, ν= Poisson's ratio, E= Young's modulus, c= cohesion, ϕ'=peak friction angle, J_{kn}= joint normal stiffness, J_{ks}= joint shear stiffness, J_{fri}= joint friction, J_{coh}= joint cohesion

4.4.4 Initial Simulations of the Bearing Pressure-Displacement Response of single Uncemented Stone Columns

The Young's modulus of the aggregate columns was estimated considering the available laboratory data (Fig. 4.17d, Duncan et al. 2007; Newton 2014) and the initial geostatic stresses at each stone column location based on cone penetration test (CPT) data (Stuedlein and Holtz 2012a). The average effective confining stress computed around each aggregate column prior to installation is approximately 55 kPa and 50 kPa for column V10PW and V10PU, respectively. Using this value as the σ'_r corresponding to the mid-point of the height of yielding (Stuedlein and Holtz 2013) under the Brauns (1978) bulging failure mechanism, the Young's Modulus estimated from the laboratory aggregate data (Eqs. 39 and 42) is approximately 40 MPa for the

well-graded aggregate columns and 25 MPa for the uniformly-graded aggregate columns (Table 8). Fig. 4.22 compares the observed and simulated q-δ curves for columns V10PW, V15PW, V10PU and V15PU. While good agreement between the column simulations and the observed q-δ responses with well-graded aggregate have been obtained, the response of the uniformly-graded aggregate columns was observed to be mixed. Fig. 4.22b indicates that the numerical response for column V10PU agrees well with the field data; however, simulation of column V15PU overestimates the measured displacements, producing a response similar to that measured for V10PU. Based on the close agreement observed between field and numerical results for columns V10PW and V10PU, these two columns were determined to be validated for the full-scale simulations and were used as references for the sensitivity analyses conducted to investigate the factors that may have influenced the response of column V15PU.

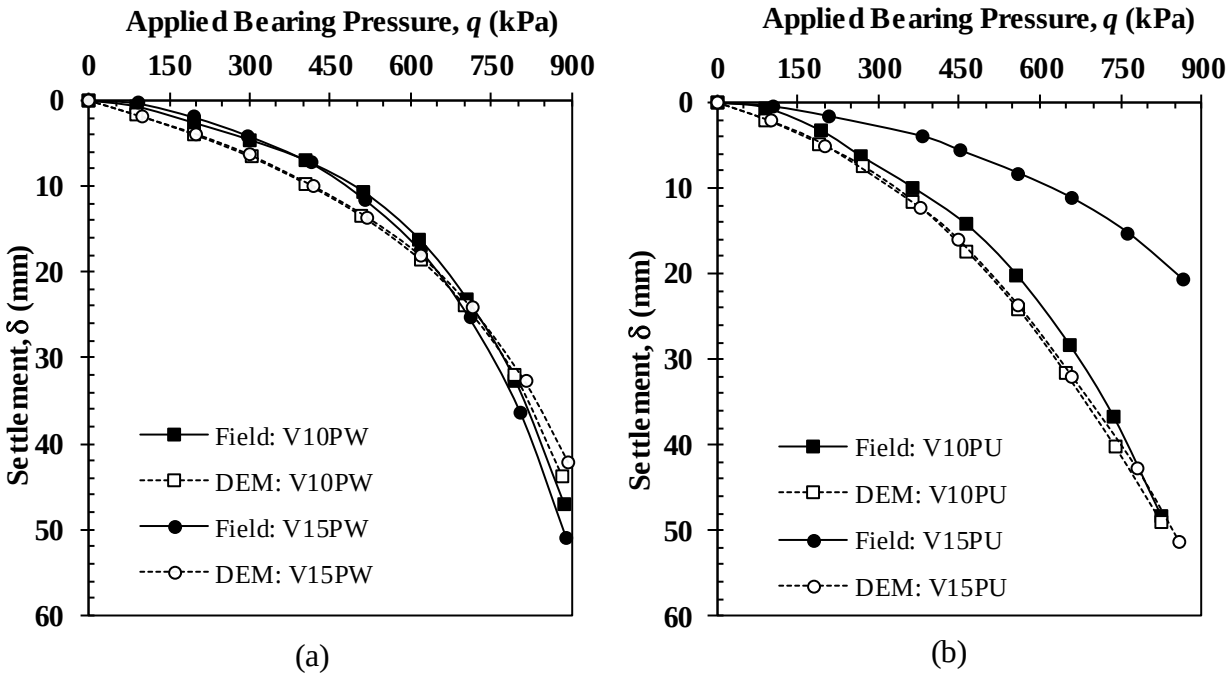

Fig. 4.22. Comparison of q-δ responses for (a) well-graded aggregate columns, and (b) uniformly-graded aggregate columns.

Table 8. Summary of model parameters used in the full-scale DEM simulations of uncemented columns V10PW and V10PU.

Material	γ [kN/m^3]	ν ---	E_{cu}/E [MPa]	s_u [kPa]	PI [%]	OCR ---	ϕ' °	ψ °
Desiccated Clay	17	0.495	30	150	---	>20	0	---
Upper Clay (CL)	18	0.495	Fig. 4.8	Fig. 4.9	26	12	0	---
Lower Clay (CH)	19	0.49	Fig. 4.8	Fig. 4.9	42	6	0	---
V10PW	18.5	0.30	40, Eq. 38	0	0	0	Eq. 36	Eq. 37
V10PU	18.5	0.30	25, Eq. 41	0	0	0	Eq. 39	Eq. 40
Foundation	23.5	0.20	30000	---	---	---	---	

4.4.5 Initial simulations of the bearing pressure-displacement response of single cemented stone columns

Figure 4.23 compares the experimental and simulated q-δ curves for columns V15U-UCSC, V15U-PCSC, and V15U-FCSC. These three columns were simulated using the modeling parameters (Table 9). As observed, the numerical responses for the uncemented column V15U-UCSC and fully cemented column V15U-FCSC agree well with the field data. However, numerical simulation of the partially cemented column V15U-PCSC substantially overestimates the measured settlements (by 2.5 times at q=1200 kPa), resulting in a response slightly less stiff than that observed for the fully cemented column V15U-FCSC. This behavior coincides with that measured for the small-scale footings reported by Golait et al. (2016), with FCSC column providing a marginally stiffer q-δ performance than PCSC. As illustrated in Fig. 4.9, the s_u profile corresponding to column V15U-PCSC is lower than that for V15U-FCSC within the

column critical length ($4D_{sc}$); therefore, possible variation in s_u is unlikely the cause of the stiffer performance of V15U-PCSC.

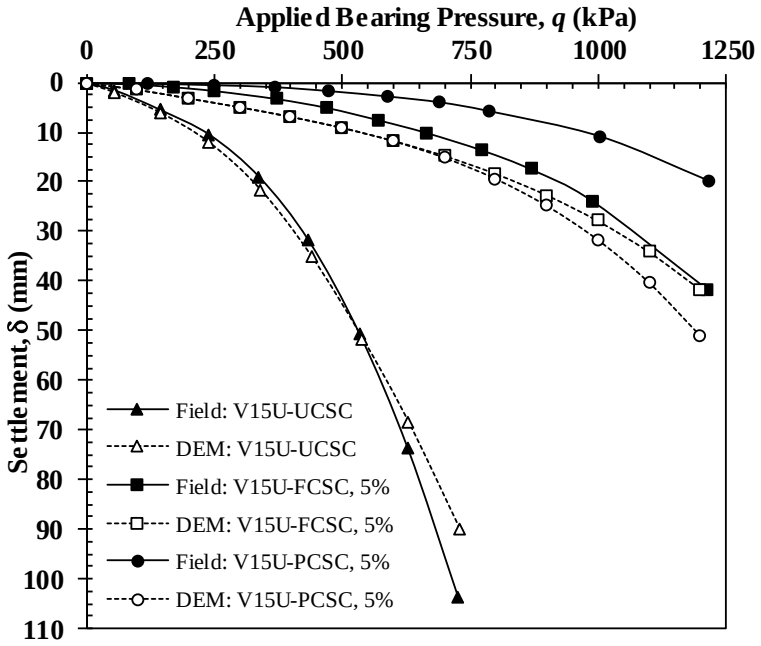

Fig. 4.23. Comparison of the computed and measured bearing pressure-displacement curves for full-scale stone columns (field data from Stuedlein 2008).

Table 9. Summary of constitutive model parameters used in the full-scale DEM simulations of cemented columns V15U-FCSC, V15-PCSC.

Model	Material	Block Material Properties					Joint Properties		
		γ	ν	E	c/s_u	ϕ'	J_{kn}, J_{ks}	J_{fri}	J_{coh}
		[kN/m^3]	---	[MPa]	[kPa]	[°]	[GPa/m^2]	[°]	[kPa]
Full-Scale	Desiccated clay (CL)	17	0.495	30	150	---	---	---	---
	Upper clay (CL)	18	0.495	Fig.4.8	Fig.4.9	---	---	---	---
	Lower clay (CH)	19	0.495	Fig.4.8	Fig.4.9	---	---	---	---
	Uncemented Aggregate	18.5	0.30	41	---	Fig.4.20b	10	40	---
	Cemented Aggregate, 5%	20.5	0.30	80	Fig.4.20c	Fig.4.20b	30	42	85
	Cemented Aggregate, 10%	20.5	0.30	220	Fig.4.20c	Fig.4.20b	80	65	400
	Foundation	23.5	0.20	30000	---	---	---	---	---

4.4.6 Initial Simulations of the Bearing Pressure-Displacement Response of Large Footings on small Uncemented Stone Column groups

A comparison between the observed and simulated bearing pressure-displacement curves for large footing G4 resting on five stone columns constructed using uncemented uniformly-graded aggregate is presented in Fig. 4.24. Constitutive modeling parameters for the uncemented granular material and the native soils were selected based on Eqs. (40 to 42) and Table 8, respectively. The total average stresses acting on the stone columns (σ_{sc}) and surrounding soil (σ_c) were monitored and recorded underneath the footing base in the DEM model, whereas the average stress on the foundation, σ_{avg}, was computed using Eq. (23) for an area replacement ratio (A_r) of approximately 30% (Table 4). The numerical average foundation stress-displacement curve agrees well with the estimated field q-δ response at the foundation center (Fig. 4.24). The numerical results also suggest a stiffer q-δ response of the adjacent soil with respect to that corresponding to the aggregate columns, which exhibits an almost linear behavior. This indicates that a higher percentage of the applied bearing pressure (q) is transferred to the soil as a result of the high strength and compressibility characteristics of the stiff crust. At q = 383 kPa, the stress concentration ratio (n) computed using Eq. (23) is approximately 0.73, whereas the ratios of stresses in the granular columns (μ_{sc}; Eq. 24) and adjacent soil (μ_c; Eq. 25) to σ_{avg} are 0.80 and 1.09, respectively.

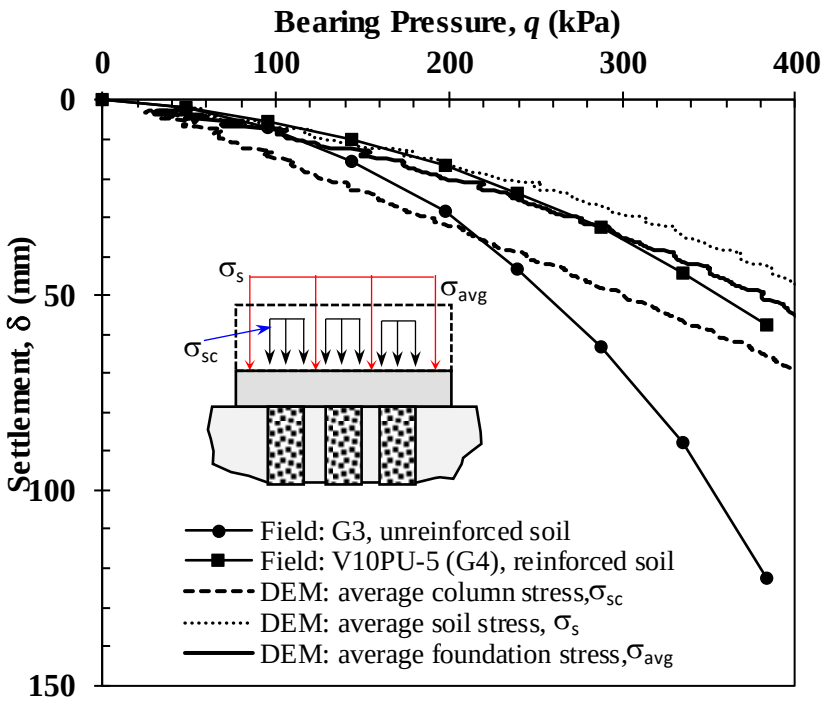

Fig. 4.24. Comparison of q-δ responses for large footing G4 resting on a small uncemented stone column group of five columns.

Lateral soil displacements adjacent to the large footing G4 were also monitored using a vertical inclinometer casing installed at depth of 10.4 m from the ground surface and distance of 0.20 m away from the footing edge as described above for G3. A comparison of the numerical and observed profiles of lateral soil displacements with depth adjacent to G4 is presented in Fig. 4.25. As observed for G3, the numerical simulation of G4 also overestimates the measured lateral movements. For q = 383kPa, the maximum numerical lateral displacement is approximately 16 mm, which differs by 4 mm (i.e., 33%) with the maximum observed movement (i.e., 12 mm) at the same depth of 0.9 m. Contour plots of the vertical displacement distributions for G3 and G4 are presented in Fig. 4.26. As observed, the contour plots indicate a significant reduction in the footing settlement of the aggregate column reinforced soil when compared with the untreated soil.

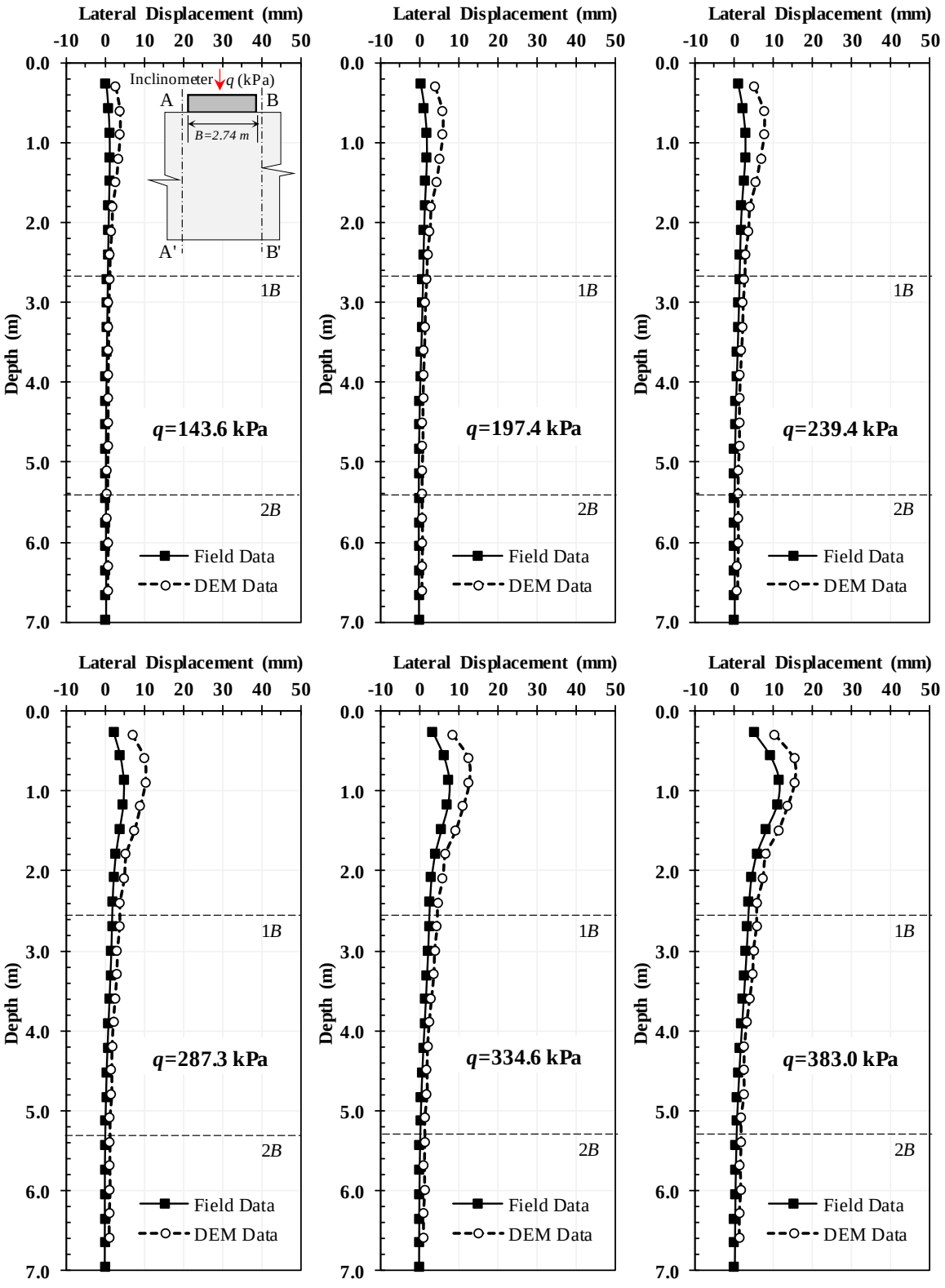

Fig. 4.25. Comparison of profiles of lateral soil movements adjacent to the large footing G4.

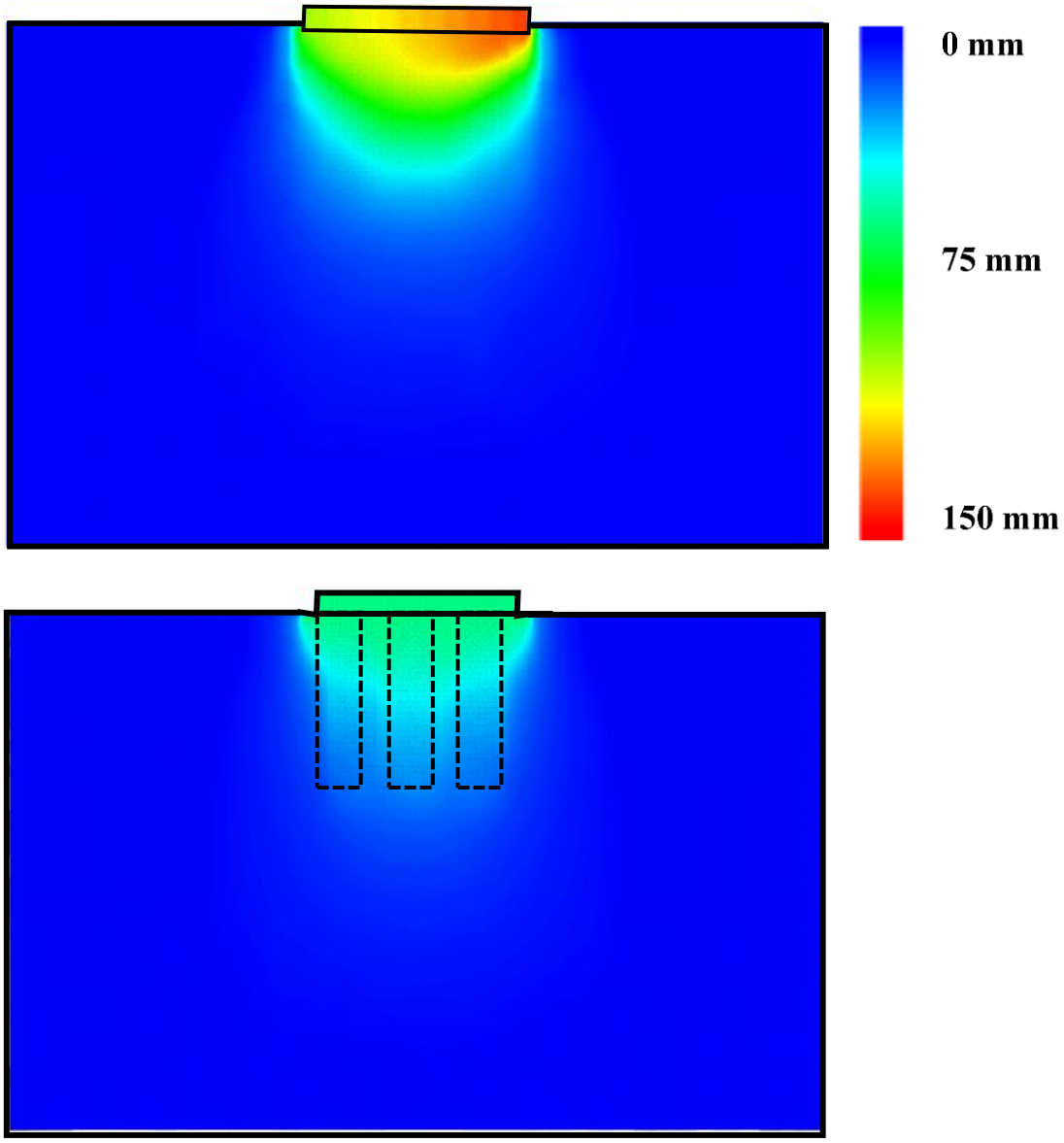

Fig. 4.26. Contour plots comparing the vertical displacement distributions for (a) large footing G3, and (b) large footing G4.

4.5 Numerical Modeling of Small-Scale Experimental Program

Since the field q-δ performance of column V15U-PCSC compared to column V15U-FCSC is contrary to what is expected, numerical simulations of the small-scale cemented stone columns were conducted to validate the results obtained from the large-scale cemented stone columns models. The model geometry was selected according to the laboratory experimental study described in Golait et al. (2016) and above section. The block generation of the surrounding soil and aggregate column was developed using hexahedron elements (8-node bricks), which are discrete and deformable based on specified constitutive responses. These individual hexahedron blocks were internally discretized into tetrahedral zones to improve the resolution of the nonlinear behavior of the clayey soil and aggregate material. The blocks comprising the stone column and those located near the column edge were further refined to enhance the accuracy of computed lateral deformation, stress distribution and failure formation along the soil-column interface. The boundary conditions were specified based on the geometry of the mild-steel tank used in the experiment, with full fixity assigned along the bottom of the model and lateral fixity applied to the vertical model sides. An illustration of the model geometry, block mesh, and boundary conditions for the small-scale DEM simulations is shown in Fig. 4.27.

4.5.1 Model Validation of the Soft Clayey Soil

The soil surrounding the column was classified as highly compressible clay (CH). The constitutive model parameters for this soil (Table 8) were obtained from the experimental data reported by Golait et al. (2009; 2016). This clay material was modeled using undrained conditions and the linear elastic-perfectly plastic stress-strain response with the Mohr-Coulomb

failure criterion. The bearing response of the unreinforced soft soil (USS) was simulated with the selected constitutive model parameters, and good agreement was obtained between the laboratory measured and the numerical q-δ responses (Fig. 4.28a). Therefore, these parameters were used to model the surrounding soil in all subsequent small-scale DEM simulations.

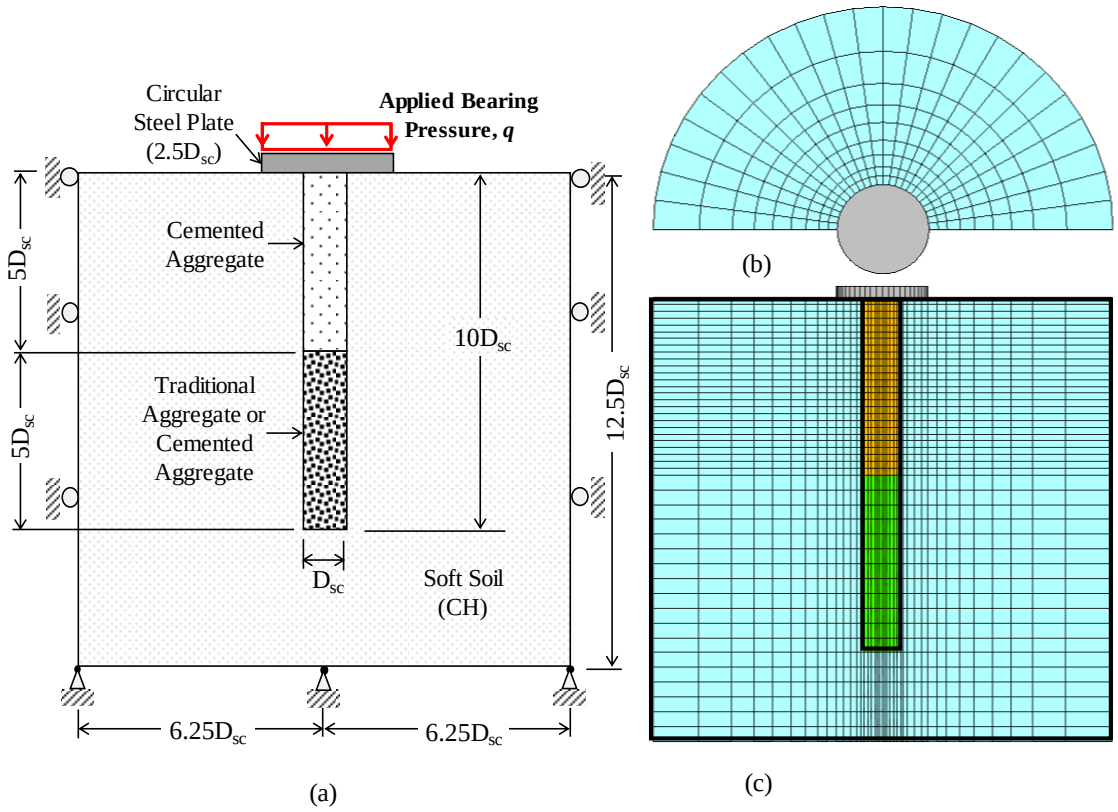

Fig. 4.27.3DEC mesh configuration and model geometry used in the numerical small-scale simulations: (a) example soil layering for a pier with slenderness ratio of 10, (b) plan view of the mesh, and (c) side view of mesh through an isolated, single stone column.

4.5.2 Model Validation of the Small-Scale Column Aggregate

Because of a lack of stress-strain response data, no triaxial test simulations were conducted for the uncemented and cemented aggregates used by Golait et al. (2016). The stiffness and strength properties of this material were selected in accordance with the values

reported by the authors (Table 10). Each discrete-deformable block forming the aggregate column was represented as an elasto-plastic element with the Mohr-Coulomb failure criterion instead of using rigid blocks.

4.5.3 Initial Bearing Pressure-Displacement Behavior of Small-Scale Cemented Stone Columns

A comparison of the bearing pressure-displacement responses for the partially cemented stone column (PCSC), fully cemented stone column (FCSC), and uncemented stone column (UCSC) is presented in Fig. 4.28b. Good agreement is observed between the computed and measured q-δ responses for all three simulated columns. The numerical results show that both cemented columns provide a similar initial linear behavior for q values less than 150 kPa, although slight differences in the initial stiffness are observed in the experiments. As q increases, however, the column FCSC exhibits a slightly stiffer q-δ response than that for column PCSC. This behavior coincides with that computed for the large-scale cemented stone columns (section 4.4.5). At δ = 17 mm (close to column failure), the bearing capacity improvement factors are approximately 1.5 and 1.6 for PCSC and FCSC, respectively, computed in terms of the bearing capacity of the uncemented stone column (UCSC).

The 3D DEM models that were developed, calibrated and validated using the small and full-scale loading tests as described in chapter were used to conduct systematic parametric investigations of the factors contributing to the response of stone-column supported footings.

Table 10. Summary of constitutive model parameters used in the small-scale DEM simulations.

Model	Material	Block Material Properties					Joint Properties		
		γ	ν	E	c/s_u	ϕ'	J_{kn}, J_{ks}	J_{fri}	J_{coh}
		[kN/m^3]	---	[MPa]	[kPa]	[°]	[GPa/m^2]	[°]	[kPa]
Small-scale	Soft Clay (CH)	12.2	0.49	10	19	10	0.18	10	19
	Uncemented Aggregate	19.6	0.30	15	---	38	0.25	35	---
	Cemented Aggregate	19.8	0.49	50	68	37	3	35	68
	Steel Plate	78.5	0.20	200000	---	---	---	---	---

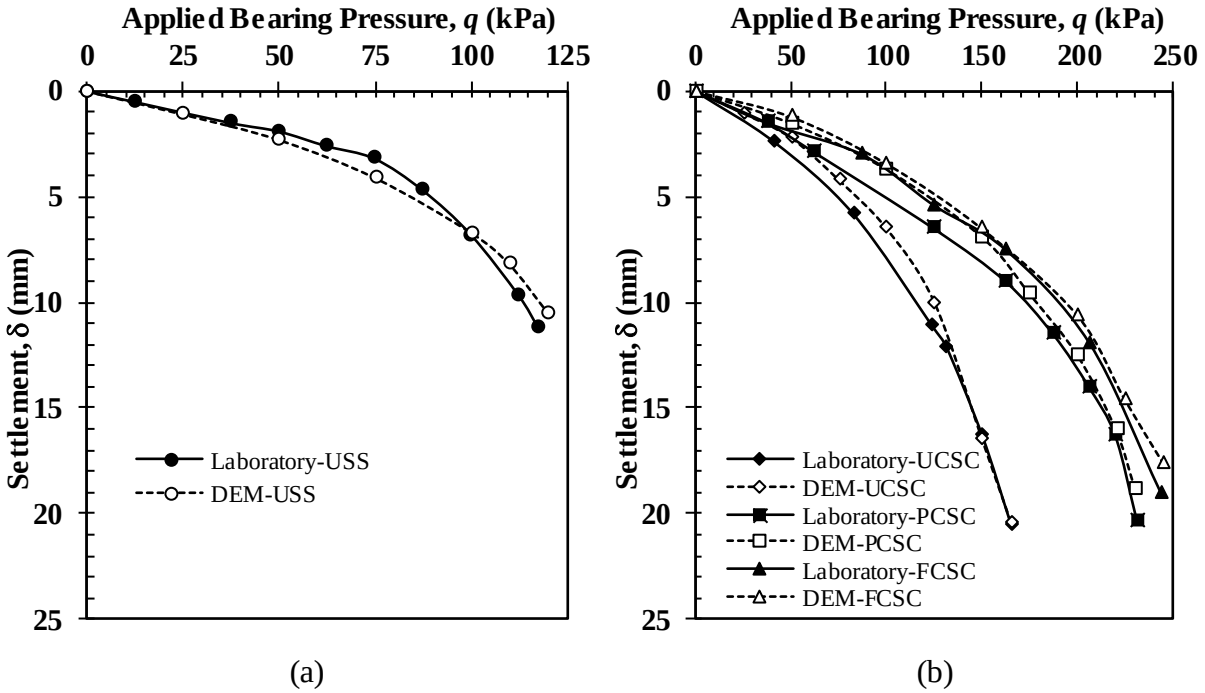

Fig. 4.28. Comparison of the bearing pressure-displacement curves for the small-scale DEM models: (a) unreinforced soft soil, and (b) cemented and uncemented stone columns reinforced soft soil (after Golait et al. 2016).

CHAPTER 5. RESULTS AND DISCUSSION OF PARAMETRIC STUDY CONDUCTED USING VALIDATED DEM MODELS

The validated DEM models were used to explore the effects of variables that have been confounded during the small and full-scale experimentations, pointing to subtleties that can affect load transfer mechanisms, such as aggregate stiffness, friction and dilation angle, s_u profile, and area replacement ratios, cement content, and column geometry. These results point to the effect of quality control-type factors in stone column construction on subsequent local load transfer characteristics and global bearing pressure-displacement performance. The DEM results are also compared with the analytical methods described in chapter 2.

5.1. Factors Affecting the Response of Single, Uncemented Stone Column-Supported Footings

5.1.1 Effect of Aggregate Gradation

5.1.1.1 Aggregate Friction Angle

Fig. 5.1 compares the q-δ responses for columns V10PW and V10PU considering the two different ϕ'_{sc} relationships described by Eqs. 37 and 40. To single out the influence of ϕ'_{sc}, E_{sc} of columns V10PW and V10PU were kept constant at 40 MPa and 25 MPa, respectively, based on the validated values. Therefore, one curve in each plot represents the validated case while the second curve has the same modulus, but a different ϕ'_{sc} relationship. The friction angle influences the response of V10PW for bearing pressures greater than 510 kPa; however, this is not observed for V10PU. At q = 885 kPa, a difference in settlement of 8 mm is observed between the two curves for V10PW, while no difference is observed for V10PU. At the initial confining stresses,

the variation of ϕ'_{sc} for both gradations (Eqs. 37 and 40) is approximately 3°. During loading, the variation of the average confining stress in the bulging zone increases for the two different aggregate gradations as the E_{sc} of the column increases from 25 MPa to 40 MPa (Fig. 5.2). Therefore, the magnitude of the effect of the aggregate friction angle depends also on the aggregate stiffness. Additional discussion of the influence of E_{sc} is given below.

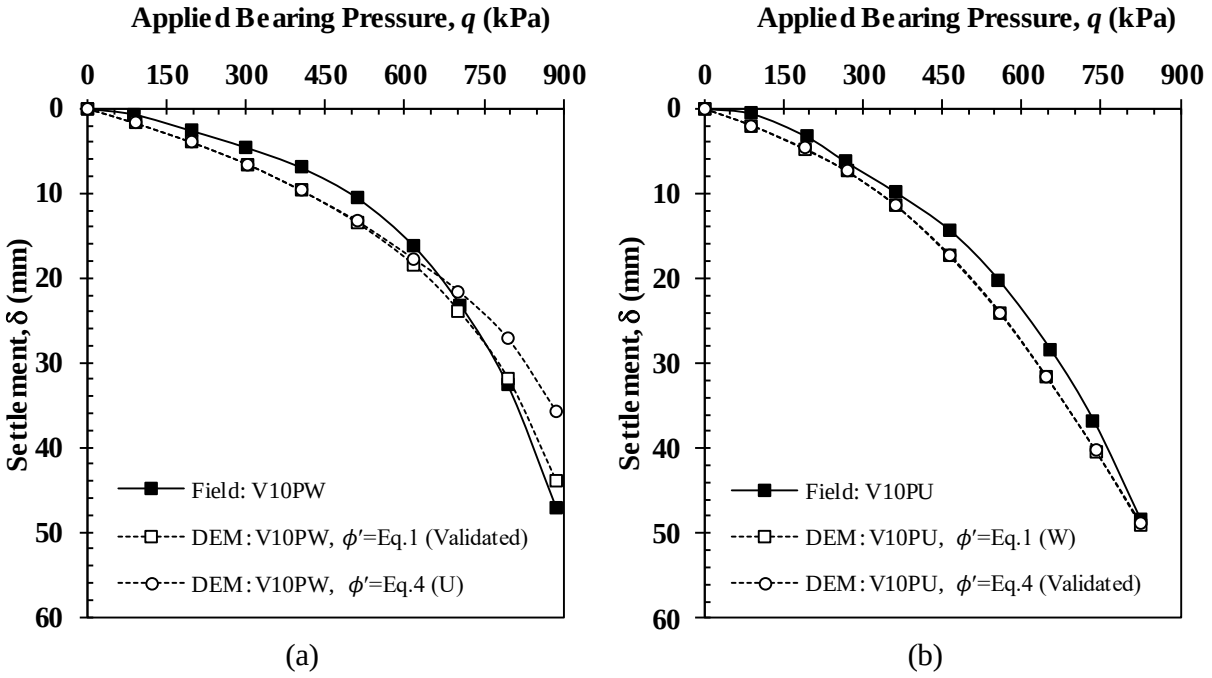

Fig. 5.1. Comparison of the effect of aggregate friction angle on the q-δ responses for (a) well-graded aggregate columns (E_{sc}=40 MPa), and (d) uniformly-graded aggregate columns (E_{sc}=25 MPa).

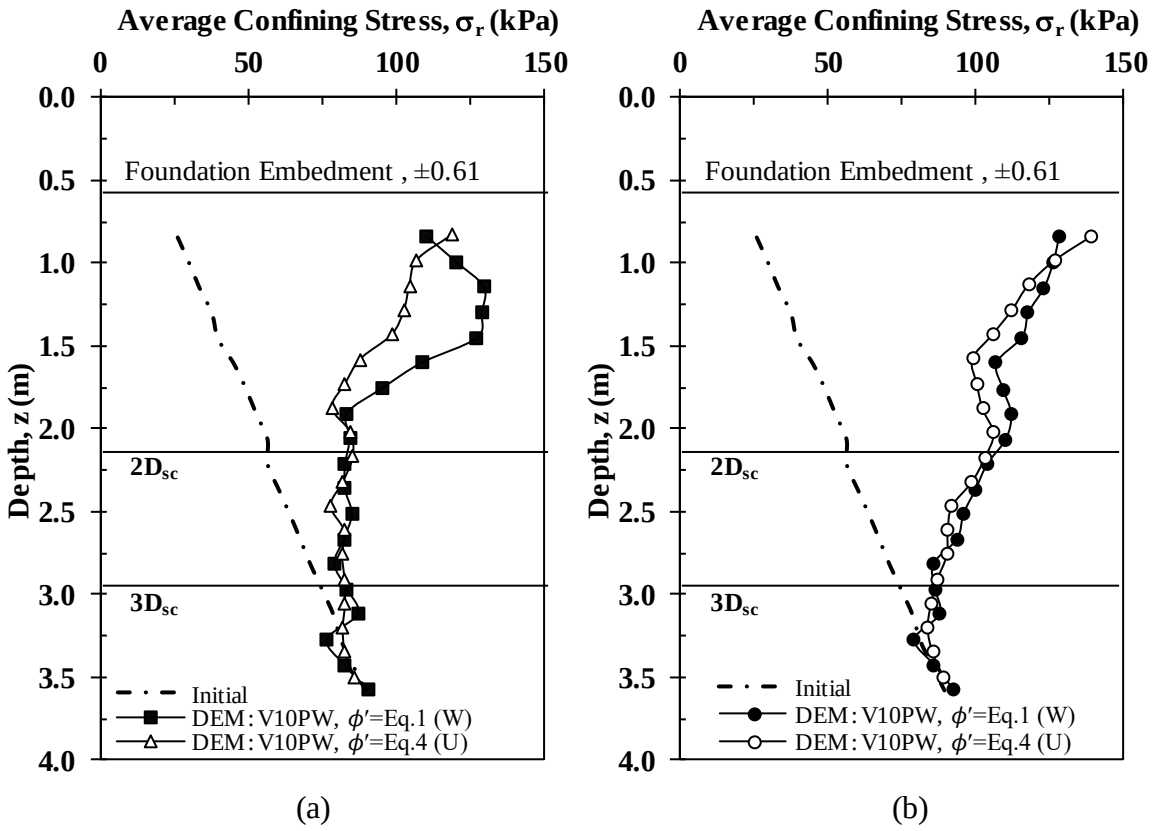

Fig. 5.2. Average confining stress distribution with depth for different column stiffness for column V10PW (a) 40 MPa and (b) 25 MPa.

5.1.1.2 Aggregate Dilation Angle

Fig. 5.3 presents the observed and simulated q-δ responses corresponding to V10PW and V10PU modeled with a zero-dilation condition, along with the reported dilation (Eqs. 38 and 41) to consider the pressure-dependence of aggregate dilatation angle. The incorporation of various ψ_{sc} in the DEM model does not appear to contribute to a variation in the simulated q-δ responses. When the applied q is small, the ψ_{sc} is positive, yet has little effect on the response because the corresponding strain is within the elastic region. As q increases, ψ_{sc} reduces which also results in minimal influence on the response.

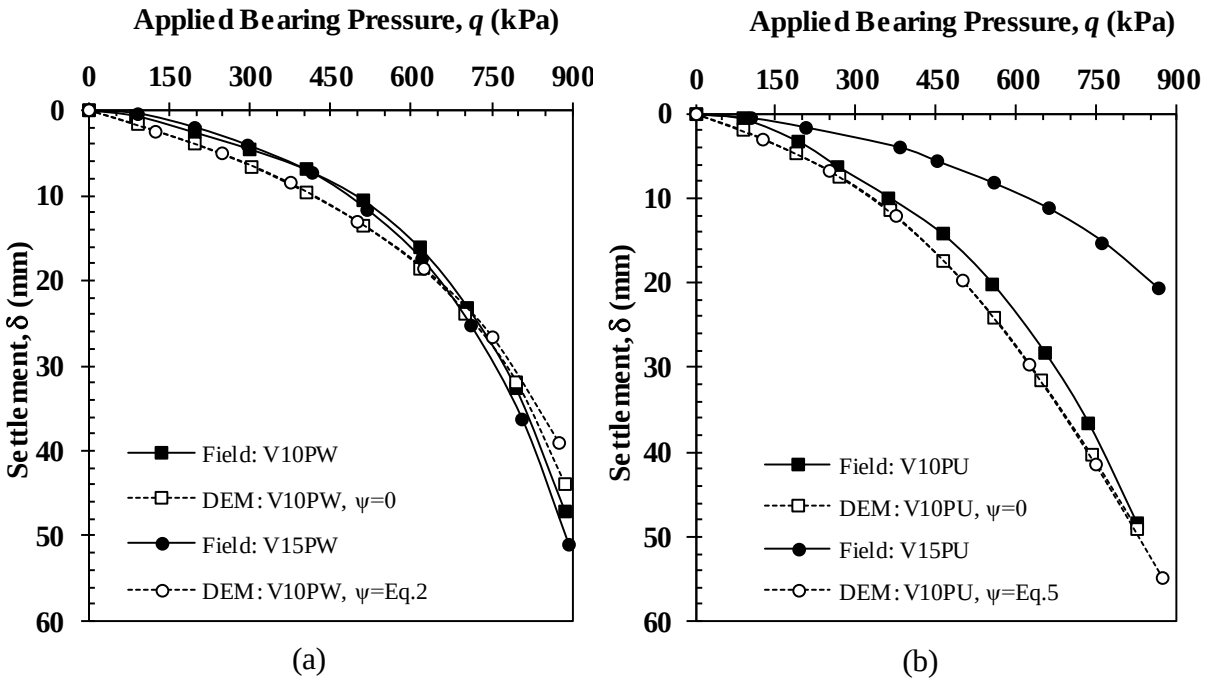

Fig. 5.3. Comparison of the effect of aggregate dilatancy angle on the q-δ responses for (a) well-graded aggregate columns, and (b) uniformly-graded aggregate columns.

5.1.1.3 Aggregate Stiffness

The effect of the initial stiffness of columns V10PW and V10PU was investigated by evaluating the pressure-dependent Young's Moduli associated with Eqs. 39 and 42. Based on in-situ conditions and an average at-rest earth pressure coefficient, K_o, of 1.3 obtained by correlation to CPT data taken prior to column installation, σ'_r was calculated as 55 kPa (corresponding to an E_{sc} of 40 MPa from Eq. 39) for V10PW and 50 kPa (corresponding to an E_{sc} of 25 MPa from Eq. 42) for V10PU. The columns were modeled in the pre-installation condition, and for a range of E_{sc} values representing the increase in initial σ'_r (and thus K_0) that might occur during installation. E_{sc} values ranging from 40 to 60 MPa for V10PW and 25 to 75 MPa for V10PU were used based on an increase in the initial σ'_r of 200 kPa. Comparing Figs.

5.4a and 5.4b, it is clear to see that for the same increase in σ'_r, the range of E_{sc} and the response for the well-graded and uniformly-graded aggregate columns is quite different. As illustrated in Fig. 5.4a, even if column installation practices result in a higher initial σ'_r, the q-δ responses of the "W" columns remain similar to the response where geostatic in situ conditions were assumed. This is due to the fact that even large increases in the initial σ'_r result in very small changes in the initial stiffness for the well-graded aggregate.

Figure 5.4b indicates, however, that the q-δ responses of the "U" columns are more sensitive to differences in the initial σ'_r. The validated case for V10PU modeled using an E_{sc} value of 25 MPa agrees well with the observed response; however, it does not capture the observed response for V15PU. As the E_{sc} values increase, the simulated response approaches the observed response for V15PU. An E_{sc} above 100 MPa is needed to capture the field q-δ response, which is over four times greater than the value selected based on the laboratory data and pre-installation in situ stresses. This would imply an increase in σ'_r of 250 kPa and a K_o of 5. Elshazly et al. (2008) used K_o values ranging from 0.85 to 1.7, Ammari and Clarke (2018) used K_o values varying from 1.5 to 3.5, whereas Castro (2017) reported K_o values ranging from 0.4 to 2.5. Stuedlein (2010) reported K_o values at the location of column V15PU prior to stone column installation ranging from 1.2 to 2.2 within the bulging depth. Because the pre-installation K_o values are relatively high, a post-installation K_o of 5 for column V15PU is possible and could have generated higher initial column stiffness conditions.

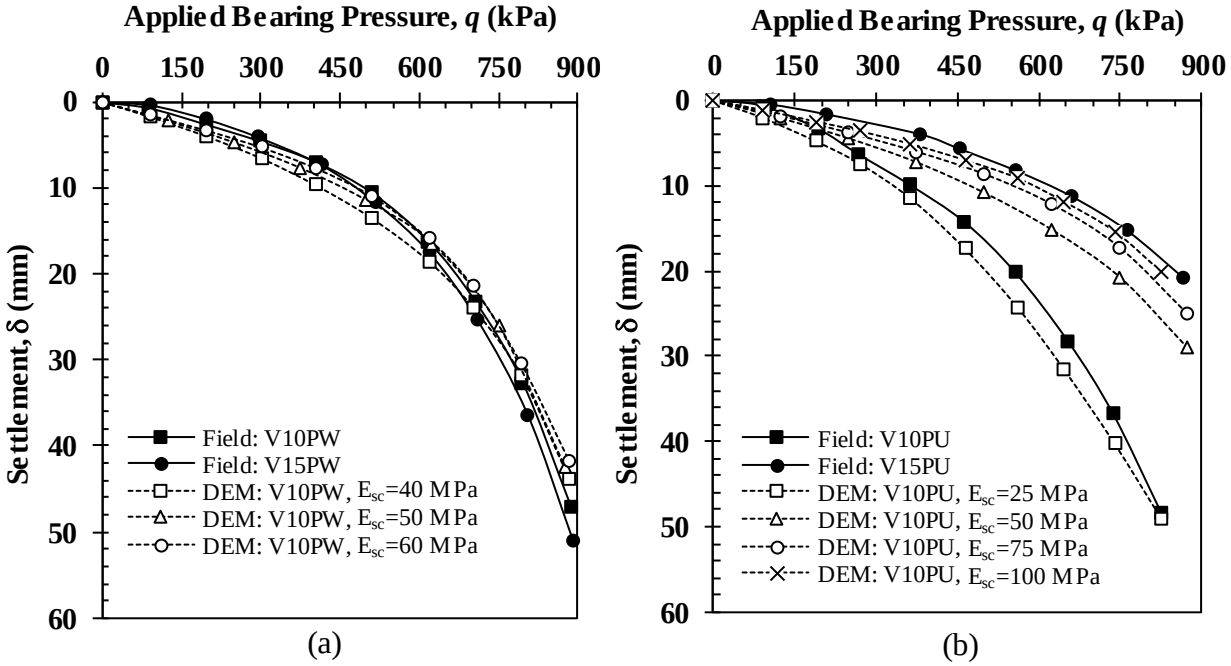

Fig. 5.4. Comparison of the effect of aggregate stiffness on the q-δ responses for (a) well-graded aggregate columns, and (b) uniformly-graded aggregate columns.

5.1.2 Effect of Column Length

Given the 1.5 m difference in length between V15PU and V10PU, the column length was also examined as a possible factor influencing the q-δ responses of these columns. In order to account for the column length, columns V10PW and V10PU were modeled using two different column lengths (i.e., 3.05 m and 4.56 m). Figure 5.5 shows that the DEM results for both column lengths are similar for bearing pressures less than 750 kPa, and only slightly vary for greater q. Vahedian et al. (2014) and Castro (2017) note that increases in length beyond the critical length, estimated as 1.5 to 3 times D_{sc} (for isolated columns), do not result in improvements in the q-δ response. Likewise, no differences in numerical or experimental q-δ responses were observed for the well-graded aggregate columns (V10PW and V15PW).

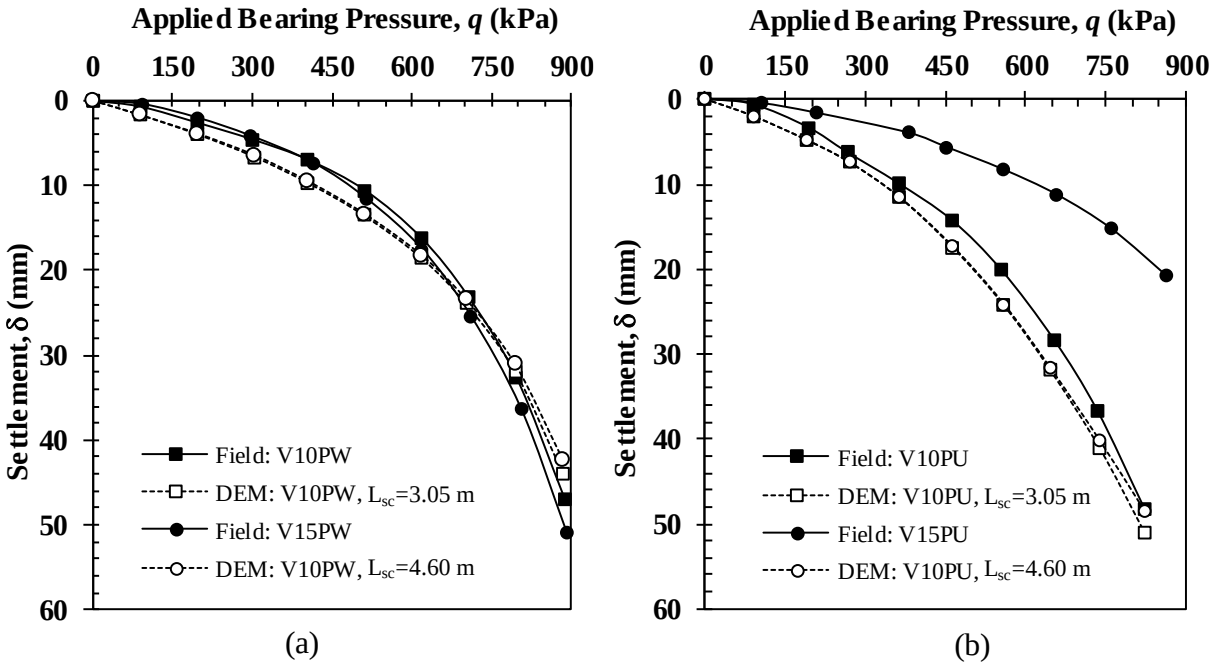

Fig. 5.5. Comparison of the effect of aggregate column length on the q-δ responses for (a) well-graded aggregate columns, and (b) uniformly-graded aggregate columns.

Existing methods to estimate the bearing capacity of single stone columns do not take into account the column slenderness ratio (L_{sc}/D_{sc}); therefore, a numerical model as presented in this study can be conducted to determine the optimal column length (L_{sc}) to satisfy the ultimate limit sate (ULS) and serviceability limit state (SLS) design requirements. Determining the optimal L_{sc} can significantly reduce the direct construction costs of a stone column project consisting of a large number of columns, providing more cost-effective designs. As summarized in Table 11, the 1.5 m (5 feet) difference in length between V15PU and V10PU would represent estimated reductions in the direct costs of $17,500 and $125,000 for projects containing 100 and 2000 columns, respectively.

Table 11. Estimations of cost savings by stone column length optimization.

Number of columns	Difference in column length [feet]	Unit-price [LF]	Cost saving
100	5	$35.00	$17, 500
1000	5	$25.00	$125, 000

5.1.3 Effect of Undrained Shear Strength

The inherent variability of the native soil s_u at the site was investigated by comparing the q-δ curves for "W" and "U" columns considering the standard deviation (σ) in s_u reported by Stuedlein et al. (2012c). Figure 5.6a, and b, presents comparisons of the aggregate columns incorporating the mean $s_u \pm \sigma$ with depth. In addition to showing that the initial mean estimate of s_u was appropriate based on the site characterization, the comparison of simulations using the upper and lower bound s_u indicates that large variations in s_u appear to only govern the large displacement response of aggregate columns. Further, possible variation in s_u cannot explain the stiffer response of V15PU relative to V10PU.

It is important to highlight that the s_u profiles used in this study were obtained prior to column installation; however, these s_u profiles could have changed due to construction. Fig. 5.6c shows the q-δ response for column V10PU simulated by multiplying its initial s_u profile by an amplification factor to consider an increase in the s_u profile after column installation. Several multipliers were used to determine the value required to represent the V15PU column. As it is observed, the initial V10PU s_u profile (58 kPa) needs to be multiplied by a factor of 2.6 in order to obtain a similar q-δ response to column V15PU. This s_u profile amplification factor of 2.6 is

considered to be disproportionally high since it is completely outside of the field s_u profiles measured by Stuedlein (2008). Unfortunately, this cannot be validated or explored any further because of a lack of experimental field data of the s_u profiles after installation.

To evaluate the influence of the surrounding soil strength and stiffness, columns V10PW and V10PU were modeled using low s_u values to represent soft clay conditions (i.e., 10kPa and 20kPa). Fig. 5.6d illustrates that a significant reduction on the bearing capacity of both columns is observed as the field average s_u (55 kPa) is lowered. For a settlement of 25 mm, it is noted from the DEM results that the bearing pressures are 55% (s_u=10 kPa) and 40% (s_u = 20 kPa) lower than the field-measured bearing pressures for both columns, respectively. Also, even though the initial response of V10PW is stiffer for settlements up to 45 mm, the differences between both q-δ curves start reducing as a result of the higher frictional response of the No. 57 gradation in comparison with the 21b gradation. This results in V10PU having a bearing capacity equal to or greater than V10PW as shown in Fig. 5.6d.

Since the geotechnical investigation at the test site was conducted in the spring season (March-April, 2005), and the stone columns were tested in the late fall season (November-December, 2005), differences in the q-δ responses for the investigated columns (e.g., V10PW, V10PU, V15PW and V15PU) could have been caused by variations in the s_u profiles associated with the seasonal variation in the moisture soil conditions at the test site. As illustrated in Fig. 5.7, the rainfall histories at the test site for the spring and fall seasons in 2005 clearly show an increase in the total amount of precipitation in the fall season as compared to the spring season. However, since groundwater levels were not monitored and CPT soundings were not performed during the fall season, a more quantitative analysis of the effects of the seasonal variation in the s_u profiles on the q-δ behaviors of the investigated columns cannot be carried out.

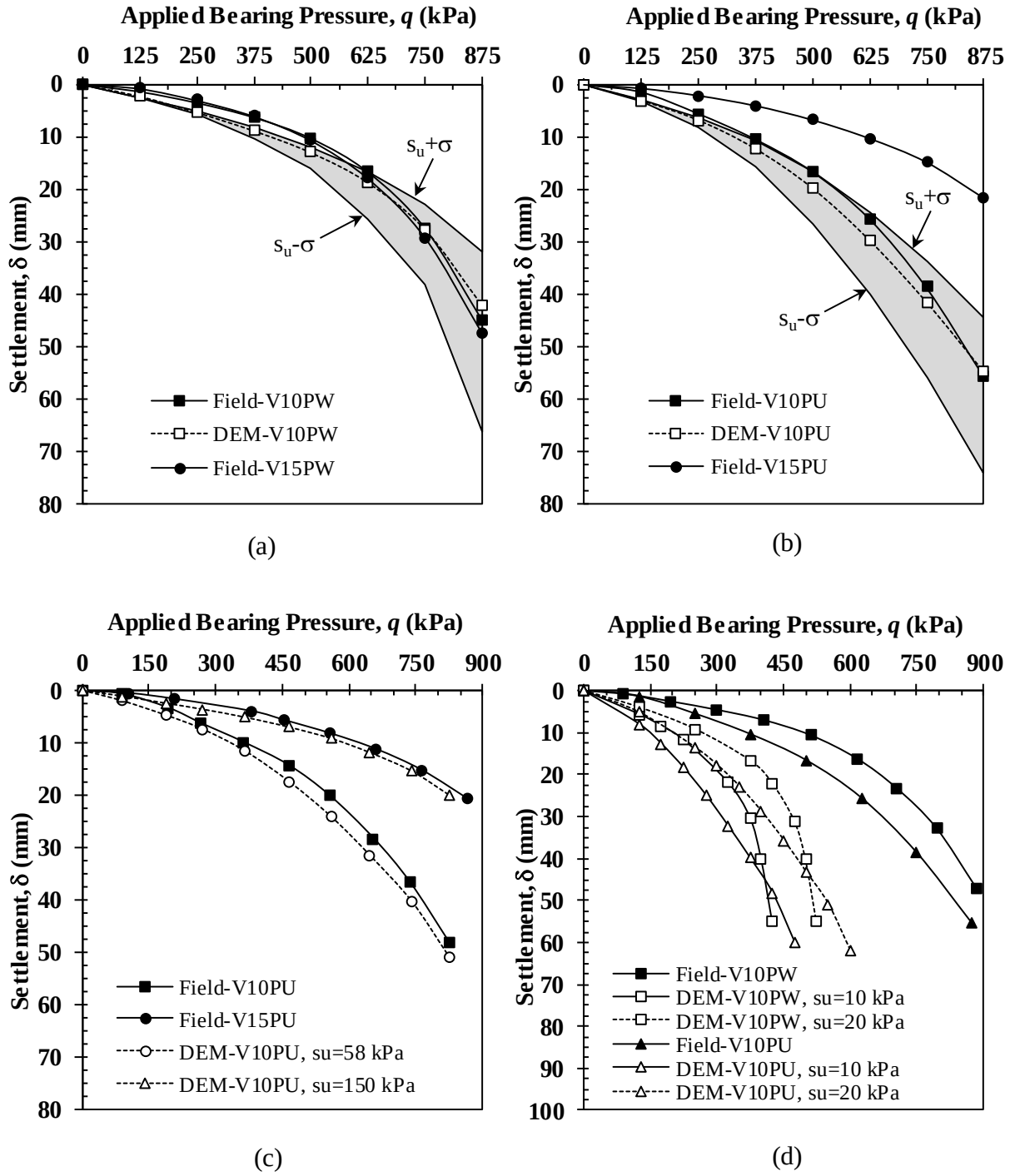

Fig. 5.6. Comparison of the effect of s_u profile on the q-δ responses for (a) well-graded aggregate columns $s_u \mp$ SD, (b) uniformly-graded aggregate columns $s_u \mp$ SD, (c) well-graded aggregate columns different s_u profiles, and (d) uniformly-graded aggregate columns different s_u profiles.

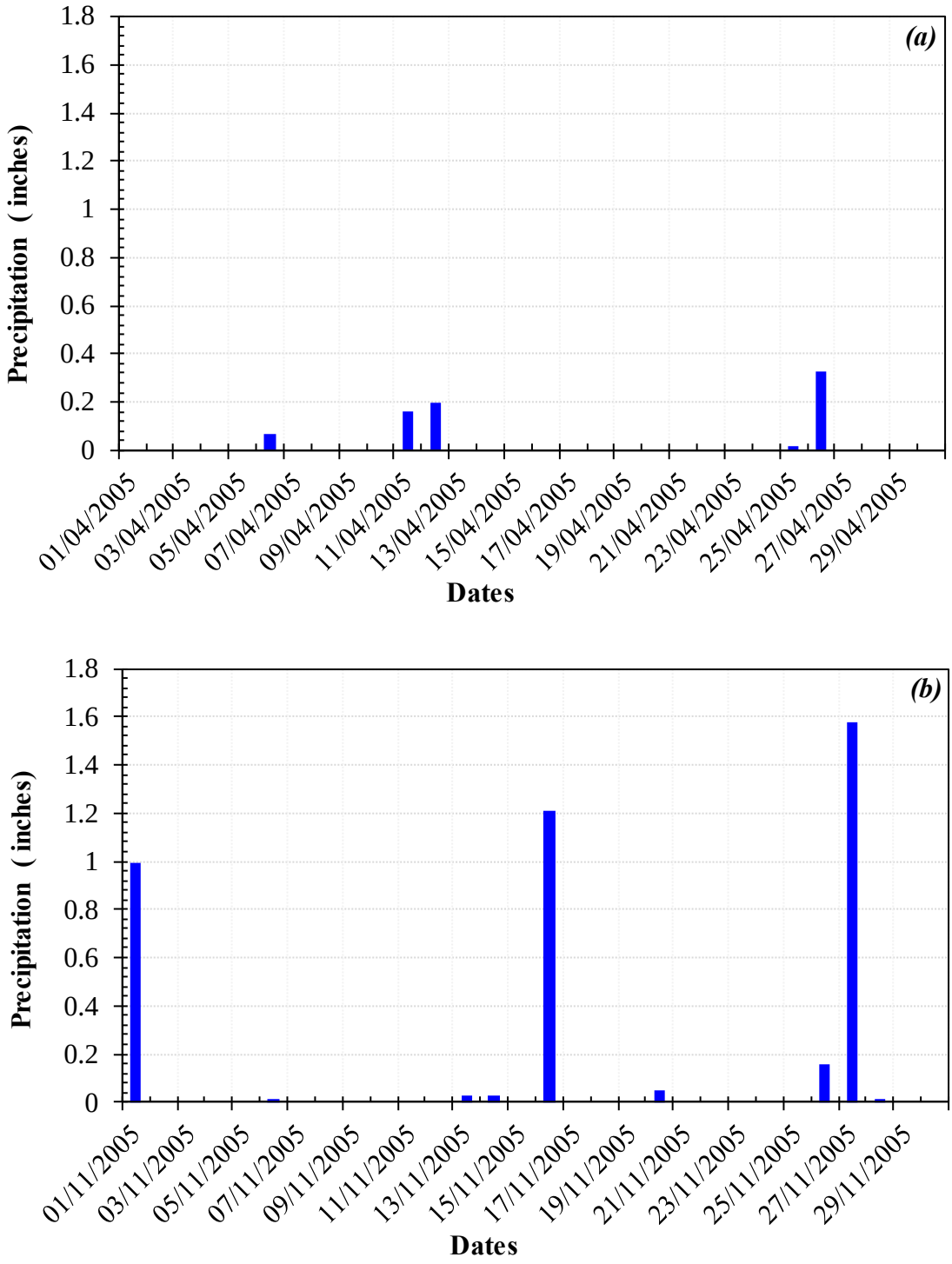

Fig. 5.7. Comparison of rainfall histories at Baytown (a) April 2005 and (b) November 2005 (data obtained from the National Oceanic and Atmospheric Administration-NOAA).

5.1.4 Effect of Area Replacement Ratio

The area replacement ratio, A_r, strongly influences the global stone column response since the confining and vertical pressure in the surrounding soil increases with increases in the loaded area (Barksdale and Bachus 1983). The influence of A_r was evaluated by modeling columns V10PW and V10PU for A_r values ranging from 10 to 50% (typical for stone column projects), and 95 and 100%, representing the common range for static plate loading tests like those conducted in Stuedlein (2008). As illustrated in Fig. 5.8, the bearing pressure-displacement responses for column V10PW are more sensitive to changes in A_r compared to V10PU. Because ϕ'_{sc} is lower for the well-graded aggregate (Fig. 4.17b), the increase in σ'_r around the column generated as A_r decreases causes a greater reduction in ϕ'_{sc} for column V10PW due to the pressure-dependence of the aggregate friction angle. For δ = 25 mm, the DEM simulations show that the estimated bearing pressures are 63% (A_r=10%), 39% (A_r=30%), and 14% (A_r=50%) lower than the field-measured bearing pressures (A_r=100%) for column V10PW. On the other hand, for V10PU, these values are 50%, 41% and 33%, indicating a narrower range in the reduction of the bearing capacity for the same change in A_r. Since the foundation diameter (0.76 m) is only 2 cm larger than V10PU (0.74 m), the increase in the confining stress around the column is localized at the top of the column and is negligible for the rest of the length of the column. Therefore, the impact of a 5% increase in A_r on the q-δ performance of column V10PU relative to V10PW is minimal and discrepancies in the q-δ responses between the two footings are likely not caused by the 2 cm difference in the column diameter.

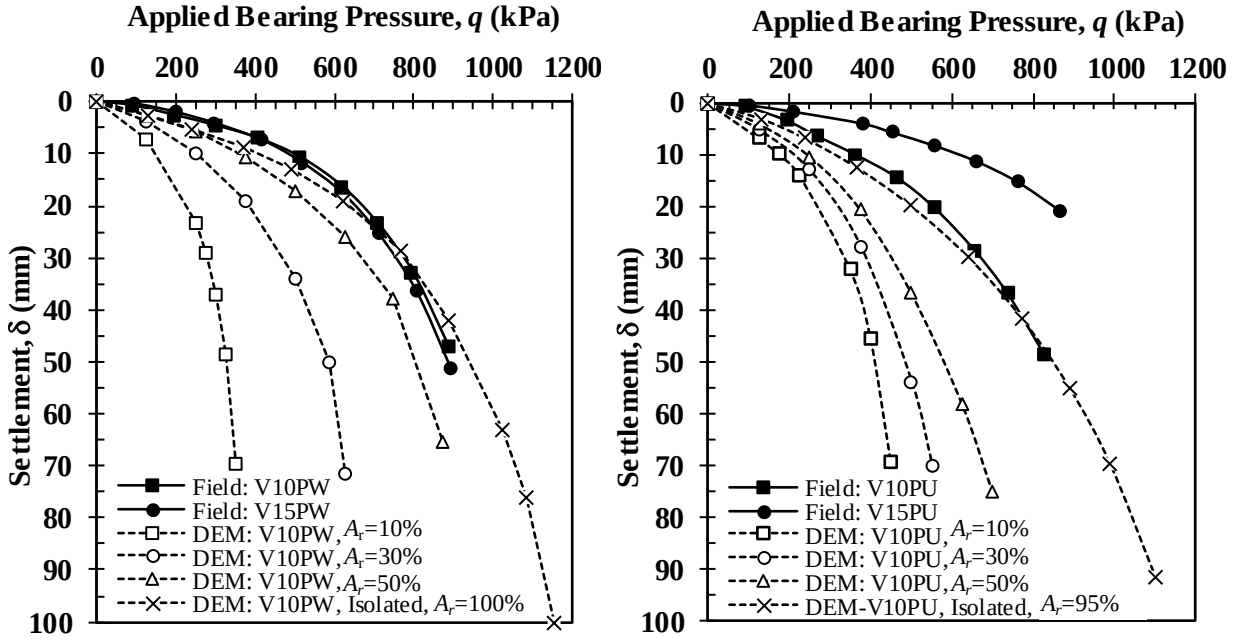

Fig. 5.8. Comparison of the effect of area replacement ratio on the q-δ responses for columns (a) V10PW, and (b) V10PU.

5.1.5 Comparison of the Stress Transfer Mechanisms, Displacements, and Capacities at the Ultimate Limit State

The calibrated DEM models facilitated simulation of the response of the aggregate columns at the ultimate limit state, including stress transfer mechanisms, displacements, and capacities. The field capacity of the two columns was estimated by extrapolation of the available q-δ data, as described by Stuedlein and Holtz (2013), and equaled 1,100 and 1,125 kPa for V10PU and V10PW, respectively. DEM simulations were carried out until settlements of approximately 100 mm. A similar extrapolation was also used for the first 50 mm of the DEM simulation data and compared to the actual DEM results up to 100 mm of settlement to evaluate the accuracy of the extrapolation. Fig. 5.9 compares the observed and DEM simulated q-

δ responses to the extrapolations of the observed and DEM simulations for columns V10PW and V10PU. The extrapolations of the DEM-based q-δ curves are in excellent agreement with the DEM simulations over the range of displacements evaluated. The extrapolated DEM simulations suggest ultimate bearing resistances that are 9 and 13% (i.e., 1,225 and 1,250 kPa) greater than that estimated by extrapolation of the observed q-δ curves for V10PW and V10PU, respectively. Differences in the initial stiffness of the q-δ curves between the two columns do not translate to significant differences at large displacements owing to the aggregate-specific pressure-dependence (i.e., Fig. 4.17), such that the capacities of the two columns are nearly identical at large displacements.

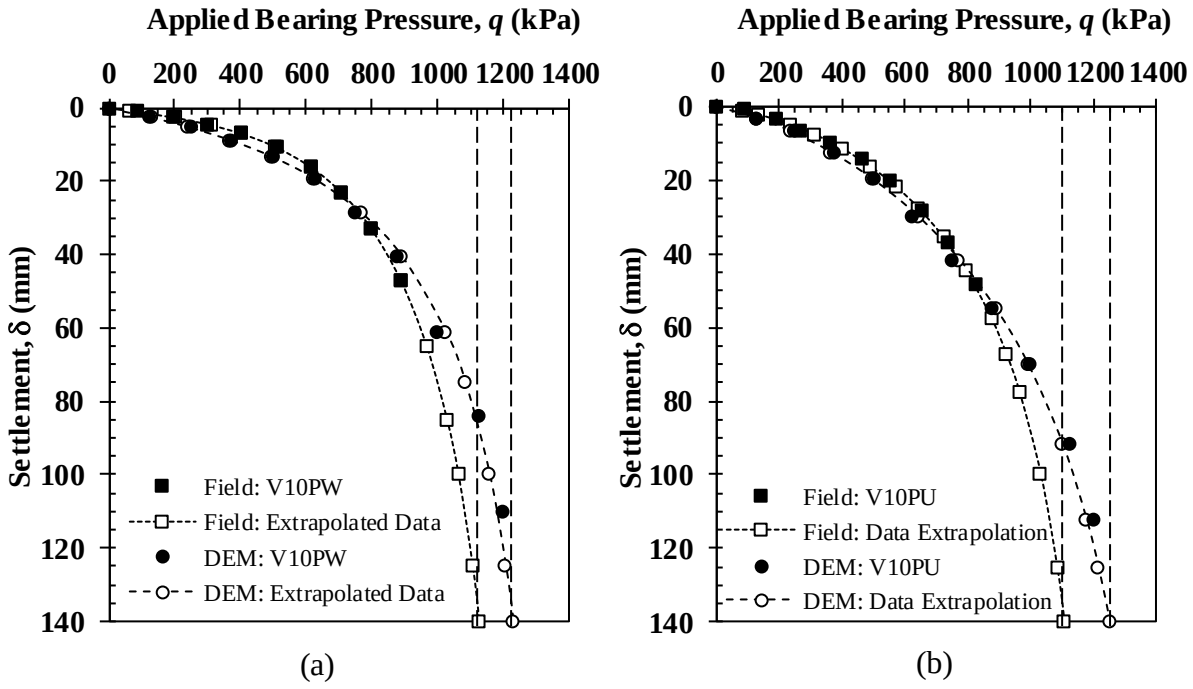

Fig. 5.9. Comparison of the full DEM bearing pressure-displacement results for columns V10PW and V10PU with extrapolated field data and similar extrapolated DEM data.

Fig. 5.10 compares the extrapolations of the observed and DEM simulated q-δ responses to the ultimate bearing capacity estimates using existing methods for columns V10PW and V10PU. As clearly observed, the ultimate bearing capacity estimates using existing methods exhibit a wide variation for both columns. On the other hand, the DEM simulations and the methods (e.g., modified Mitchell 1981 and Hughes et al. 1975) proposed by Stuedlein et al. (2013) indicate better agreement with the extrapolated field data compared to the other existing methods. The modified methods were developed using back-calculations of the extrapolated field data; hence, good agreement with the observed data is expected. The numerical results show that conducting a DEM simulation incorporating site specific soil conditions and variations in the aggregate stiffness and strength based on the actual gradation used to construct the column could provide better estimations of the ultimate bearing capacity of a single stone column. Therefore, this could result in an improvement in selecting an appropriate factor of safety for bearing capacity and a reduction in construction costs associated with field verification testing (e.g., plate load testing).

The evolution of the average confining stress (σ'_r), radial displacement, and settlement distributions with depth for columns V10PW and V10PU for q = 1,200 kPa (i.e., near the ultimate state) are presented in Fig. 5.11. Average σ'_r was calculated for each 0.3 m height of the column by averaging the radial stresses for the "ring" of blocks surrounding the column. The radial displacements were tracked at the edge of the stone column for each 0.3 m height of the column.

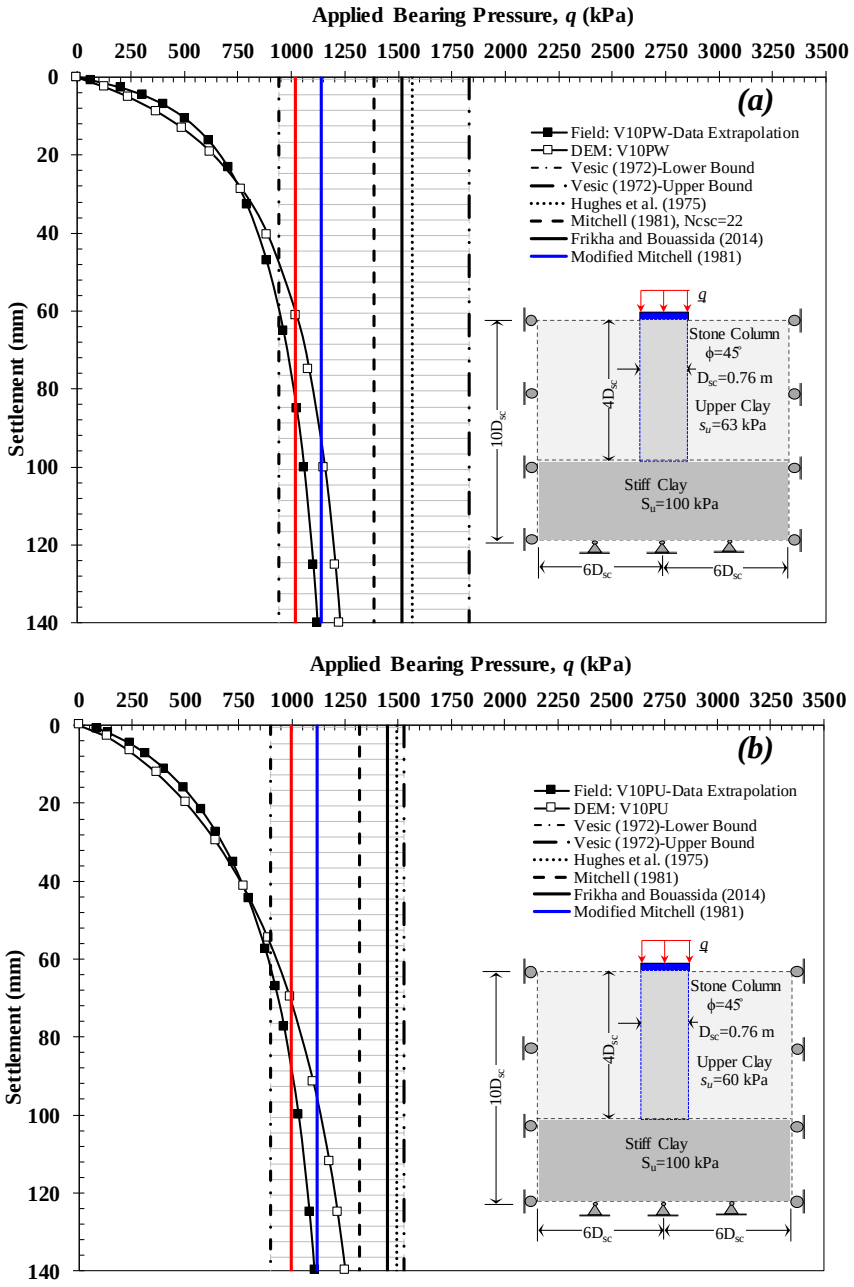

Fig. 5.10. Comparison of the full DEM bearing pressure-displacement results with extrapolated field data and bearing capacity estimations using existing methods for (a) column V10PW, and (b) column V10PU.

Comparison of the σ'_r and radial displacement distributions indicate that the bulging zone develops largely within a length of approximately $2D_{sc}$ for V10PW which agrees with the typical reported range of $2D_{sc}$ to $3D_{sc}$ (Barksdale and Bachus 1983; Castro 2017). However, column

V10PU exhibits a bulging zone extending beyond $3D_{sc}$, and the average increase in the confining pressure within the range of $2D_{sc}$ to $3D_{sc}$ is 16% greater than that estimated for column V10PW. This variation is not only controlled by the differences in the s_u profiles corresponding to each column location, but also by the difference in initial stiffness. Column V10PU exhibited an E_{sc} of 25 MPa compared to 40 MPa for column V10PW based on the laboratory-validated simulations. Therefore, the increase in the settlement and confining stress distributions with depth for column V10PU is greater than that for column V10PW as shown in Fig. 5.11b, and c, contributing in part to the greater large-displacement capacity.

The DEM simulations also provide an opportunity to evaluate the accuracy of various cavity expansion factors, k_p, proposed to compute the bearing capacity of aggregate columns (e.g., Hughes et al. 1975; Stuedlein and Holtz 2013). The average σ'_r estimated from the DEM simulations of V10PW within the bulging zone (i.e., 0.80 m to 2.0 m) is approximately 185 kPa for q = 1,200 kPa, representing an increase in σ'_r of 145 kPa from the initial, unloaded condition. The ratio of average increase in σ'_r and average s_u corresponding to the bulging zone length (51 kPa) results in $k_p = 2.84$, significantly lower than the $k_p = 4$ recommended by Hughes et al. (1975). On the other hand, the empirical equation proposed by Stuedlein and Holtz (2013) results in $k_p = 2.82$, within 1% of that derived from the DEM simulations, owing to the ability to capture pressure-dependency in the empirical approach. Similarly, $k_p = 2.15$ for the DEM simulations of V10PU computed using $s_{u,\,avg}$ =58 kPa and σ'_r = 165 kPa, compared to 2.63 estimated using the methodology proposed by Stuedlein and Holtz (2013), or within 18% (as compared to 46% derived using Hughes et al. 1975). Despite some differences between the numerical and semi-empirical methods (Stuedlein and Holtz 2013 and Hughes et al. 1975), the estimated k_p are relatively consistent.

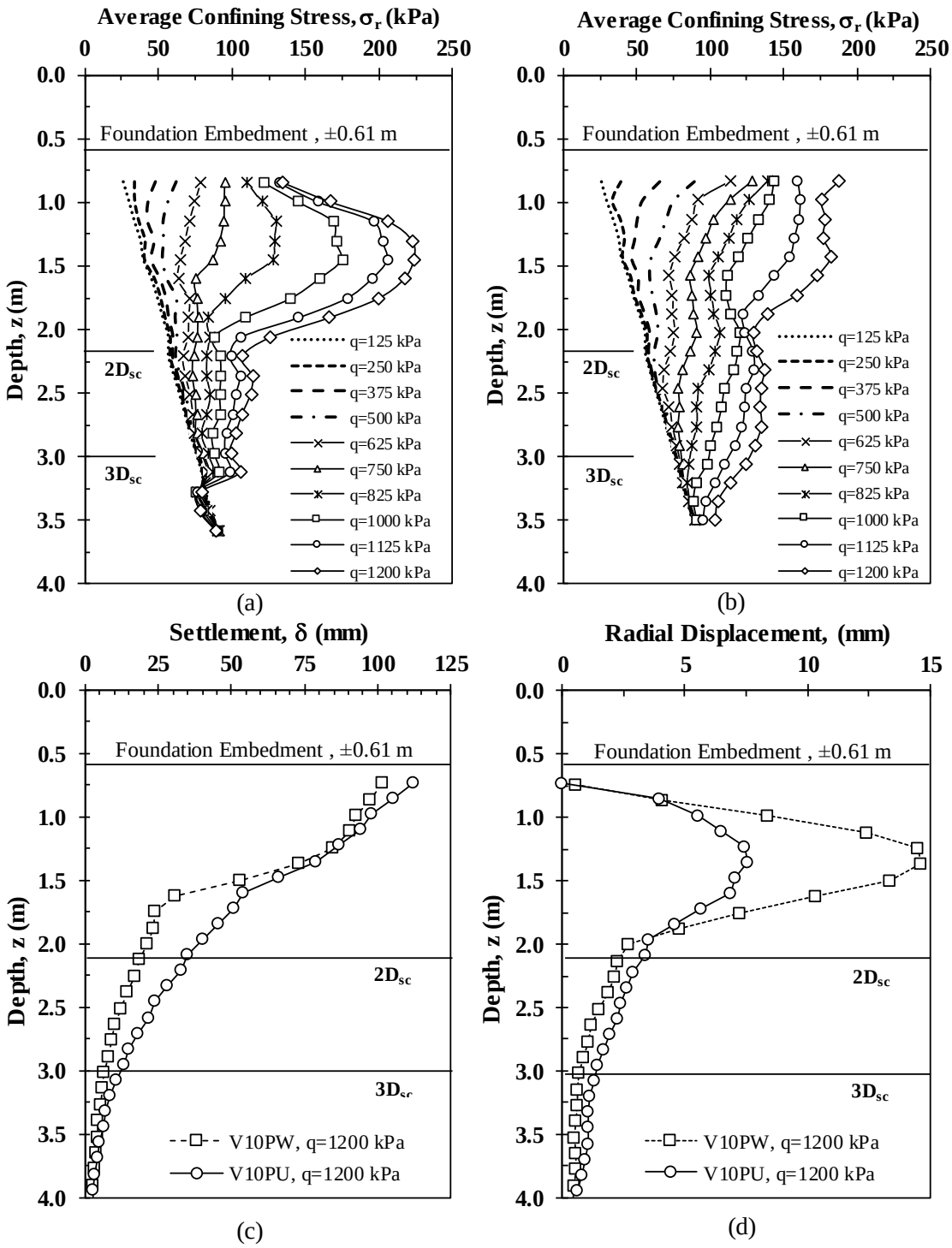

Fig. 5.11. Average confining stress distribution for V10PW, (b) average confining stress distribution for V10PU, (c) settlement distribution with depth for V10PW and V10PU, and (d) radial displacement distribution with depth for V10PW and V10PU.

Fig. 5.12 compares the variation of the bearing capacity factor (N_c) as a function of A_r for columns V10PW and V10PU. The average undrained shear strengths ($s_{u,\,avg.}$) of the clayey soil within the bulging depth are 51 kPa and 58 kPa for V10PW and V10PU, respectively. For both columns, the DEM simulations suggest that there is a linear variation of N_c for different settlements (i.e., 10 and 25 mm) and failure condition as A_r varies from 10 to 50%. The bearing capacity factors at the failure condition for isolated conditions (A_r=100%) are approximately 24 and 22 for columns V10PW and V10PU, respectively. These values are slightly above the typical value used to determine q_{ult} (≈20s_u) of isolated stone columns as reported by Castro (2007). Based on these N_c values, the factors of safety (FS=q/q_{ult}) to satisfy foundation serviceability limit state were estimated from the DEM results. For δ=25 mm, on the other hand, the estimated FS values are approximately 1.5 and 2.0 corresponding to V10PW and V10PU, respectively.

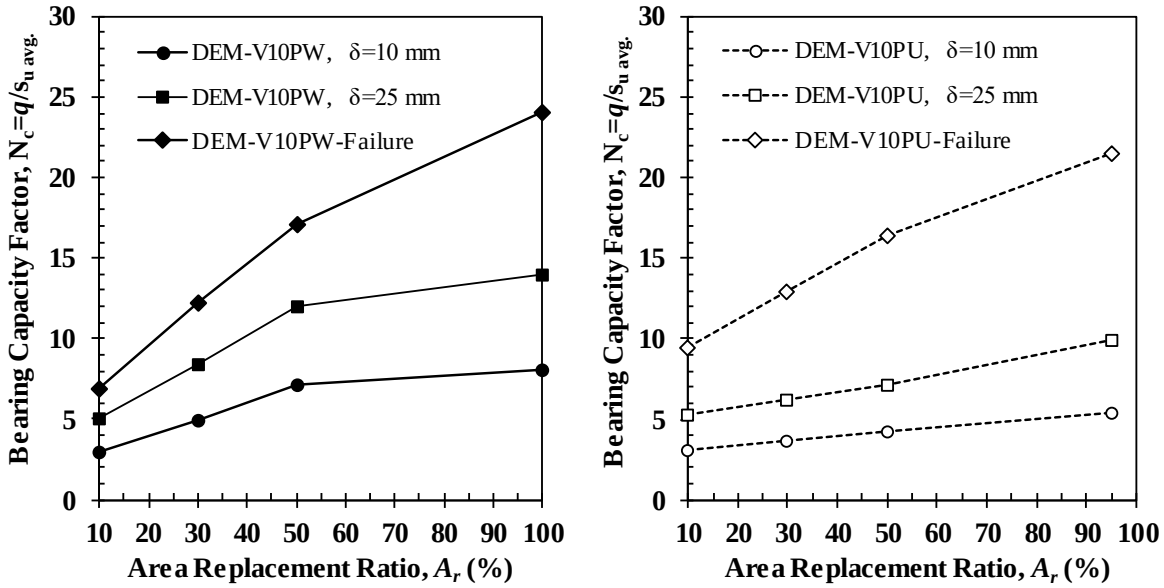

Fig. 5.12. Comparison of the bearing capacity factor variation as a function of the area replacement ratio for different settlement values and failure condition (a) V10PW and (b) V10PU.

5.2. Comparison of Load Transfer Mechanism, and Bearing Pressure-Displacement Response of Single, Cemented Stone Column-Supported Footings

5.2.1 Settlement and Vertical Stress Distributions in Small-Scale DEM models

Distributions of the vertical displacement (δ-z) and stress (σ_v-z) with depth below the edge (A-A') and center (B-B') of the foundations on the small-scale granular columns are presented in Fig. 5.13, for an applied q of approximately 150 kPa. A significant reduction (2.3 times at the soil surface) in the settlement for both foundations supported on cemented columns is observed compared to UCSC (Fig. 5.13a, and c). This settlement reduction largely occurs within the upper half of the column length (equal to 2B; B = 0.10 m), with no differences in the δ-z between the cemented and uncemented columns for depths greater than 2.5B. On the edge of the foundation, minimal influence on the σ_v-z in the matrix soil is observed between all three columns. For depths greater than 2B, the σ_v-z are essentially the same for all columns (Fig. 5.13c); however, a substantial increase in the σ_v-z occurs below the foundation center of the cemented columns in comparison with UCSC (Fig. 5.13d). This increase in σ_v is expected due to the stiffer response of the cemented columns, resulting in a maximum increase in σ_v for PCSC and FCSC of approximately 2.8 and 3.8 times, respectively, at a depth of 0.3B.

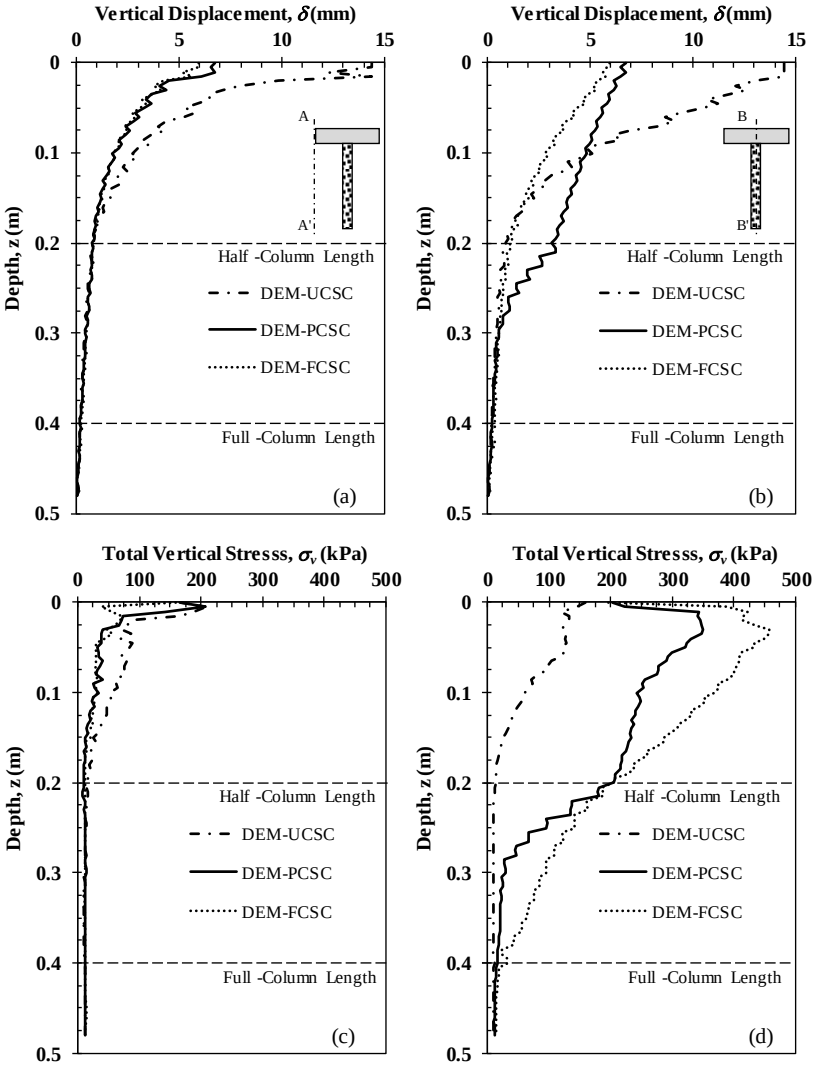

Fig. 5.13. Comparison of computed settlement and vertical distributions for small-scale stone column DEM simulations for q = 150 kPa: (a) settlement distribution in the soil matrix (A-A'), (b) settlement distribution along shaft (B-B'), (c) vertical stress distribution in the soil matrix (A-A'), and (d) vertical stress variation with depth in the column center (B-B').

5.2.2 Effect of Cement Content on q-δ Performance of Investigated Full-Scale Cemented Stone Columns

The effect of the cement content on the q-δ behavior of columns V15U-PCSC and V15U-FCSC was investigated by modeling these columns with the aggregate stiffness and strength properties determined from triaxial simulations (Tables 7, and 9). As illustrated in Fig. 5.14, the

bearing pressure-displacement responses for both columns V15U-PCSC and V15U-FCSC modeled with the constitutive parameters for 10 % cement exhibit an almost linear initial behavior for q less than 1000 kPa and are significantly stiffer than those simulated for 5% cement. At q=1200 kPa, simulation of column V15U-PCSC-10% suggests a settlement reduction of 30 mm (i.e., 59%) when compared to V15U-PCSC-5%, whereas the simulated response of V15U-FCSC-10% indicates a settlement reduction of 66% (i.e., 28 mm) in reference to V15U-FCSC-5%. For $\delta = 25$ mm, the bearing capacity improvement factor of the partially cemented stone columns is 2.3 and 3.3 for columns V15U-PCSC-5% and V15U-PCSC-10%, respectively, in comparison with the observed q-δ response of V15U-UCSC. For the fully-cemented stone columns, the improvement factor is 2.4 and 4.4 for columns V15U-FCSC-5% and V15U-FCSC-10%, respectively, with respect to V15U-UCSC, indicating a significant improvement in the column bearing capacity due to the cement inclusion at the serviceability limit state. Fig. 5.14a shows that modeling column V15U-PCSC with material properties corresponding to 10% cement provides a better approach to the field data than when simulated using 5% cement; however, the numerical results still overestimate the measured settlements.

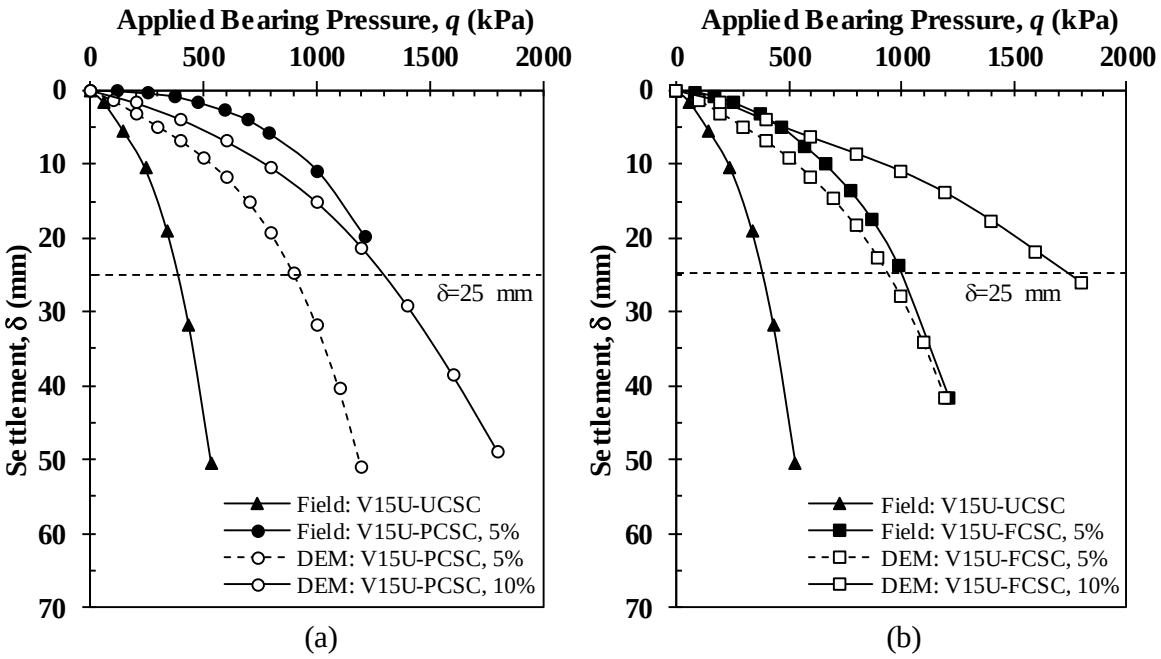

Fig. 5.14. Comparison of the numerical and measured bearing pressure-displacement responses for large-scale uncemented stone column (V15U-UCSC) and cemented stone columns (V15U-PCSC and V15U-FCSC) simulated with 5 and 10% cement content: (a) partially cemented and (b) fully cemented (field data from Stuedlein 2008).

5.2.3 Comparison of the Behavior of the Full-Scale Cemented Stone Columns at the Ultimate Limit State

Lateral and vertical stress distributions, displacements and capacities of the full-scale cemented aggregate columns at the ultimate limit state were investigated using the calibrated 3D DEM models. The field capacities of the uncemented aggregate column and cemented stone columns were computed based on extrapolations of the field-measured data following the approach described by Stuedlein and Holtz (2013), and equaled 900, 2,250, and 1,900 kPa for V15U-UCSC, V15U-PCSC, and V15U-FCSC, respectively. A comparison of the extrapolations of the observed and numerical q-δ responses for columns V15U-UCSC, V15U-PCSC, and V15U-FCSC is presented in Fig. 5.15. The DEM q-δ responses closely agree with the field

observed responses in the range of displacement evaluated for columns V15U-UCSC and V15U-FCSC, indicating ultimate bearing resistances that are 6 and 5% (i.e., 950 and 2,000 kPa) greater than that estimated by extrapolation of the observed responses for V15U-UCSC and V15U-FCSC, respectively. However, the simulated response for the partially cemented column (V15U-PCSC) clearly underestimates the observed and extrapolated bearing pressures, with an ultimate bearing resistance (i.e., 1800 kPa) that is 20% less than that obtained from the extrapolation of the observed q-δ curve. The bearing capacity ratio (BCR) of the partially cemented columns simulated with modeling parameters for 5 and 10% cement is approximately 1.9 and 3.1 for columns V15U-PCSC-5% and V15U-PCSC-10%, respectively, when compared to column V15U-UCSC. On the other hand, for the fully-cemented aggregate columns, BCR is estimated as 2.2 and 3.3 for V15U-FCSC-5% and V15U-FCSC-10%, respectively, with reference to V15U-UCSC. This indicates that the partially cemented stone columns simulated with aggregate properties for either 5 or 10% cement provide BCR values very similar to those for the fully cemented aggregate column simulations at ultimate limit state.

The average confining stress (σ'_r), radial displacement, vertical stress, and settlement distributions with depth for columns V15U-UCSC, V15U-PCSC, and V15U-FCSC for q = 750 kPa (i.e., maximum applied bearing pressure for V15U-UCSC) are shown in Fig. 5.16. The σ'_r and radial displacement distributions suggest a bulging zone development within the upper half of the column length for V15U-UCSC, with an increase in the average σ'_r (i.e., 108 kPa) in this zone that is 77% greater than for the cemented aggregate columns (i.e., 61 kPa). The increase in the vertical stress distribution with depth for column V15U-FCSC is greater than that for the rest of the simulated columns (Fig. 5.16c), resulting from its greater stiffness. The DEM results also indicate a significant reduction in the δ-z distribution with depth within a length of

approximately $3D_{sc}$, with 82 and 96% reduction in δ at the column top for 5% and 10% cemented stone columns, respectively, when compared to the uncemented column.

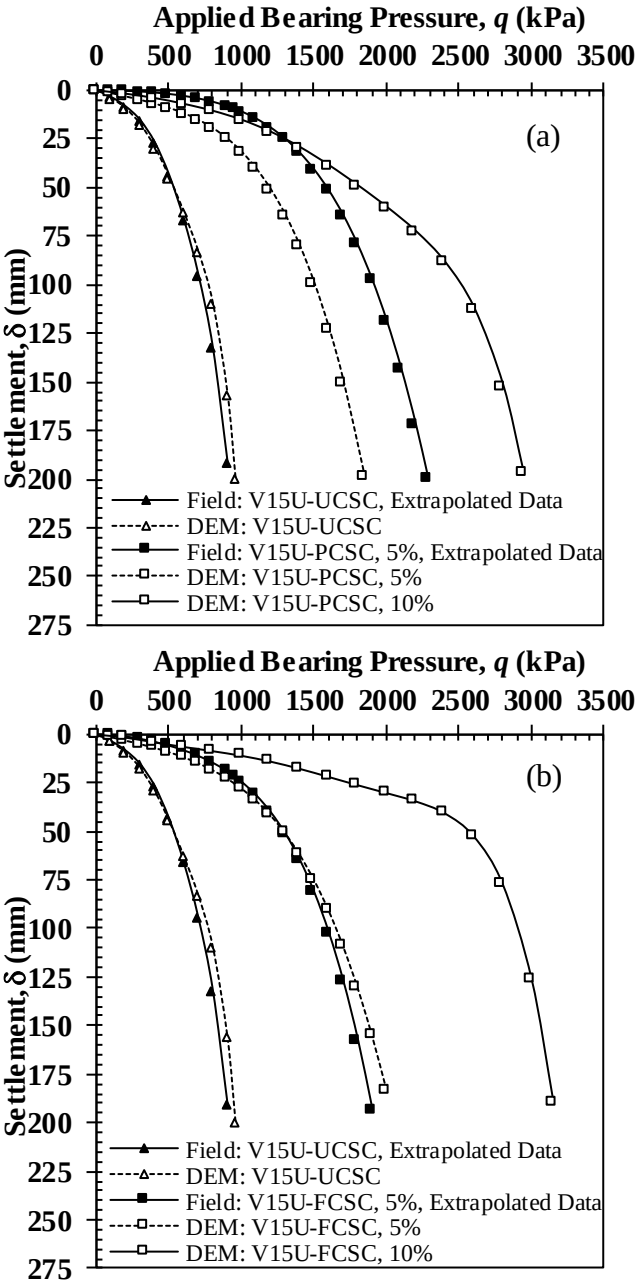

Fig. 5.15. Comparison of the full DEM bearing pressure-displacement results for large-scale uncemented stone column (V15U-UCSC) and cemented aggregate columns (V15U-PCSC and V15U-FCSC) simulated with 5 and 10% cement content with extrapolated field data: (a) partially cemented and (b) fully cemented (field data from Stuedlein 2008).

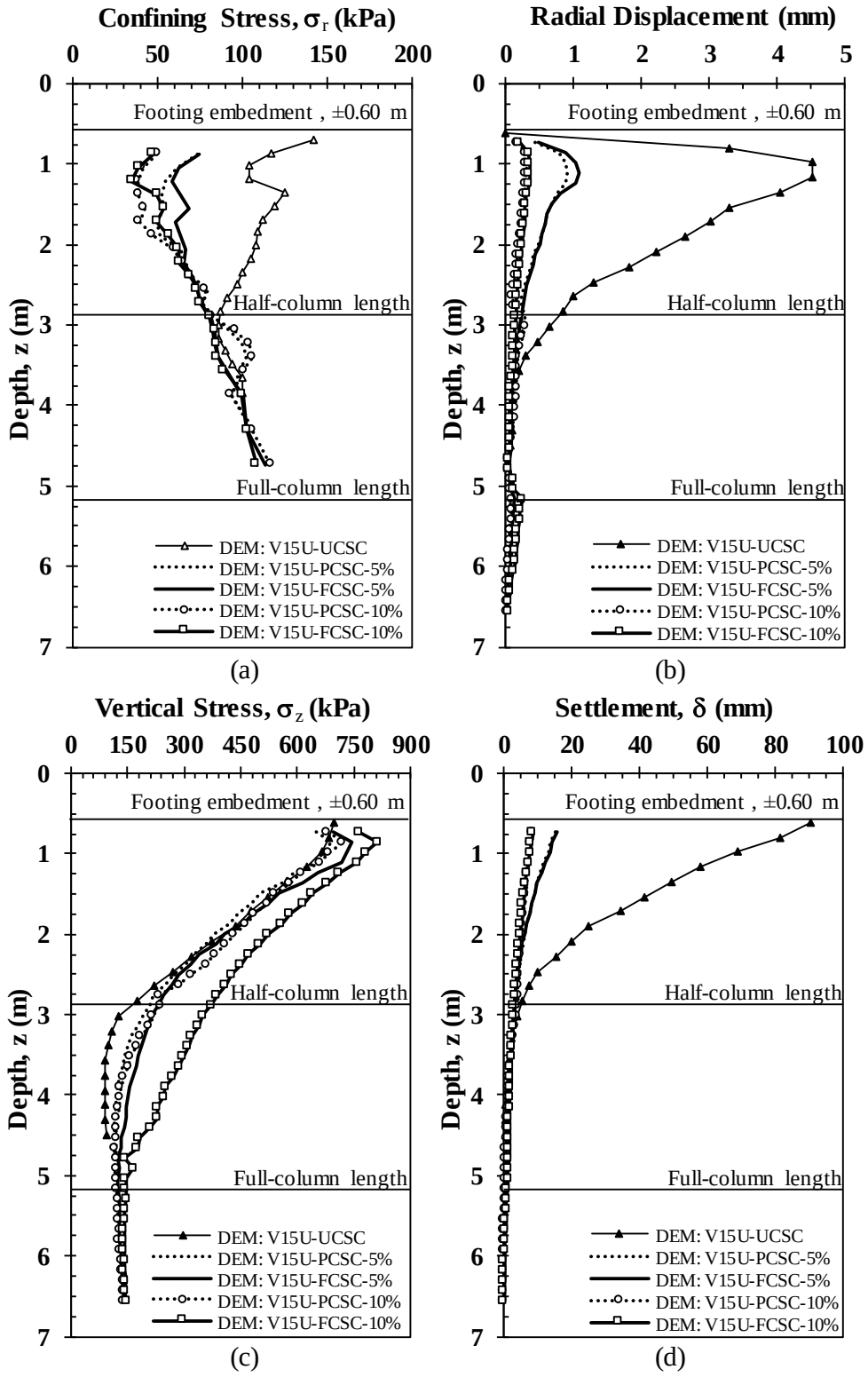

Fig. 5.16.Comparison of the DEM stress and displacement distributions with depth for full-scale uncemented aggregate column (V15U-UCSC) and cemented stone columns (V15U-PCSC and V15U-FCSC) for a bearing pressure of 750 kPa: (a) average confining stress, (b) radial displacement, (c) vertical stress, and (d) settlement.

A comparison of the average confining stress, radial displacement, vertical stress and settlement distributions with depth for full-scale cemented stone columns (V15U-PCSC and V15U-FCSC) at the ultimate limit state is presented in Fig. 5.17. While columns simulated with 5% cement modeling parameters exhibit a bulging zone within a depth of approximately $2D_{sc}$ (typical for uncemented single stone columns), no bulging zone is developed in the upper column half for the columns simulated with 10% cement. The average σ'_r computed from the DEM results of columns V15U-PCSC-5% and V15U-FCSC-5% within the bulging zone (i.e., 0.80 m to 2.2 m) is approximately 190 kPa, indicating an increase in σ'_r of 140 kPa from the initial, unloaded condition. On the other hand, for columns V15U-PCSC-10% and V15U-FCSC-10%, the increase in σ'_r is approximately 36% of the estimated value for the 5% cement columns. The DEM simulations of the partially cemented stone columns show an increase in the average σ'_r (i.e., 98 kPa) in the lower column half (Fig. 5.17a), resulting from the lower stiffness and strength of the uncemented aggregate within this zone. Because of the floating support condition, there is an increase in the radial displacement at the column tip that is 10 and 27 times greater than the maximum radial displacement (i.e., 1.4 mm) within the bulging zone for columns V15U-PCSC-10% and V15U-FCSC-10%, respectively. Contour plots comparing the vertical and radial displacement distributions at ultimate limit state (i.e., δ=200 mm) for columns V15U-UCSC, V15U-FCSC-5% and V15U-FCSC-10% are presented in Fig. 5.18, and 19. As observed, there is a minimal increase in the vertical displacement distributions for columns V15U-UCSC and V15U-FCSC-5% for depths greater than the haft of the column length, with no increase in the vertical displacement at the tip of the columns (Fig. 5.18a, and b). This indicates that most of the applied q is radially transferred to the soil by lateral deformation of the column (i.e., bulging) within the upper column half as observed in Fig. 5.19a and b.

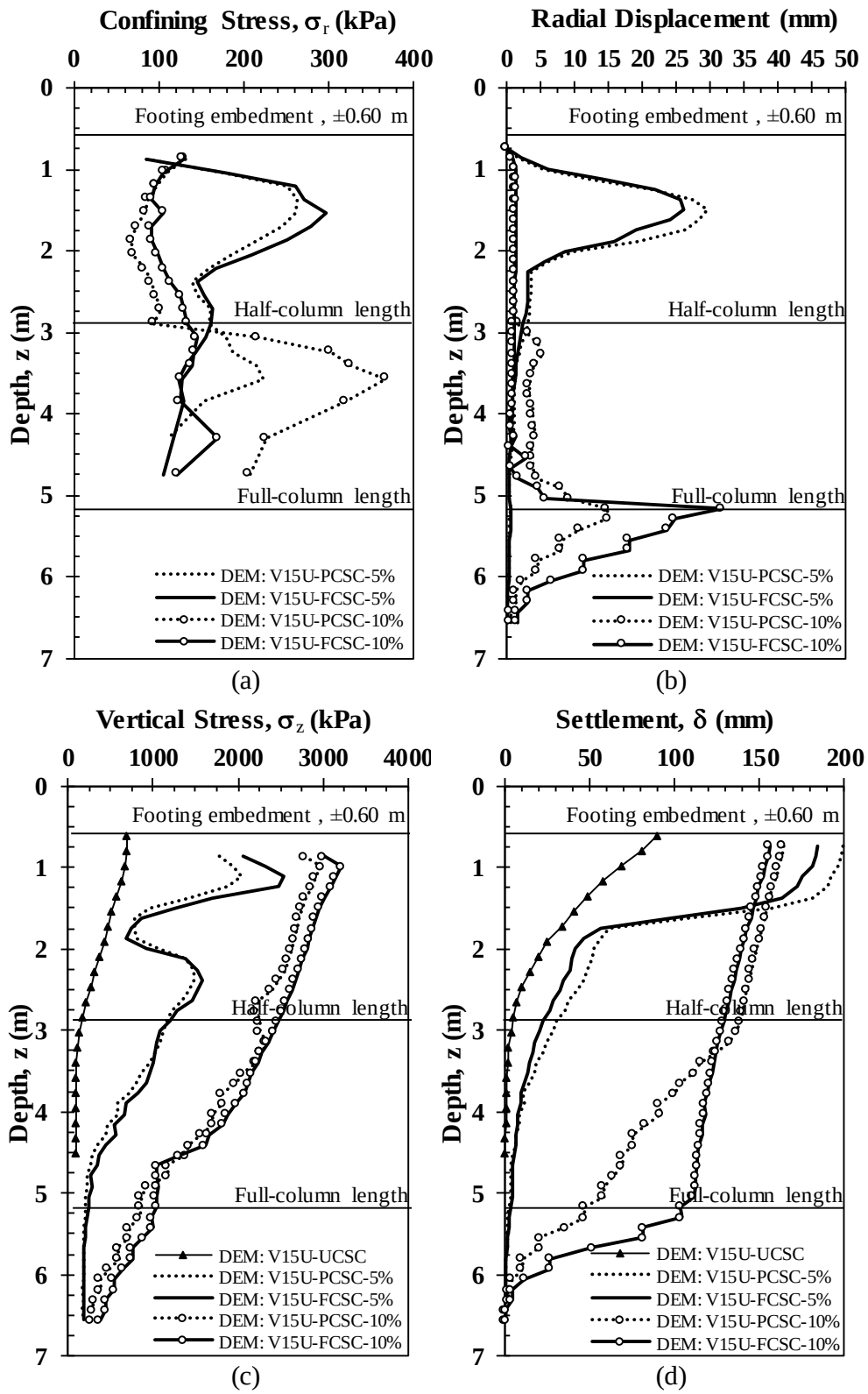

Fig. 5.17. Comparison of the DEM stress and radial displacement distributions with depth for full-scale cemented stone columns (V15U-PCSC and V15U-FCSC) at ultimate limit state: (a) average confining stress, and (b) radial displacement, (c) vertical stress, and (d) settlement.

Fig. 5.18c shows an increase in the vertical displacement distribution within the lower column half for column V15U-FCSC-10% in comparison with columns V15U-UCSC and V15U-FCSC-5%, with approximately 75% of the footing settlement transferred to the column tip. Column V15U-FCSC-10% exhibit no bulging formation within the upper column half, but an increase in the radial displacement at the tip of the column (Fig. 5.19c). This represents that this column behaves more like a rigid element where the applied *q* is largely transferred to the surrounding soil by side friction and end-bearing (similar to vertically loaded piles).

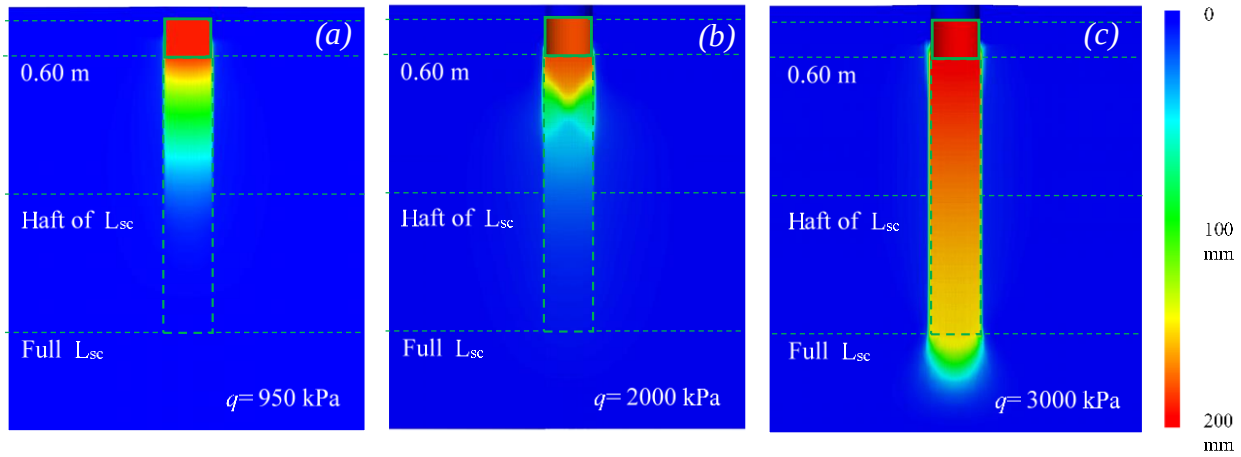

Fig. 5.18. Contour plots comparing the vertical displacement distributions at ultimate limit state for the: (a) V15U-UCSC, (b) V15U-FCSC -5%, and (d) V15U-FCSC -10%.

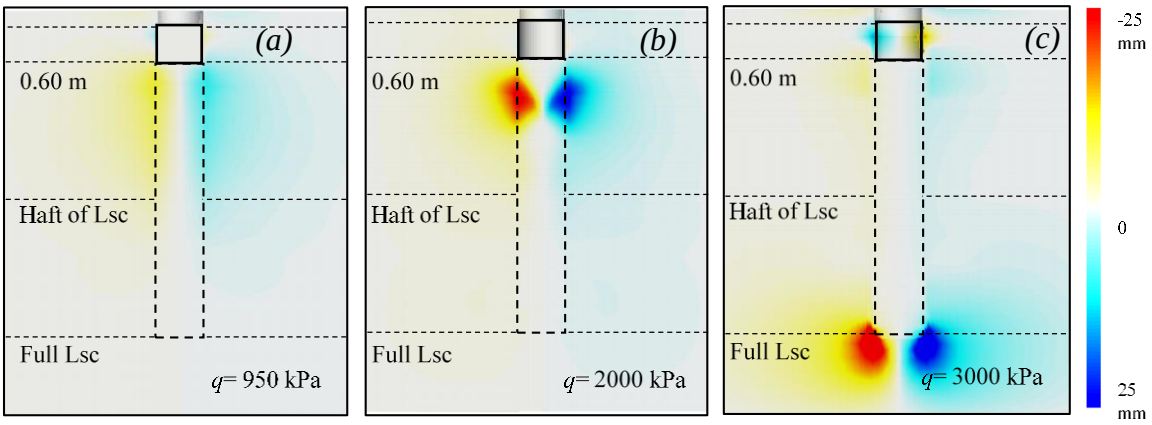

Fig. 5.19. Contour plots to compare the radial displacement distributions at ultimate limit state: (a) V15U-UCSC, (b) V15U-FCSC -5%, and (d) V15U-FCSC -10%.

5.3. Comparison of Load Transfer Mechanism, and Bearing Pressure-Displacement Response of Large Footings Supported on Small, Uncemented Stone Column Group

5.3.1 Comparison of the q-δ Responses of Alternative Geometric Models for Footing V10PU-5 (G4)

Three-dimensional simplified single-column configurations of field test conditions for footing G4 were conducted to evaluate the effectiveness of these alternative approaches to estimate the q-δ responses of footings on a small stone column group. A model of a single stone column with an equivalent diameter representing the same total cross-sectional area of the five columns and a unit cell-model were developed (Fig. 4.7). The q-δ curve obtained from the equivalent diameter model is in close agreement with not only the 3D DEM model representing the actual column configuration (5-columns) used in the field, but also with the observed q-δ response presented in Fig. 5.20. On the other hand, the numerical results of the DEM simulation developed using the unit cell-model indicate a stiffer q-δ response of this model compared to that observed in the field. The close boundary conditions used in the unit-cell model due to the close column spacing configuration for footing G4 prevented the column from deforming laterally, resulting in an almost linear q-δ behavior of the column-footing system for all applied bearing pressures. At q = 383 kPa, the unit-cell model underestimated the observed settlement (i.e., 58 mm) by 75%, indicating a poor performance of this model to simulate individual columns within a small column group.

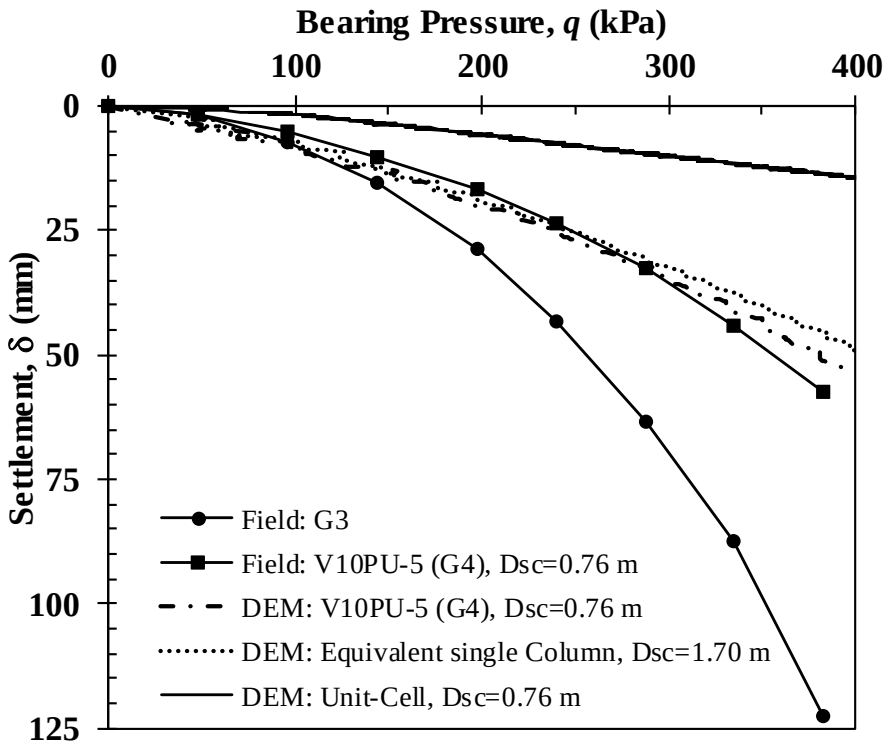

Fig. 5.20. Comparison of q-δ responses for large footing G4 resting on a small uncemented stone column group of five columns using alternative single column models.

5.3.2 Comparison of the q-δ Responses for Footing V10PU-5 (G4) and V15PU-5 (G6)

Given the differences in length between V10PU-5 (G4) and V10PU-5 (G6) (i.e., 1.50 m), the column length was examined as a possible factor influencing the q-δ responses of these large footings. Both footings were simulated using the same s_u profile to only focus on the difference in the length. Fig. 5.21 illustrates that the DEM results for both column lengths are almost the same for bearing pressures less than 250 kPa. Beyond this value, there is a slight difference in the q-δ curve, with the longer columns G6 (4.56 m) providing a settlement of 6% less than the 3.05 m long columns (G4). This behavior agrees with what was estimated for the single, uncemented stone columns (i.e., V10PW and V15PW) as discussed above but is opposite

to what was observed in the field for G4 and G6. Because the differences in the q-δ responses are negligible, the length does not result in a stiffer q-δ response for column G4 with respect to column G6, and it confirms that there is very little influence of column length above 4 times D_{sc} for these investigated columns.

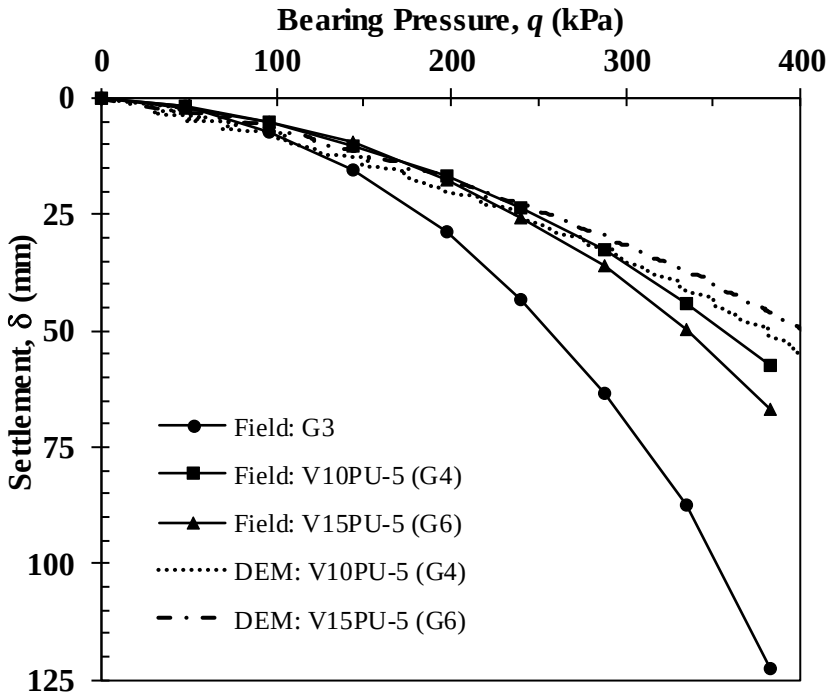

Fig. 5.21. Comparison of q-δ responses for large footing G4 and G6 considering the difference in the column lengths.

5.3.3 Comparison of the performance of the Full-Scale Footings on Uncemented Stone Column group at the Ultimate Limit State

The calibrated DEM models were also used to estimate the ultimate bearing resistance of footing G4 beyond the field measurements. In order to obtain a suitable estimate of the bearing pressure of G4 at failure, the capacity of this footing was estimated for the field-measured

response by extrapolation of the q-δ curves for settlements ranging from 0 to 60 mm using the approach described by Stuedlein and Holtz (2013). A comparison of the average column stress-displacement with the field data is presented in Fig. 5.22a. The numerical results indicate that for the same settlement, the average stress acting on the columns is less than the applied pressure on the footing as a result of the stiffer crust layer. However, as q increases, the stress in the surrounding soil approaches its ultimate capacity, resulting in an increase in the column stress as shown in Fig. 5.22a. This indicates that the stress concentration factor (n) increases (i.e., 0.50 to 1.31) as q also increases (i.e., 100 kPa to 700 kPa). Fig. 5.22b compares the DEM simulated q-δ responses to the extrapolations of the measured field-response data for V10PU-5 (G4). The average foundation stress obtained from the DEM simulations agree with the observed q-δ data for settlements less than 60 mm. Beyond this magnitude of deformation, the DEM results appear to be stiffer than the response expected from extrapolation of the observed q-δ field response. At δ = 200 mm, the DEM simulation provides an ultimate bearing resistance (i.e., bearing capacity; 725 kPa) that is 11% greater than the value estimated from the extrapolated field data (equal to 650 kPa) as illustrated in Fig. 18b. The ultimate bearing capacity of G4 was computed using Barksdale and Bachus method (Eq.30), resulting in a q_{ult} (i.e., 964 kPa) 48% greater than that estimated from the extrapolated field data (Fig. 5.22b).

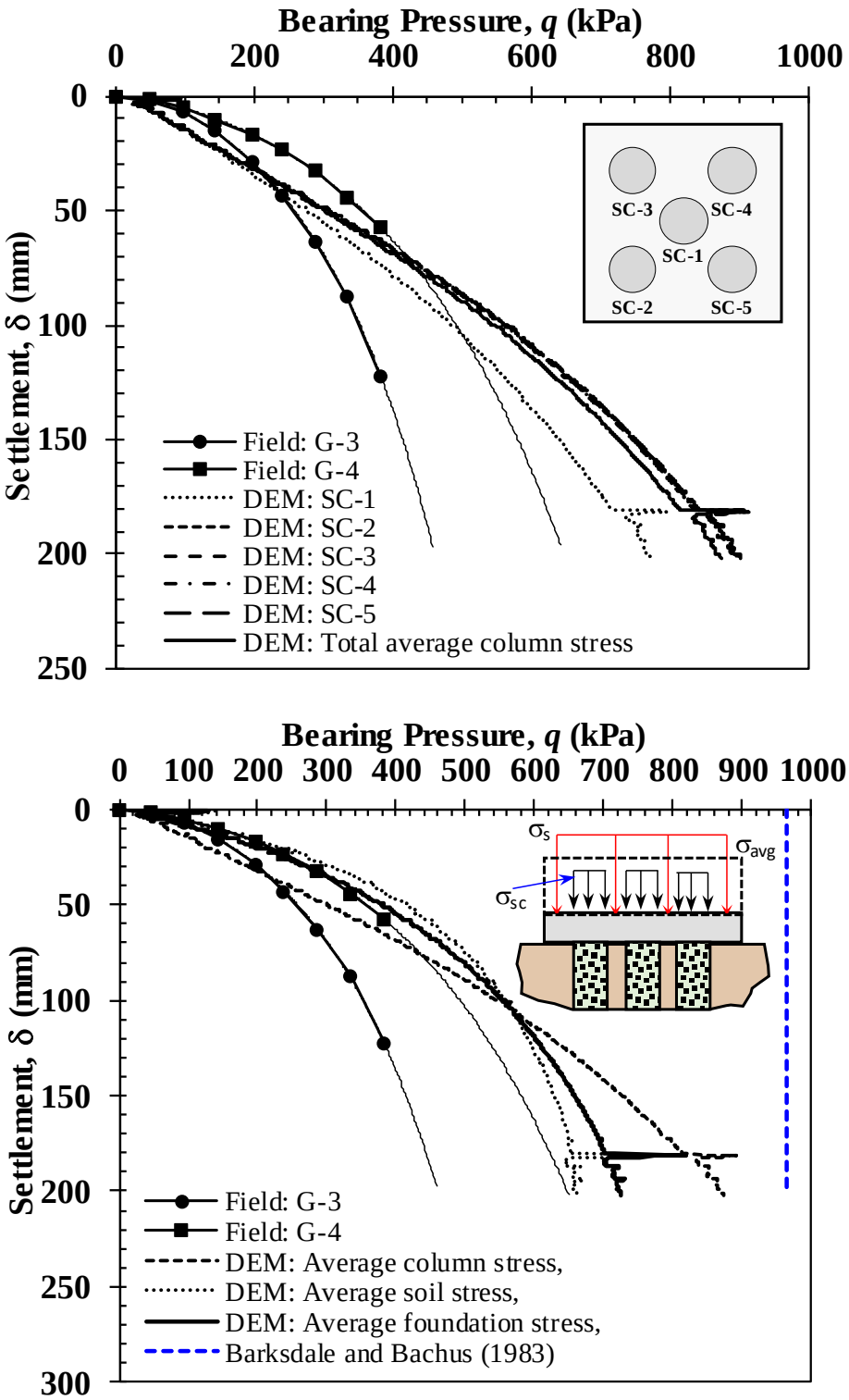

Fig. 5.22. Comparison of the full DEM bearing pressure-displacement results for footing V10PU-5 (G4) with extrapolated field data.

CHAPTER 6. SUMMARY AND CONCLUSIONS

Full-scale loading tests reported by Stuedlein and Holtz (2012a), small-scale loading tests reported by Golait et al. (2016) and corresponding laboratory investigations were used as a basis for the numerical investigation of factors affecting the global response of isolated foundations supported on uncemented and cemented aggregate column reinforced soil. The main parameters investigated in this study included the pressure-dependence of the aggregate friction angle and dilation angle, column length and stiffness, area replacement ratio, undrained shear strength of the surrounding soil, and cement content. In general, the 3D DEM simulations were shown to replicate the observed bearing pressure-displacement curves, and the validated models could be used to systematically investigate aggregate column performance, resulting in the following conclusions:

1. In general, the 3D DEM simulations presented were shown to accurately capture the complex stress transfer and bearing pressure-displacement response of aggregate columns. Incorporating friction angle-gradation dependence in the DEM model was a key factor in improving the accuracy of the bearing pressure-displacement response of the stone columns at the serviceability level.
2. The effects of the initial conditions and aggregate gradation on pressure-dependent strength and stiffness were shown to represent critical factors in the performance of the aggregate columns.
3. The extent of the bulging zone does not appear to be affected by the length of the column for the slenderness ratios investigated.
4. For conditions approaching the ultimate limit state, the maximum average confining stresses estimated from the DEM simulations are greater than 150 kPa within a depth

range less than $2D_{sc}$, which represents a reduction on ϕ'_{sc} of 8° for both gradations. Therefore, it is important to consider the pressure-dependent ϕ'_{sc} corresponding to the radial stress changes as the ultimate limit state is approached.

5. The Young's modulus of the aggregate columns was found to be the main parameter affecting the stone column q-δ performance and the degree of influence was determined to be dependent on the aggregate gradation. Because Young's Modulus varies nonlinearly with confining pressure, variations in the initial radial stress acting on the columns results in different initial column stiffnesses and discrepancies in the q-δ responses of the columns. The influence of increasing radial stresses on the q-δ responses of the uniformly-graded aggregate columns was greater due to the larger range of corresponding initial stiffnesses.
6. The cavity expansion factors, k_p, derived from the DEM simulations are significantly lower than the value originally proposed by Hughes et al. (1975), but agree well with the values determined using the empirical modifications to existing methods proposed by Stuedlein and Holtz (2013).
7. The 3D DEM simulations provided good agreement with the observed and extrapolated data of the cemented aggregate columns investigated, indicating a substantial improvement in the q-δ curves due to the cement-coated aggregate inclusion as compared to the uncemented stone columns for serviceability and ultimate limit states.
8. Numerical results of small- and full-scale partially-cemented stone columns exhibited slightly lower bearing pressure capacities than those fully constructed with cemented aggregate. Hence, the effectiveness of conventional stone columns can be significantly improved by incorporating cemented aggregate into the upper half of the column length;

however, using cemented aggregate in the full column length might be more feasible in terms of construction convenience.

9. Increases in cement content in the aggregate mixture from 5 to 10%, showed improvements in bearing capacity factors in the simulated columns of approximately 2 and 3, respectively, as compared to uncemented columns at the ultimate state condition.
10. Full-scale columns simulated with 5% cement exhibited bulging failure within the upper half of the column similar to uncemented columns, whereas the columns modeled with 10% cement aggregate properties showed a settlement and load transfer mechanism similar to vertically loaded piles.
11. The full-scale DEM simulations of large footings on small groups of stone columns were shown to provide good estimations of bearing pressure-displacement responses compared to field data. The unit-cell model of these large footings, however, exhibited poor performance in estimating the bearing pressure-displacement response. A single aggregate column model developed using an equivalent diameter (i.e., same area replacement ratio that the five columns) produced a closer estimation of the bearing pressure-displacement behavior to the field data.

The DEM results show that gradation-specific parameters influence the global response of stone columns and should be incorporated into the design. Because the aggregate types and gradations used in production vary, it is recommended that aggregate and gradation specific laboratory tests be used to quantify the strength and stiffness design parameters, instead of assuming typical values. This study was limited to stone columns and plate loading tests conducted on the Beaumont clay formation. Therefore, these recommendations are based on

aggregate columns that fit into the bounds of the data and loading used in this numerical investigation.

REFERENCES

Adalier, K., Elgamal, A., Meneses, J., and Baez, J. (2003). "Stone columns as liquefaction countermeasure in non-plastic silty soils." *Soil Dynamics and Earthquake Engineering, Elsevier, Vol. 23, No. 7, pp. 571-584, DOI: 10.1016/S0267-7261(03)00070-8.*

Ambily, A. and Gandhi, S. (2007). "Behavior of stone columns based on experimental and FEM analysis." *Journal of Geotechnical and Geoenvironmental Engineering, ASCE, Vol. 133,*
No. 4.

Ammari, K. and Clarke, B. (2018). "Effect of vibro stone-column installation on the performance of reinforced soil." *Journal of Geotechnical and Geoenvironmental Engineering, ASCE, Vol. 144, Issue 9.*

Ashford, S., Rollins, K., Case Bradford, V., Weaver, T., and Baez, J. (2000). "Liquefaction mitigation using stone columns around deep foundations: Full scale test results." *Transportation research record, 1736, 110-118.*

Balaam, N., Brown, P., and Poulos, H. (1977). " Settlement analysis of soft clays reinforced with granular piles." *Proceedings, 5th Southeast Asian Conference on Soil Engineering, July 2-4, Bangkok, Thailand.*

Balaam, N., and Booker, J. (1981). "Analysis of rigid rafts supported by granular piles." *Int. J. Numerical. and Analytical Methods in Geomech., 5, 379–403.*

Barksdale, R. and Bachus, R. (1983). "Design and construction of stone columns." *Rep. No. FHWA/RD 83/026, Federal Highway Administration, Washington, DC.*

Brauns, J. (1978). "Initial bearing capacity of stone columns and sand piles." *Vol. I, Proc., Soil Reinforcing and Stabilizing Techniques in Engineering Practice, New South Wales Institute of Technology, Sydney, Australia, 497-512.*

Bouassida, M., and Frikha, W. (2014). "Prediction of stone column ultimate bearing capacity using expansion cavity model." *Ground Improv., 168, 106-115.*

Castro, J. and Sagaseta, C. (2009). "Consolidation around stone columns. Influence of column deformation." *International Journal for Numerical and Analytical Methods in Geomechanics. Vol. 6, 851-877.*

Castro, J. (2017). "Modeling Stone Columns." *Materials, 10(7), 782.*

Chen, B. and Mayne, P. (1996). "Statistical relationships between piezocone measurements and stress history of clays." *Canadian Geotechnical Journal, Vol. 33, NRC Press, Canada. 488-498.*

Cundall, P. (1988). "Formulation of a three-dimensional distinct element model-Part I. A scheme to detect and represent contacts in a system composed of many polyhedral blocks." *Rock Mechanics and Geomechanics, 107-116.*

Duncan, J. and Chang, C. (1970). "Nonlinear analysis of stress and strain in soils." *Journal of Soil Mechanics and Foundations Division,* ASCE, Vol. 96, No. SM5, Reston, *Virginia, USA.*

Duncan, J. and Buchignani, A. (1987). "An engineering manual for settlement studies." *Berkeley: University of California.*

Duncan, J., Brandon, T., Jian, W., Park, Y., Griffith, T., Corton, J., and Ryan, E. (2007). "Densities and friction angles of granular materials with standard gradations 21b and #57." *Center for Geotechnical Practice and Research, Virginia Polytechnic Institute*.

Elshazly, H., Elkasabgy, M., and Elleboudy, A. (2008). "Effect of inter-column spacing on soil stresses due to vibro-installed stone columns." *Interesting Findings. Geotech. Geol. Eng. 2008, 26, 225–236.*

Fox, N. and Cowell, M. (1998). "Geopier foundation and soil reinforcement manual." *Geopier Foundation Company, Scottsdale, AZ.*

Gibson, R. and Anderson, W. (1961). "In situ measurement of soil properties with the pressuremeter." *Civil Engineering and Public Works Review, Vol. 56, No. 658, 615-618.*

Golait, Y., Satyanarayana, V., and Raju, S. (2009). "Concept of under reamed cemented stone columns for soft clay ground improvement. " *Proc., Indian Geotechnical Conf. 2009, Vol. 1, Allied, Mumbai, India,356–360.*

Golait, Y., and Padade, A. (2016). " Analytical and experimental studies on cemented stone columns for soft clay ground improvement." *International Journal of Geomechanics, © ASCE, Vol. 17, Issue 4, 04016100.*

Goughnour, R. and Bayuk, A. (1979a). "Analysis of stone column-soil matrix interaction under vertical load." *Proceedings of the International Conference on Soil Reinforcement: Reinforced Earth and Other Technologies, Vol. I, Paris, France. 271-277.*

Greenwood, D. (1970). "Mechanical improvement of soils below ground surface." *Proc., Conf. on Ground Engineering, Institution of Civil Engineers, London.*

Han, J. and Ye, SL. (2001). "A simplified solution for the consolidation rate of stone column reinforced foundations." *Journal of Geotechnical and Geoenvironmental Engineering; 127(7):597–603.*

Hanna, A., Etezad, M., and Ayadat, T. (2013). "Mode of failure of a group of stone columns in soft soil." *International Journal of Geomechanics (American Society of Civil Engieers-ASCE),* 87-96.

Hu, W., Wood, D. M., and Stewart, W. (1997). "Ground improvement using stone column foundations: Result of model tests." *Int. Conf. on Ground Improvement Techniques, CI-Premier, Singapore, 247-256.*

Hughes, J. and Withers, N. (1974). "Reinforcing of soft cohesive soils with stone columns." *Ground Eng., 7(3), 42–49.*

Indraratna, B., Ngo, N., Rujikiatkamjorn, C., and Sloan, S. (2015). "Coupled discrete element–finite difference method for analysing the load-deformation behaviour of a single stone column in soft soil." *Computer and Geotechnics, 63:267–278.*

Itasca Consulting Group Inc. (2013). "3DEC version 5.0 user's guide, Minneapolis, Minnesota USA."

Kelly, P. (2014). "Soil structure interaction and group mechanics of vibrated stone column foundations." *Ph.D. thesis, Univ. of Sheffield.*

Kulhawy, F. and Mayne, P. (1990). "Manual on estimating soil properties for foundation design." *EL-6800, Research Project 1493-6, Electric Power Research Institute, Palo Alto Institute, 304.*

Madhav, M. and Vitkar, R. (1978). "Strip footing on weak clay stabilized with a granular trench or pile." *Can. Geotech. J., 15(4), 605-609.*

Mahar, L., and O'Neill, M. (1983). "Geotechnical characterization of desiccated clay." *J. Geotech. Eng., 109(1), 56–71.*

McCabe, B., and Nimmons, G. (2009). "A review of field performance of stone columns in soft soils." *Geotech. Eng., 162, 323-334.*

McCabe, B. and Killeen, M. (2016). "Small stone-column groups: mechanisms of deformation at serviceability limit state." *International Journal of Geomechanics, © ASCE, ISSN 1532-3641.*

Meyerhof, G. (1963). "Some recent research on the bearing capacity of foundations." *Canadian Geotechnical Journal, 1, 16-26. http://dx.doi.org/10.1139/t63-003.*

Meyerhof, G. (1965). "Shallow Foundations." *Journal of the Soil Mechanics and Foundation Division, ASCE, Vol. 91. No. SM2, pp. 21-31.*

Mitchell, J. (1981). "Soil improvement-state-of-the-art report." *Proc., 10th Int. Conf. on Soil Mechanics and Foundation Engineering, Session 12, Int. Society of Soil Mechanics and Foundation Engineering, London, Vol. 4, 506-565.*

Mitchell, J. and Huber, T. (1985). "Performance of a stone column foundation." *Journal*

of Geotechnical Engineering, ASCE, Vol. I, No. 2, Reston, Virginia, USA.

Nazari, J., and Ghazavi, M. (2014). "A simple analytical method for calculation of bearing capacity of stone-column." *Int. J. of C. Eng., Vol. 112, 15-25.*

Newton, C. (2014). "Drained response of uncemented and cemented aggregates used with aggregate pier ground improvement." *MS Thesis, Oregon State University.*

Ngo, N. T., Indraratna, B. and Rujikiatkamjorn, C. (2016). "Load-deformation behavior of a stone column using the coupled DEM-FDM method." *Proceedings of the joint geotechnical and structural engineering congress., 1618-1626.*

O'neill, M., & Yoon, G. (1995). "Engineering properties of overconsolidated Pleistocene soils of Texas gulf coast." *Transportation Research Board, Issue: 1479, 81-88.*

Poorooshasb, G., and Meyerhof, G. (1997). "Analysis of behavior of stone columns and lime columns." *Computer and Geotechnics, Vol 20, Issue 1, 47–70.*

Priebe, H. (1976). "Abschätzung des setzungsverhaltens eines durch stopverdich-tung verbesserten baugrundes." *Die Bautechnik, (53), 5, 160-13.*

Raju, V., and Sondermann, W. (2005). "Ground improvement using deep vibro techniques." *Ground Improvement Case Histories. Indraratna, B and Chu, J., Elsevier Geo-Engineering Book Series Vol.3, 601-638.*

Rayamajhi, D., Nguyen, T., Ashford, S., Boulanger, R., Lu, J., Elgamal, A., and Shao, L. (2014a). "Numerical study of shear stress distribution for discrete columns in liquefiable soils." *Journal of Geotechnical and Geoenvironmental Engineering, ASCE, Vol. 140, No. 3, pp. 04013034, DOI: 10.1061/(ASCE)GT.1943-5606.0000970.*

Rayamajhi, D., Nguyen, T., Ashford, S., Boulanger, R., Lu, J., Elgamal, A., and Shao, L. (2014b). "Reinforcing effects of soil-cement columns in liquefiable sand." *Network for Earthquake Engineering Simulation (distributor), Dataset. Schofield, A. N.* (1981).

Siahaan, F., Indraratna, B., and Rujikiatkamjorn, C. (2015). "Three-dimensional modelling of the behavior of stone columns using the discrete element method." *Geomechanics from Micro to Macro. © 2015 Taylor & Francis Group, London, ISBN 978-1-138-02707-7.*

Schaefer, V., Abramson, L., Drumheller, J., and Sharp, K. (1997). "Ground improvement, ground reinforcement, ground treatment. Developments 1987-1997." *ASCE Geotechnical Special Publications No. 69, 1997.*

Schaefer, V., and Berg, R., (2014). "Geotechnical solutions for soil improvement, rapid embankment construction, and stabilization of the pavement working platform." *Transportation Research Board, SHRP-2 Report S2-R02-RW-1.*

Schaefer, V., Berg, R., Collin, J., Christopher, B., DiMaggio, J., Filz, G., Bruce, D., and Ayala, D (2017). " Ground modification methods - Reference Manual Volume I." *FHWA-NHI-16-027.*

Stuedlein, A. (2008). "Bearing capacity and displacement of spread footings on aggregate pier reinforced clay." *Ph.D. thesis, Univ. of Washington, Seattle.*

Stuedlein, A., and Holtz, R. (2010). "Undrained displacement behavior of spread footings in clay." *The art of foundation engineering practice, honoring Clyde N. Baker, Jr., P.E., S.E., GSP 198, ASCE, Reston, VA, 653-669.*

Stuedlein, A. (2010). Discussion, "Performance monitoring of a rammed aggregate pier foundation supporting a mechanically stabilized earth wall." *Journal of Performance of Constructed Facilities, ASCE, Vol. 24, No. 3, pp. 289-292.*

Stuedlein, A. and Young, J. (2012). "Uplift performance of multi-helix anchors in desiccated clay." *Journal of the Deep Foundations Institute, Vol. 6, No. 2, 13-25.*

Stuedlein, A., and Holtz, R. (2012a). "Analysis of footing load tests on aggregate pier reinforced clay." *J. Geotech. Geoenviron. Eng., 10.1061/ (ASCE)GT.1943-5606.0000677, 1091–1103.*

Stuedlein, A., Kramer, S., Arduino, P., and Holtz, R. (2012b). "Geotechnical characterization and Rajarandom field modeling of desiccated clay." *J. Geotech. Geoenviron. Eng., 10.1061/(ASCE)GT.1943-5606.0000723, 1301–1313.*

Stuedlein, A., Kramer, S., Arduino, P., and Holtz, R. (2012c). "Reliability of Spread Footing Performance in Desiccated Clay." *J. Geotech. Geoenviron. Eng., 10.1061/(ASCE)GT.1943-5606.0000706, 1314–1325.*

Stuedlein, A. and Holtz, R. (2013). "Bearing capacity of spread footings on aggregate pier reinforced clay." *J. Geotech. Geoenviron. Eng., 10.1061/(ASCE)GT.1943-5606.0000748, 49–58.*

Stuedlein, A., and Holtz, R. (2014). "Displacement of spread footings on aggregate pier reinforced clay." *J. Geotech. Geoenviron. Eng., 10.1061/(ASCE)GT.1943-5606.0000982, 36–45.*

Stuedlein, A., Abdollahi, A., Mason, H., and French, R. (2015). "Shear wave velocity measurements of stone column improved ground and effect on site response." *International Foundation and Equipment Expo (2015), 2306-2317.*

Tan, X., Konietzky, H., Fruhwirt, T., and Dan, D. (2015). "Brazilian tests on transversely isotropic rocks: Laboratory testing and numerical simulations." *Rock Mech. Rock Eng. 48 (4), 1341-1351.*

Tan, X., Konietzky, H., and Chen, W. (2016). "Numerical simulation of heterogeneous rock using discrete element model based on digital image processing." *Rock Mech. Rock Eng. 49 (12), 4957-4964.*

Tan, X., Zhao, M., and Chen, W. (2018). "Numerical simulation of a single stone column in soft clay using the discrete-element method." *International Journal of Geomechanics, © ASCE, ISSN 1532-3641.*

Vahedian, A., Mahini, S., and Aghdaei, S. (2014). "A short state of the art review on construction and settlement of soft clay soil reinforced with stone column." *Int. J. Eng. Tech., Vol. 6, 420-425.*

Van Impe W., and De Beer, E. (1983). "Improvement of settlement behavior of soft layers by means of stone columns." *8th European Conference on Soil Mechanics and Foundation Engineering, Helsinki, vol. 1, 309–312.*

Vautrain, J. (1977). "Reinforced earth wall on stone columns in soil". *Proc. Int. Symp. On Soft Clay, Asian Inst. Technol., Bangkok, 613-626. Also in Bull. Liaison Labs. P et Ch. Special issue VI E, April 1978, 188-194.*

Wehr, W. (1999). "Schottersäulen-Das verhalten von einzelnen säulen und säulengruppen." *Geotechnik, 22(1), 40-47.*

Vermeer, P. and Borst, R. (1984). "Non-associated plasticity for soils, concrete and rock." *Stevin-Laboratory of the Department of Civil Engineering of the Delft University of Technology, Rijswijk, ZH.*

Vesic, A. (1972). "Expansion of cavities in infinite soil mass." *Journal of Soil Mechanics and Foundation Engineering Division, ASCE, No. SM3, Vol. 98, 265-290.*

White, D., Pham, H., and Hoevelkamp, K. (2007). "Support mechanisms of rammed aggregate piers. I: Experimental results." *J. Geotech. Geoenviron. Eng., 133(12), 1503–1511.*

Wissmann, K., White, D., and Lawton, E. (2007). "Load test comparisons for rammed aggregate piers and pier groups." *Soil improvement— Geo-Denver 2007, ASCE, Reston, VA, 1–11.*

Wood, D., Hu, W., and Nash, D. (2000). "Group effects in stone column foundations: Model tests." *Geotechnique, 50(6), 689-698.*

Zhang, L., Zhao, M., Shi, C., and Zhao, H. (2013). "Settlement calculation of composite foundation reinforced with stone columns." *J. Geomech., 248-256.*